

THE ENERGY LEVELS OF  $^{134}\text{Cs}$

By

© ALBERT GARLAND LEE

A Thesis

Submitted to the School of Graduate Studies  
in Partial Fulfilment of the Requirements

for the Degree

Doctor of Philosophy

McMaster University

October, 1982

THE ENERGY LEVELS OF  $^{134}\text{Cs}$  ..

Doctor of Philosophy (1982)

McMaster University

(Physics)

Hamilton, Ontario

Title: The Energy Levels of  $^{134}\text{Cs}$

Author: Albert Garland Lee, B.Sc. (University of Manitoba)

M.Sc. (York University)

Supervisor: Dr. R.G. Summers-Gill

Number of Pages: xiii, 169

## Abstract

The energy levels of  $^{134}\text{Cs}$  were investigated with single particle transfer reactions,  $^{133}\text{Cs}(d,p)$  and  $^{135}\text{Ba}(t,\alpha)$ , and via  $\gamma$ -ray spectroscopy studies,  $^{133}\text{Cs}(d,p\gamma)$  and  $^{130}\text{Te}(^7\text{Li},3n\gamma)$ . The  $^{133}\text{Cs}(d,p)$  reaction revealed twentyfive levels up to 936 keV. The  $l$ -values and spectroscopic factors were extracted for twenty-three of these levels. Four prominent  $l_n = 2$  and three prominent  $l_n = 0$  levels were found. Eleven  $l_n = 5$  levels were also identified.

The  $^{135}\text{Ba}(t,\alpha)$  reaction showed nineteen levels up to 1319 keV, but  $l$ -values and spectroscopic factors were extracted for only eleven of these levels. Four strong  $l_p = 4$  and seven  $l_p = 2$  levels were identified.

High resolution singles and coincidence  $\gamma$ -ray studies in the  $^{133}\text{Cs}(d,p\gamma)$  and  $^{130}\text{Te}(^7\text{Li},3n)$  reactions gave data on the de-excitation of the levels in  $^{134}\text{Cs}$ . The  $^{133}\text{Cs}(d,p\gamma)$  study provided detailed information on the levels of  $^{134}\text{Cs}$ . These data provided confirmation of some of the  $(n,\gamma)$  work of Alexeev et al. (1975, 1978).

A level scheme for  $^{134}\text{Cs}$  was deduced from the accumulated data. Tentative spin and parity assignments

were made for some of the levels. Simple shell model p-n configurations,  $[\pi g_{7/2}, (v d_{3/2})^{-1}]$ ,  $[\pi g_{7/2}, (v s_{1/2})^{-1}]$ ,  $[\pi g_{7/2}, (v h_{11/2})^{-1}]$  and  $[\pi d_{5/2}, (v d_{3/2})^{-1}]$ , were invoked to make the spin assignments. The (d,p) and (t, $\alpha$ ) particle data were used to make shell model configuration assignments to some of the energy levels. Poor agreement between the shell model configurations determined in the present study and those assigned by Alexeev et al. (1978) was found.

## Acknowledgements

I have received help and encouragement from many people during the course of this work. I wish to especially thank one group of people who were particularly helpful: Dr. R.G. Summers-Gill, my supervisor, for his guidance and assistance on the long experimental runs and for his diverse research program which enabled me to learn about many aspects of experimental nuclear physics, Dr. J.A. Kühner and Dr. R.H. Tomlinson, the other members of my supervisory committee, for their advice and encouragement, Dr. D.G. Burke, for his friendship and many helpful discussions, Dr. J.A. Cameron, for his wit and his very interesting but diverting ideas, Dr. J.C. Waddington, for his refreshing new ideas, Kevin Lenestour and Aquila Islam, former members of the research group, for their help on the experimental runs, the operations staff, for maintaining the accelerator in good working order, the electronics staff for keeping the computers running, my fellow graduate students, Victor, Ron, Arlene, Fred, Anne, Michel and Brian, for their comradeship,

Miss S. den Blekker, for her help in typing this thesis,  
Mrs. H. Yardley and Mrs. E. Luker, for their patient  
scanning of the nuclear emulsions,

Mr. A.M. Smith, for his assistance in producing the  
drawings for the thesis,

Christine Nawalkowsky for her moral support and for  
reminding me of the humorous side of life, and

Miss C.L. Swift, a very special friend, for giving me  
support and encouragement when I needed it and for  
helping me with the figures in this thesis.

I would also like to thank the Natural Science and  
Engineering Research Council for providing financial  
support to my supervisor for this work and McMaster  
University for providing me with financial assistance.

## Table of Contents

Chapter	Page
1. Introduction	1
2. Nuclear Theory	9
2.1 Introduction	9
2.2 Nuclear Shell Theory	9
2.3 $^{134}\text{Cs}$ Shell Model Considerations	15
2.4 Nuclear Reactions	17
2.4.1 Distorted Wave Born Approximation	19
2.4.2 Spectroscopic Factors	23
2.5 Electromagnetic Transitions	26
3. The $^{133}\text{Cs}(d,p)^{134}\text{Cs}$ Reaction	31
3.1 Introduction	31
3.2 Experimental Set-up	32
3.3 Data Analysis	35
4. The $^{135}\text{Ba}(t,\alpha)^{134}\text{Cs}$ Reaction	47
4.1 Introduction	47
4.2 Experimental Set-up	48
4.3 Data Analysis	55

## Table of Contents (continued)

Chapter	Page
5. $\gamma$ -ray Studies	65
5.1 Introduction	65
5.2 Experimental Set-up	67
5.2.1 The $^{133}\text{Cs}(d,p\gamma)^{134}\text{Cs}$ Reaction	67
5.2.2 The $^{130}\text{Te}(^7\text{Li},3n)^{134}\text{Cs}$ Reaction	72
5.3 Data Analysis	75
5.3.1 The $^{133}\text{Cs}(d,p\gamma)^{134}\text{Cs}$ Reaction	75
5.3.1.1 Singles $\gamma$ -ray Measurements	76
5.3.1.2 Coincidence Measurements	87
5.3.2 $^{130}\text{Te}(^7\text{Li},3n)^{134}\text{Cs}$ Reaction	90
5.3.2.1 Decay Spectrum	93
5.3.2.2 Excitation Functions	96
5.3.2.3 Coincidence Measurements	98
5.3.2.4 Singles Measurements	98
6. Discussion and Interpretation	101
6.1 Introduction	101
6.2 Energy Level Scheme	102
6.3 Additional Levels in $(n,\gamma)$ Level Scheme	145
6.4 Shell Model Configurations in $^{134}\text{Cs}$	147
6.5 Summary	152

Table of Contents (continued)

Chapter	Page
Bibliography	156
Appendix A	161
Appendix B	166

## List of Tables

Table	Page
3.1 Optical Model Parameters for the $^{133}\text{Cs}(d,p)^{134}\text{Cs}$ Reaction at 12 MeV	41
3.2 Energy Levels, $l_n$ -values and Spectroscopic Factors for the (d,p) Reaction at 12 MeV	44
3.3 Centroid Energies of $^{133}\text{Xe}$ , $^{135}\text{Ba}$ and $^{134}\text{Cs}$ for $l_n = 0, 2$ and $5$	46a
4.1 Isotopic Composition of the $^{135}\text{BaO}$ Target	49
4.2 Optical Model Parameters for the $^{135}\text{Ba}(t,\alpha)^{134}\text{Cs}$ Reaction at 15 MeV	56
4.3 Energy Levels, $l_p$ -values and Spectroscopic Factors for the (t, $\alpha$ ) Reaction at 15 MeV	59
4.4 Centroid Energies of $^{137}\text{Cs}$ , $^{134}\text{Cs}$ and $^{139}\text{La}$ for $l_p = 2$ and $4$	64
5.1 Isotopic Composition of the $^{130}\text{TeO}$ Target	73
5.2 $\gamma$ -ray Energies and Relative Yields in the ( $^{133}\text{Cs} + d$ ) Reactions at 12 MeV	80
5.3 $\gamma$ -ray Gates and Coincident $\gamma$ -rays for $^{134}\text{Cs}$	89
5.4 Residual Activity in $^{130}\text{Te}$ Target	94
5.5 $\gamma$ -ray Gates and Coincident $\gamma$ -rays $^{134}\text{Cs}$	100

List of Tables (continued)

Table	Page
6.1 Branching Ratios for the $\gamma$ -ray Transitions.	119
A-1 Differential Cross-Sections from $^{133}\text{Cs}(d,p)$ Reaction	162
B-1 Differential Cross-Sections from $^{135}\text{Ba}(t,\alpha)$ Reaction	167

## List of Figures

Figure	Page
1.1 Level scheme of Alexeev et al. (1975)	4
3.1 $^{133}\text{Cs}(d,p)$ particle spectrum at $40^\circ$	39
3.2 Angular distributions and the DWBA fits for the levels populated in the $^{133}\text{Cs}(d,p)$ reaction	43
4.1 $^{135}\text{Ba}(t,\alpha)$ reaction spectrum at $15^\circ$	54
4.2 Angular distributions and the DWBA fits for the levels populated in the $^{135}\text{Ba}(t,\alpha)$ reaction	57
4.3 Angular distributions for the first two states in $^{137}\text{Cs}$	62
5.1 Singles $\gamma$ -ray spectrum from ( $^{133}\text{Cs} + d$ ) reaction at 12 MeV	77
5.2 Coincidence spectra from the $^{133}\text{Cs}(d,p\gamma)$ reaction	91
5.3 Decay spectrum of the $^{130}\text{Te}$ target	95
5.4 Excitation functions for the 157, 205 and 295 keV lines in the ( $^{130}\text{Te} + ^7\text{Li}$ ) reaction	97
5.5 Coincidence spectra from the $^{130}\text{Te}(^7\text{Li},3n)$ reaction	99

List of Figures (continued)

Figure	Page
6.1 Level scheme from $(n, \gamma)$ study	103
6.2 Level scheme from the present study	106

## Introduction

The nuclear force has been a subject of study since the discovery of the neutron, fifty years ago. To date, a complete picture of the nuclear force has not been formulated. Simplified models of the nucleus are used to explain and understand the results of experimental studies. One of the most successful of these models is the nuclear shell model.

The nuclear shell model has been most successful in describing the structure of even-even, odd A and lower mass odd-odd nuclei. Full calculations are more difficult and restrictions must be imposed to allow the calculations to be performed for heavier odd-odd nuclei and nuclei far from the closed shells. One approach to shell model calculations makes use of a phenomenological effective proton-neutron interaction. The parameters describing the effective interaction are obtained from fits to experimental level energies. The study of the odd-odd nuclei is significant since the low-lying energy levels in these nuclei involve the coupling of a proton to a neutron. As more experimental information becomes available, the shell model calculations can be extended to nuclei of higher mass and further from the closed

shells.

The  $^{134}\text{Cs}$  nucleus has fifty-five protons, five more than the closed shell at  $Z=50$  and seventy-nine neutrons, three short of the closed shell at  $N=82$ . Many of the low-lying levels of this nucleus should be describable in terms of simple proton-neutron shell model configurations.

$^{134}\text{Cs}$  is only one of the odd-odd  $N=79$  nuclei. The others are  $^{130}\text{Sb}$ ,  $^{132}\text{I}$ ,  $^{136}\text{La}$ ,  $^{138}\text{Pr}$ ,  $^{140}\text{Pm}$  and  $^{142}\text{Eu}$ . The  $^{130}\text{Sb}$  (Nunnally and Loveland, 1977) and  $^{132}\text{I}$  (Fransson et al., 1968 and Yousif et al., 1981) nuclei have been studied via beta decay. Electron capture studies leading to  $^{138}\text{Pr}$  (Bultsev et al., 1974) and  $^{140}\text{Pm}$  (Westgaard et al., 1973) also have been carried out. The decay of  $^{136\text{m}}\text{La}$  was studied by Gritsyna et al. (1966) and Goncharov et al. (1977). The levels of  $^{136}\text{La}$  were examined in the  $^{135}\text{Ba}(^3\text{He},d)$  and  $^{135}\text{Ba}(\alpha,t)$  reactions (Khan, 1977). The  $\gamma$ -ray transitions in  $^{136}\text{La}$  were studied in the  $^{136}\text{Ba}(p,n)$  reaction (Summers-Gill and Oluwole, 1978). The decay of  $^{136\text{m}}\text{La}$  has also been studied in the  $^{133}\text{Cs}(\alpha,n)$  and  $^{136}\text{Ba}(p,n)$  reactions (Summers-Gill et al., 1980).

Experimental studies have also been done on  $^{134}\text{Cs}$ . The spins of the ground state and 2.9 hour

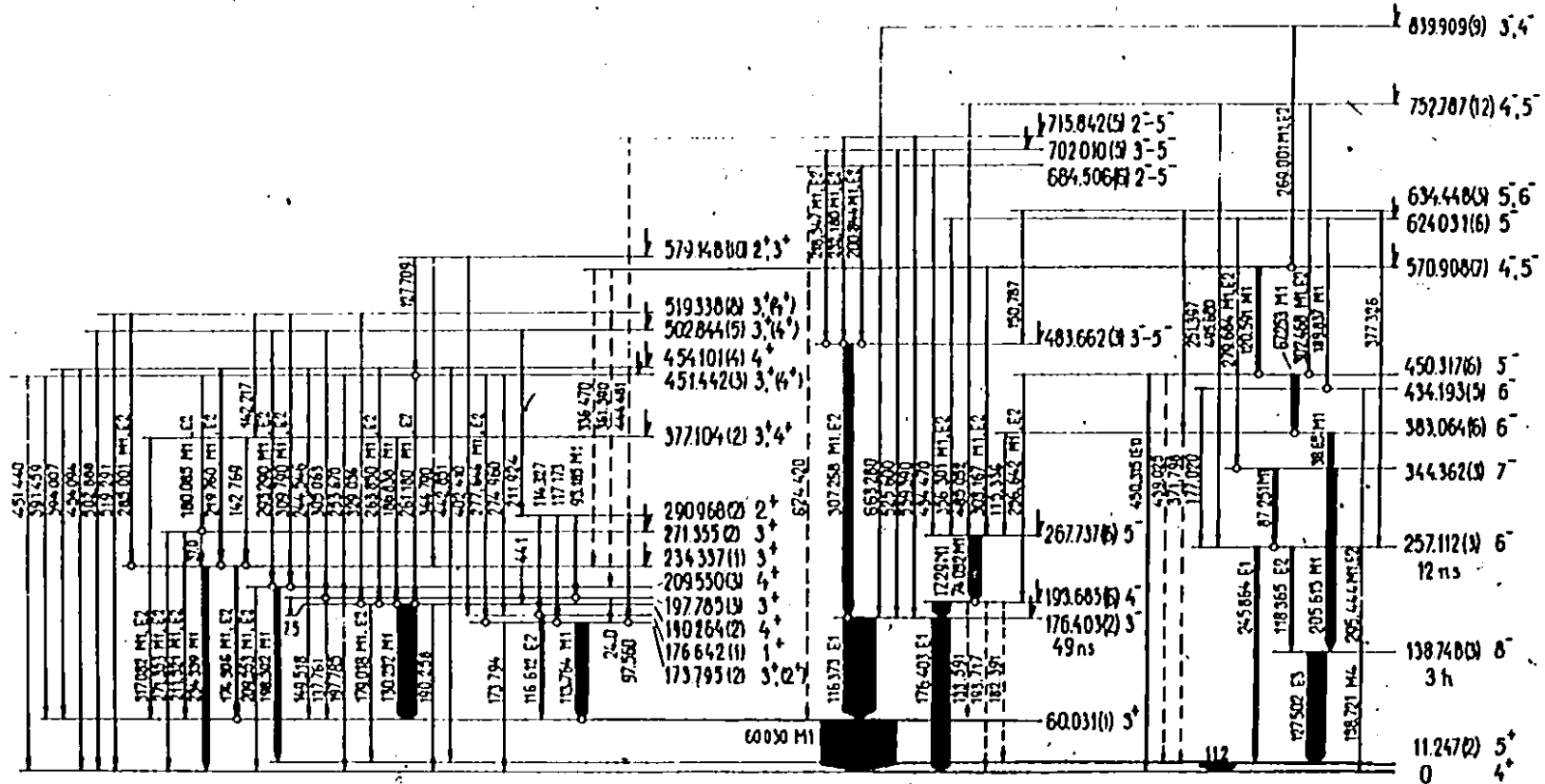
isomer were determined in atomic beam studies (Fuller 1976). Sunyar et al. (1954) studied the decay of  $^{134m}\text{Cs}$ . The 2.9 hour isomer at 138 keV decays by two  $\gamma$ -ray transitions, 127.5 and 138.7 keV. The 127.5 keV transition is followed by an 11.2 keV transition to the ground state. Sunyar et al. determined the multipolarities for the three transitions and deduced the spin of the 11 keV state to be  $5^+$ .

A number of thermal neutron capture studies have been done. The high energy capture  $\gamma$ -rays were measured by Archer et al. (1966) and Berestovoi et al. (1968). Archer et al. also measured some low energy transitions in coincidence with the capture  $\gamma$ -rays.

Alexeev et al. (1975) conducted a detailed study of  $^{134}\text{Cs}$  with the  $^{133}\text{Cs}(n,\gamma)$  reaction. A bent crystal spectrometer provided very precise determinations of the  $\gamma$ -ray energies. Internal conversion electron measurements were made to determine the transition multipolarities for many of the  $\gamma$ -rays. Gamma-gamma coincidence measurements were also made. These data were used to deduce the energy level scheme depicted in figure 1.1. The transition multipolarities provided the parities for the energy levels. The ordering of the levels and the placement of the  $\gamma$ -ray transitions were based on the  $\gamma$ - $\gamma$  coincidence,  $\gamma$ -ray intensity and  $\gamma$ -ray energy data. Spin assignments for the levels were deduced from the

Figure 1.1

The  $^{134}\text{Cs}$  level scheme of Alexeev et al. (reproduced from Nucl. Phys. A248, 249 (1975)). A circle at the end of the transition means that the coincidences between this transition and the low-lying ones have been used for constructing the scheme. Dashed lines are used to indicate energetically possible transitions (for which multipolarities have not been determined) between opposite parity levels. Dots are used to mark transitions which were not found but which are necessary to explain the coincidences obtained.



POPULATED BY PRIMARY TRANSITIONS

116 Cs 19

multipolarities of the transitions placed in the scheme.

Alexeev et al. (1978) have also run a limited shell model calculation to determine the energies of the members of the  $[\pi g_{7/2}, (\nu h_{11/2})^{-1}]$  and  $[\pi d_{5/2}, (\nu h_{11/2})^{-1}]$  multiplets. After apparent success with the levels of  $^{122}\text{Sb}$ , they interpreted a number of the negative parity states in  $^{134}\text{Cs}$  in terms of the p-n multiplets from a comparison of the calculated and experimental level energies.

Recently, a new review of the  $A = 134$  nuclei was published by Sergeenkov and Sigalov (1981). Many of the spin assignments made by Alexeev et al. (1975) were not adopted by the reviewers. The p-n configurations assigned by Alexeev et al. (1978) were adopted by the reviewers. There appear to be numerous misprints in the review article, so the present study makes reference to the original papers rather than the review article.

The present study was initiated to gain more information about the energy levels in  $^{134}\text{Cs}$  and to try to determine the nature of the levels in terms of the shell model. A number of reactions can be used to populate the energy levels of  $^{134}\text{Cs}$ . Three single particle transfer reactions were considered,  $^{133}\text{Cs}(d,p)$ ,  $^{135}\text{Ba}(t,\alpha)$ , and  $^{135}\text{Cs}(d,t)$ . The  $(d,p)$  and  $(d,t)$  reactions involve neutron transfers to populate the  $^{134}\text{Cs}$  nucleus. These reactions provide an insight into the neutron hole

contributions to the p-n configurations for the levels. The (t, $\alpha$ ) reaction transfers a proton from the target to the outgoing particle. This reaction gives information on the proton contributions to the p-n configurations.

Only two of these single particle transfer reactions were used to study the levels of  $^{134}\text{Cs}$ . Enriched  $^{135}\text{Cs}$  target material was not available. Both  $^{135}\text{Cs}$  and  $^{137}\text{Cs}$  are produced in uranium fission reactions. It is necessary to separate the two isotopes. Unfortunately, both are radioactive, with half-lives of  $2.3 \times 10^6$  years for  $^{135}\text{Cs}$  and 30.2 years for  $^{137}\text{Cs}$ . In separating the isotopes, the apparatus would become contaminated with  $^{137}\text{Cs}$ , so no one was willing to provide us with samples of the enriched  $^{135}\text{Cs}$  isotope. The (d,t) experiment could not be performed with the unenriched material since the energy levels of  $^{136}\text{Cs}$  from the  $^{137}\text{Cs}(d,t)$  reaction are not known and the triton groups from this reaction overlap the triton groups from the  $^{135}\text{Cs}(d,t)$  reaction. The Q-values were determined from the atomic mass tabulation of Wapstra (1977) to be -2.01 and -2.57 MeV for the  $^{137}\text{Cs}(d,t)$  and the  $^{135}\text{Cs}(d,t)$  reactions respectively. The levels of  $^{136}\text{Cs}$  would completely mask the levels of  $^{134}\text{Cs}$  since the ground state of  $^{134}\text{Cs}$  would appear at about 560 keV with respect to the ground state of  $^{136}\text{Cs}$ .

The levels of  $^{134}\text{Cs}$  were also examined via two

$\gamma$ -ray spectroscopy experiments  $^{133}\text{Cs}(d,p\gamma)$  and  $^{130}\text{Te}(^7\text{Li},3n\gamma)$ : Both singles and coincidence  $\gamma$ -ray data were collected. The  $\gamma$ -ray data from the  $(d,p\gamma)$  experiment greatly augmented the particle spectroscopy data. The  $(d,p)$   $\gamma$ -ray data provided information about the decay modes of the levels populated in the  $(d,p)$  particle spectroscopy experiment and revealed some levels which were not directly populated.

The  $^{130}\text{Te}(^7\text{Li},3n)$  reaction was performed in the hope of finding some levels of higher spin which would not be populated by the  $(d,p)$  reaction. The  $^7\text{Li}$  ion is capable of transferring more angular momentum into the nucleus. Unfortunately, this reaction did not prove as useful as was expected. Perhaps the reason for this is that inappropriate bombarding energies were selected for the experiment.

Another reaction,  $^{134}\text{Xe}(p,n\gamma)$ , was considered as a means of investigating  $^{134}\text{Cs}$ . It was possible to obtain target material that was enriched in  $^{134}\text{Xe}$  but but it would have higher abundances of other xenon isotopes. This target material was very expensive. The  $\gamma$ -ray spectra from protons on the xenon target would contain lines from several cesium nuclei, such as  $^{132}\text{Cs}$ ,  $^{134}\text{Cs}$  and  $^{136}\text{Cs}$ . Since there is very little information available on the levels of these cesium nuclei, it would be difficult to identify the  $\gamma$ -rays. The  $\gamma$ -ray spectra

would have many close lying lines since these nuclei have high level density and similar level structures. It was doubtful whether useful information on the levels of  $^{134}\text{Cs}$  could be learned from this target. Since the high expense for the target could not be well justified the reaction was not tried.

The present study provided data which are consistent with the placement and spin assignments of many energy levels in the level scheme shown in figure 1.1. Additional levels were also found and placed in the scheme (see figure 6.2). Shell model configurations are identified for some of the low-lying levels. A discussion of the new level scheme and how it differs from the scheme of Alexeev et al. is presented in chapter 6. This follows a description of experiments performed and the data obtained in the present study.

## Nuclear Theory

### 2.1 Introduction

Understandings of the nuclear shell model, the single particle transfer reactions and the electromagnetic transitions are crucial to the analysis and interpretation of the experimental data on the nuclear structure of  $^{134}\text{Cs}$ . For this purpose a general description of the theoretical background is provided. Detailed mathematical descriptions of the shell model already exist (eg. Bertsch, 1972 and Brussaard and Glaudemans, 1978). Similarly, many works describing the mathematical details of direct reactions have been published (eg. Satchler, 1980). The electromagnetic interaction is treated in many works (eg. Siegbahn, 1965, Preston, 1962 and Hamilton; 1978). This chapter gives only a discussion of the basic assumptions and approximations used in the models and provides the formulae pertinent to the analysis and interpretation of the data.

### 2.2 Nuclear Shell Theory

The nuclear shell model has been a very useful tool in the study of the structure of nuclei. This model has helped to explain many nuclear properties such as spin, magnetic moment, and the ordering of the energy

levels.

The shell model is based on the assumption that in first order the nucleons move independently in a spherically symmetric average potential. The three dimensional isotropic harmonic oscillator potential has been used extensively to predict the properties of even-even and odd-A nuclei. The shell closures, i.e. magic numbers, at nucleon numbers 2, 8, 20, 28, 50, 82, and 126 are obtained by a modified harmonic oscillator potential - addition of a strong spin orbit potential and a flattening of the potential well bottom.

In filling the shell model orbitals, the protons and neutrons must obey the Pauli exclusion principle. It is expected that pairs of like nucleons occupy the same level by coupling with their spins antiparallel. As each pair of like nucleons couple their single particle angular momenta,  $j$ -values, to give zero resultant angular momentum, the ground state spin of odd-A nuclei must be given by the spin of the last unpaired nucleon. Also the ground state spin of all even-even nuclei must be zero. Thus, the model assumes  $j$ - $j$  coupling and that  $j$  is a valid quantum number. The assumption that  $j$  is a good quantum number can sometimes be relaxed, when the particle state is taken as the superposition of several  $(n, j)$ -states that are close in energy.

This simple form of the shell model works well for predicting the ground state properties of the even-even and odd-A nuclei. It does not predict anything for the properties of the odd-odd nuclei as there is no way to determine which member of the multiplet arising from the coupling of the spins of the nucleons has the lowest energy. This inadequacy in the model is due to the fact that this extreme single particle model assumes no correlations between unlike nucleons. That is, the protons and neutrons are assumed not to interact. It is assumed that the protons (neutrons) fill orbitals independent of the number of neutrons (protons) in the nucleus. The shell model can be made more realistic by considering the nucleons in closed shells to form an inert core and introducing a residual interaction between the nucleons in the unfilled orbitals. The predictions for the ground state properties of even-even nuclei are not altered by these changes to the shell model.

Experimental studies of odd-odd nuclei just beyond closed cores indicate that the residual interaction is predominantly a short range attractive force. Anti-parallel and parallel angular momentum couplings are lowered more in energy than couplings to an in between value of  $J$ . A more detailed description of the residual interaction may be found in Preston (1962).

The Nordheim (1950) rules, as modified by Bren-

nan and Bernstein (1960), summarize the effect of the residual interaction on the spin multiplet formed by coupling the spins of the odd proton and the odd neutron. For particle-particle or hole-hole multiplets, the spin of the lowest-lying level of the multiplet is:

$$J_1 - j_2, \text{ if } N \text{ is odd, and}$$

$$J_1 + j_2; \text{ if } N \text{ is even,}$$

where  $N = j_1 + j_2 + l_1 + l_2$  is the Nordheim number,  $j_1$  and  $j_2$  are the spins of the two particles (holes) and  $l_1$  and  $l_2$  are the orbital angular momenta of the particles (holes). For particle-hole multiplets, the spin of the lowest-lying level of the multiplet is  $j_1 + j_2 - 1$ . The modified Nordheim rules have been very successful in predicting the ground state spins of nuclei whose configurations contain only particles or holes (Brennan and Bernstein, 1960). The rule which predicts the ground state spins of nuclei whose configurations are particle-hole multiplets is less successful. The Nordheim rules appear to lose their validity when the configurations are not lowest seniority. The seniority quantum number is the number of nucleons remaining after the removal of all pairs of nucleons coupled to  $J = 0$  and  $T = 1$ .

The properties of many nuclei have been successfully described by shell model calculations in recent years, especially when the number of particles involved is not large (eg. Wong, 1966). There are several

methods for treating the residual interaction in these calculations. In one approach, the free nucleon-nucleon interaction is assumed for the residual interaction and the nuclear matrix elements are calculated from the reaction matrix (Kuo and Brown, 1966, 1967). Another approach treats the interaction phenomenologically. Several forms of the p-n residual interaction have been employed in the calculations, e.g. surface delta interaction or gaussian interaction. The form of the surface delta interaction potential (Green and Moszkowski, 1965) is:

$$V_{ij}^{\text{SDI}} = -4\pi A_T \delta(\alpha_{ij}) \delta(r_i - R) \delta(r_j - R)$$

where  $\alpha_{ij}$  is the angle between the position vectors of the interacting nucleons and  $R$  is the nuclear radius. The isospin dependent strengths,  $A_T$ , are found by fitting two body surface delta interaction matrix elements to the experimental data over a range of mass numbers.

The use of a phenomenological interaction has made it easier to perform shell model calculations where experimental data are available. Many of the restrictions that existed because matrices were limited in size have been removed in the light nuclei. An effective Hamiltonian, based on a surface delta interaction, was determined by Koops and Glaudemans (1977). Many calculations on (fp) shell nuclei have been done with this Hamiltonian. The level energies in Ni and Cu nuclei

were least squares fitted to determine the Hamiltonian. The shell model calculations of van Hienen et al. (1976) produced good agreements with the experimental spectroscopic factors in the Zn isotopes. The use of a renormalized effective charge in the calculations well reproduced the experimental B(E2) values in the Zn isotopes. More recently, Shikata et al. (1981) successfully described the M1 and E2 properties of many Zn, Ga and Ge nuclei with the same effective Hamiltonian.

When the mass is larger and more particles and holes are involved the calculations become more difficult. Restrictions are needed because the matrices involved are much larger than in the (fp) shell. Several shell model calculations have been performed in the light rare earth region. Wildenthal (1969) performed extensive calculations on the N = 82 nuclei, for A = 138-145. Macphail (1973) ran lowest seniority shell model calculations on the odd-odd N = 83 nuclei,  $^{140}\text{La}$ ,  $^{142}\text{Pr}$  and  $^{144}\text{Pm}$ , with good success. Calculations have also been done on the odd-odd N = 81 nuclei,  $^{138}\text{La}$  and  $^{140}\text{Pr}$ , by Islam (1975) and Helton (1973).

Recently, Alexeev et al. (1978) performed shell model calculations on  $^{122}\text{Sb}$  and  $^{134}\text{Cs}$ . They used a residual interaction of the form:

$$V = (V_0 + V_1 \tau_s) e^{(-r^2/r_0^2)}$$

where  $\tau_S = 1/4[1 - (\sigma_p \cdot \sigma_n)]$  is the singlet operator,  $V'_0$  is the renormalized parameter of Wigner forces,  $V_1$  is the parameter of the singlet force, which is not renormalized,  $r$  is the relative distance between the quasi-particles and  $r_0$  is the range parameter. The force parameters in the residual interaction were obtained from fits to the levels of the particle-hole configurations. Experimental data from (d,p) and (d,t) reactions were available to identify the configurations when Alexeev et al. (1978) made the comparison for  $^{122}\text{Sb}$ . The authors reported good agreement between the calculated and experimental parity levels for  $^{122}\text{Sb}$ . The calculated and experimental branching ratios were found to agree to about a factor of two. However, no particle transfer reaction data were available for  $^{134}\text{Cs}$ , so they simply chose configurations to suit their conscience. Configuration assignments to ten negative parity states in  $^{134}\text{Cs}$  were made from a comparison of the calculated and experimental level energies.

### 2.3 $^{134}\text{Cs}$ Shell Model Considerations

The levels in  $^{134}\text{Cs}$  are expected to originate from the p-n configurations involving the five valence protons and the three neutron holes. The neighboring odd-Z  $^{133}\text{Cs}$  nucleus has a  $7/2^+$  ground state ( $1g_{7/2}$

proton) and two close lying  $5/2^+$  states at 81 and 161 keV (Lederer and Shirley, 1978). Lowest seniority shell model considerations predict only one  $5/2^+$  state due to a  $2d_{5/2}$  proton. Low-lying states at 384 ( $3/2^+$ ), 437 ( $1/2^+$ ) and 605 ( $11/2^-$ ) keV are probably due to protons in the  $2d_{3/2}$ ,  $3s_{1/2}$  and  $1h_{11/2}$  orbitals, respectively.

The neutron orbitals are  $2d_{3/2}$ ,  $3s_{1/2}$  and  $1h_{11/2}$  as will be explained in section 3.1.

In the lowest seniority scheme, the levels of  $^{134}\text{Cs}$  arise from the odd proton coupling to the odd neutron. The positive parity states arising from these couplings are:

$$\begin{aligned}
 [\pi g_{7/2}, (v d_{3/2})^{-1}] &= 5^+, 4^+, 3^+, 2^+ \\
 [\pi g_{7/2}, (v s_{1/2})^{-1}] &= 4^+, 3^+ \\
 [\pi d_{5/2}, (v d_{3/2})^{-1}] &= 4^+, 3^+, 2^+, 1^+ \\
 [\pi d_{5/2}, (v s_{1/2})^{-1}] &= 3^+, 2^+ \\
 [\pi d_{3/2}, (v d_{3/2})^{-1}] &= 3^+, 2^+, 1^+, 0^+ \\
 [\pi d_{3/2}, (v s_{1/2})^{-1}] &= 2^+, 1^+ \\
 [\pi s_{1/2}, (v d_{3/2})^{-1}] &= 3^+, 2^+, 1^+, 0^+ \\
 [\pi s_{1/2}, (v s_{1/2})^{-1}] &= 1^+, 0^+ \\
 [\pi h_{11/2}, (v h_{11/2})^{-1}] &= 11^+, 10^+, 9^+, 8^+, 7^+, 6^+, \\
 &5^+, 4^+, 3^+, 2^+, 1^+, 0^+.
 \end{aligned}$$

The negative parity states are:

$$\begin{aligned}
 [\pi g_{7/2}, (v h_{11/2})^{-1}] &= 9^-, 8^-, 7^-, 6^-, 5^-, 4^-, 3^-, 2^- \\
 [\pi d_{5/2}, (v h_{11/2})^{-1}] &= 8^-, 7^-, 6^-, 5^-, 4^-, 3^- \\
 [\pi d_{3/2}, (v h_{11/2})^{-1}] &= 7^-, 6^-, 5^-, 4^-
 \end{aligned}$$

$$[\pi s_{1/2}, (\nu h_{11/2})^{-1}] - 6^-, 5^-$$

$$[\pi h_{11/2}, (\nu d_{3/2})^{-1}] - 7^-, 6^-, 5^-, 4^-$$

$$[\pi h_{11/2}, (\nu s_{1/2})^{-1}] - 6^-, 5^-.$$

The members of the  $[\pi g_{7/2}, (\nu d_{3/2})^{-1}]$  configuration are expected to be among the lowest-lying levels in  $^{134}\text{Cs}$ . The lowest-lying negative parity states are expected to arise from the  $[\pi g_{7/2}, (\nu h_{11/2})^{-1}]$  configuration. The states involving the  $d_{5/2}$  neutron should also be found at relatively low excitation since the  $5/2^+$  state is very near the  $7/2^+$  state in  $^{133}\text{Cs}$ .

#### 2.4 Nuclear Reactions

Nuclear reactions can be divided into two categories, direct reactions and compound nucleus reactions. Compound nucleus reactions are characterized by resonances whose widths are of the order of a few electron volts. Associated with these narrow energy resonances, the time scale on which the processes occur are of the order of  $10^{-16}$  sec. In compound nucleus reactions, the energy of the incident projectile is distributed over the whole nucleus. Many different nuclear configurations may be excited and decay back to other configurations. Thus, the initial and final states are generally uncorrelated as the final state has "forgotten" the origins of its formation. The differential cross-sections for compound nucleus processes are usually non-isotro-

pic. If there are no interference effects, the cross-sections display a fore and aft symmetry. Large fluctuations in the cross-section may occur as the incident projectile energy is varied.

Direct nuclear processes occur on much shorter time scales, of the order of  $10^{-22}$  sec. The associated energy resonances are correspondingly much broader, of the order of a few million electron volts. In the direct reaction, the incident projectile interacts with only a few nucleons of the target. Thus, there is a strong correlation between the initial and final states of the struck nucleus. The reaction cross-sections vary smoothly with the incident projectile energy. The fore and aft symmetry of the compound nucleus cross-sections is missing. The angular distributions display oscillatory patterns akin to the diffraction patterns observed in optical phenomena. The shapes of the angular distributions depend upon the orbital angular momentum of the transferred particles. Analysis of the angular distributions provides information on the  $g$ -values of the transferred nucleons and the spectroscopic strengths for the levels populated. The spectroscopic strength gives a measure of the overlap of the final nuclear state with the target nuclear state and the transferred particle occupying a shell model state.

Single particle transfer reactions, stripping

and pick-up reactions, have been used extensively to obtain nuclear structure information. The stripping reaction transfers a nucleon from the incident projectile to the target nucleus and the pick-up reaction transfers a nucleon from the target to the incident projectile.

#### 2.4.1 Distorted Wave Born Approximation

The DWBA model is very useful in the analysis of direct reaction experiments. Many detailed descriptions of the DWBA model have been written (e.g. Satchler, 1980, Austern, 1970 and Jackson, 1970), so it is not necessary to present more than a brief description of the model and its basic assumptions in this work. To treat the direct reaction process exactly requires knowledge of the exact nature of the nuclear force. Also full anti-symmetrized many-body wavefunctions and many-body matrix elements present formidable complexities to the calculations. Some approximations and assumptions are required to perform the calculations. These approximations reduce the many-body quantities to manageable proportions. The approximations are accomplished with the use of the optical model.

For a reaction  $A(a,b)B$ , the transition amplitude has the form:

$$T = \int \psi_b^{(-)*} \langle \phi_B | V_{bx} + V_{bA} - U_b | \phi_{aA}^{(+)} \rangle d^3r_x d^3r_b$$

where the subscript,  $x$ , denotes the transferred particle.  $\psi_b^{(-)}$  is the outgoing wave and  $\phi_B$  is the wavefunction for the final state.  $\psi_{aA}^{(+)}$  is a wavefunction involving the target,  $A$ , and the incident projectile,  $a$ . It is an exact solution to the problem and contains information on all of the possible reaction processes, such as elastic and inelastic scattering and particle transfer.  $V_{bx}$  describes the interaction between the outgoing and transferred particles.  $V_{bA}$  denotes the interaction between the outgoing particle and the target nucleus.  $U_b$  represents a distorting potential. The transmission amplitude used in most DWBA calculations, such as the computer code, DWUCK4 (Kunz, 1974), has the form:

$$T = \int \psi_b^{(-)*} \langle \phi_B | V_{bx}(\underline{r}) | \phi_A \phi_0 \rangle \psi_a^{(+)} d^3r_x d^3r_b$$

where  $\phi_A$  is the target wavefunction,  $\phi_0$  is a wavefunction for the projectile (internal). In this transition amplitude for DWBA calculations, the exact wavefunction has been replaced by a product of the wavefunctions of the target, the projectile ground state and a distorted wave to reproduce the elastic scattering data. Also the interactions represented by  $V_{bA}$  and  $U_b$  have been omitted because the interactions are approximately equal, so  $V_{bA} - U_b = 0$ .

It is assumed that the single particle transfer reaction is much weaker than elastic scattering. Single

particle transfer reactions are treated as first order perturbations of the elastic scattering process. Usually this is the case.

The cross-sections are calculated with an optical model potential. This requires that the distorted waves be wavefunctions of the optical potential. The form of the optical potential which is used in the calculations is:

$$V(r) = V_c + V f(X_R) + i[W f(X_I) + W_D (df(X_I)/dX_I)] - 4(V_{SO}/r)(df(X_{SO})/X_{SO})(L \cdot S)$$

$$f(X_i) = 1/[1 + e^{X_i}]$$

$$X_i = (r - r_{oi} A^{1/3})/a_i \quad (i = R \text{ for real, } I \text{ for imaginary and so for spin orbit})$$

where  $V_c$  is a Coulomb potential for a spherical charge distribution of radius  $r_{oc} A^{1/3}$ ,

$V$  is the real well depth for a volume Woods-Saxon potential,

$W$  is the imaginary well depth for a volume Woods-Saxon potential,

$W_D$  is the imaginary depth for a surface Woods-Saxon potential,

$V_{SO}$  is the well depth for a spin orbit potential,

$r_{oi}$  is the potential well radius parameter,

$a_i$  is the potential well diffuseness and

A is the mass number of the target.

The parameters of the optical model are selected to reproduce the elastic scattering cross-sections. The elastic scattering data determine the wavefunctions of the projectile outside of the region of the nucleus. Any wavefunctions with the same phase shifts at large distances from the nucleus will reproduce the elastic cross-sections. However, these wavefunctions can give very different DWBA reaction cross-sections. Thus, these ambiguities in the optical model parameters lead to uncertainties in the DWBA cross-sections.

The experimental cross-sections, for the stripping reaction that transfers a nucleon to the  $(n\ell j)$  orbital of the target nucleus, is related to the distorted wave Born approximation (DWBA) cross-section by:

$$\frac{d\sigma_{n\ell j}^{\text{exp}}}{d\Omega} = \frac{N}{2j+1} S_{n\ell j}(J_B) \frac{2J_B+1}{2J_A+1} \frac{d\sigma_{n\ell j}^{\text{DWBA}}}{d\Omega}$$

where  $J_A$  is the spin of the target,  $J_B$  is the spin of the final state, and  $j$  is the spin of the transferred nucleon.  $S_{n\ell j}(J_B)$  is the spectroscopic factor for the final state.  $N$  is a normalization factor which depends upon the types of incoming and outgoing particles involved in the reaction (1.55 for the  $(d,p)$  reaction). The corresponding relationship for the pick-up reaction is:

$$\frac{d\sigma_{\text{exp}}}{d\Omega_{nlj}} = \frac{N}{2j+1} S_{nlj}(J_B) \frac{d\hat{\sigma}_{\text{DWBA}}}{d\Omega_{nlj}}$$

The normalization factor for the  $(t, \alpha)$  reaction is usually taken as 23 although the best value is somewhat uncertain.

For this work, DWBA calculations were performed with the computer code, DWUCK4 (Kunz, 1974). The computer code uses a zero range approximation. The 6-fold integration for the transition amplitude is reduced to 3-fold integration by assuming  $V_{bx}(\underline{r}) \rightarrow V_0(\underline{r})$  has zero range. Finite range effects are treated with a local energy approximation (Buttle and Goldfarb, 1964). The non-locality of the optical potential is also included in the computer code (Perey and Buck, 1962).

#### 2.4.2 Spectroscopic Factors

The spectroscopic factor contains all of the structure information. It is a measure of the single particle component of the final state. The spectroscopic factor represents the overlap of the final nuclear state and the initial nuclear state coupled to the transferred nucleon, i.e.

$$S = [ \langle \psi_i \otimes \psi_{tn} | \psi_f \rangle ]^2,$$

where  $\psi_i$ ,  $\psi_{tn}$ , and  $\psi_f$  are the wavefunctions of the target nucleus, the transferred nucleon, and the residual

nucleus respectively. The  $\otimes$  symbol represents the anti-symmetrized vector coupling of the two wavefunctions. The same spectroscopic factor appears in the pick-up and stripping reaction expressions relating the cross-sections. The pick-up reaction spectroscopic factor is identically equal to the stripping reaction spectroscopic factor since only the overlap of the initial and final wavefunctions is involved.

There are two useful sum rules that can be applied to the spectroscopic factors. The sum rules for stripping and pick-up reactions are:

$$\sum_{J_B} \frac{2J_B + 1}{2J_A + 1} S_{n\ell j}(J_B) = N_{\ell}^h \quad (\text{stripping})$$

$$\sum_{J_B} S_{n\ell j}(J_B) = N_{\ell}^p \quad (\text{pick-up})$$

where  $N_{\ell}^h$  is the number of holes in the orbital,  $n\ell j$ , in the target nucleus, and  $N_{\ell}^p$  is the number of particles in the orbital,  $n\ell j$ , in the target nucleus. It should be noted that both of these sum rules are independent of the spin of the final states as one experimentally measures  $((2J_B+1)/(2J_A+1))S_{n\ell j}$  in stripping reactions and the factor  $(2J_B+1)$  does not appear in the sum rule for pick-up reactions. The energy centroid for the levels with a particular  $(n\ell j)$ -value is given by:

$$E_{n\lambda j} = \frac{[\sum_{J_B} ((2J_B+1)/(2J_A+1)) S_{n\lambda j}(J_B) E(J_B)]}{[\sum_{J_B} ((2J_B+1)/(2J_A+1)) S_{n\lambda j}(J_B)]} \quad (\text{stripping})$$

$$E_{n\lambda j} \approx \frac{[\sum_{J_B} S_{n\lambda j}(J_B) E(J_B)]}{[\sum_{J_B} S_{n\lambda j}(J_B)]} \quad (\text{pick-up})$$

The  $^{134}\text{Cs}$  nucleus was populated in two separate single particle transfer reactions, the  $^{133}\text{Cs}(d,p)^{134}\text{Cs}$  and the  $^{135}\text{Ba}(t,\alpha)^{134}\text{Cs}$  reactions. The (d,p) reaction transfers a neutron from the incoming deuteron to the  $^{133}\text{Cs}$  target. The low-lying energy levels that are populated in the (d,p) reaction should originate from the coupling of the ground state proton configuration of the  $^{133}\text{Cs}$  target to the transferred neutron. The ground state of  $^{133}\text{Cs}$  is known to have spin  $7/2^+$  (Lederer and Shirley, 1978). It is believed, from nuclear shell model considerations, that this  $7/2^+$  ground state is due to a proton in the  $1g_{7/2}$  subshell. It is shown in section 3.1, that  $\lambda_n$ -values of 0, 2, and 5 corresponding to neutrons filling vacancies in the  $3s_{1/2}$ ,  $2d_{3/2}$ , and  $1h_{11/2}$  orbitals are expected in the (d,p) reaction. The spins of the levels resulting from the coupling of the odd ground state proton in the  $^{133}\text{Cs}$  target to the transferred neutron are:

$$[\pi g_{7/2}, (\nu s_{1/2})^{-1}] = 4^+, 3^+$$

$$[\pi g_{7/2}, (\nu d_{3/2})^{-1}] = 5^+, 4^+, 3^+, 2^+$$

$$[\pi g_{7/2}, (\nu h_{11/2})^{-1}] = 9^-, 8^-, 7^-, 6^-, 5^-, 4^-, 3^-, 2^-.$$

The  $(t, \alpha)$  reaction removes a proton from the odd-N nucleus  $^{135}\text{Ba}$ . The low-lying levels of  $^{134}\text{Cs}$  that are populated in this reaction are expected to result from the coupling of the ground state neutron hole configuration of  $^{135}\text{Ba}$  and the odd proton that remains when one proton is picked up. The ground state spin of the  $^{135}\text{Ba}$  target is  $3/2^+$ , which is expected to arise from a neutron hole in the  $2d_{3/2}$  neutron orbital. The discussion in section 4.1 shows that  $l_p$ -values of 2 and 4, corresponding to pulling out a proton from the  $2d_{5/2}$  or  $1g_{7/2}$  orbitals are expected for this reaction. The spins of the levels arising from the coupling of the odd ground state neutron hole in the  $^{135}\text{Ba}$  target to the transferred proton are:

$$[1g_{7/2}, (nd_{3/2})^{-1}] = 5^+, 4^+, 3^+, 2^+$$

$$[nd_{5/2}, (nd_{3/2})^{-1}] = 4^+, 3^+, 2^+, 1^+$$

Thus, not all of the configurations shown in section 2.3 are expected to be populated in these single particle transfer reactions.

There are four neutron holes in the  $^{133}\text{Cs}$  target so the total spectroscopic strength is expected to be four in the  $^{133}\text{Cs}(d, p)$  reaction. There are six valence protons in the  $^{135}\text{Ba}$  target so the total spectroscopic strength should be six in the  $^{135}\text{Ba}(t, \alpha)$  reaction.

## 2.5 Electromagnetic Transitions

The electromagnetic operators are well known and the electromagnetic interaction is well understood. The study of electromagnetic transitions between nuclear states can provide information on the spins and parities of the levels. The modes of electromagnetic transitions between levels place constraints on the possible spins of the levels.

Electromagnetic transitions between nuclear levels occur as electric or magnetic interactions. The electromagnetic operators governing these interactions are easily expressed in terms of spherical harmonics.

The nuclear structure information is contained in the matrix element of the initial state,  $|i\rangle$ , the appropriate electromagnetic operator,  $Q_{L\mu}^\sigma$ , and the final state,  $|f\rangle$ . These matrix elements are related to the transition probabilities in the following way:

$$T_{ij}(\sigma, L) = \frac{8\pi(L+1)}{L[(2L+1)!!!]^2} \left( \frac{1}{\lambda} \right) \left( \frac{\omega}{c} \right)^{2L+1} B(\sigma L, J_i \rightarrow J_f)$$

where  $\sigma$  is the type of radiation (electric or magnetic),  $L$  is the multipolarity of the transition and  $B(\sigma L, J_i \rightarrow J_f)$  is the reduced transition probability:

$$B(\sigma L, J_i \rightarrow J_f) = \frac{1}{(2J_i + 1)} \sum_{M_i, M_f} |\langle J_f M_f | Q_{L\mu}^\sigma | J_i M_i \rangle|^2.$$

The subscript,  $\mu (=M_i - M_f)$ , is the z-projection of the

angular momentum carried away by the photon. The transition probability assumes that the wavelength,  $2\pi c/\omega$ , of the photon is much larger than the nuclear dimension,  $R$ .

The transition probability is commonly expressed in terms of Weisskopf units. The transition probabilities for some low order multipoles are as follows:

$$1.50 \times 10^{14} A^{2/3} E_Y^3 \text{ sec}^{-1} \text{ for E1}$$

$$3.15 \times 10^{13} E_Y^3 \text{ sec}^{-1} \text{ for M1}$$

$$7.25 \times 10^7 A^{4/3} E_Y^5 \text{ sec}^{-1} \text{ for E2}$$

$$1.20 \times 10^8 A^{2/3} E_Y^5 \text{ sec}^{-1} \text{ for M2}$$

$$1.10 \times 10^2 A^2 E_Y^7 \text{ sec}^{-1} \text{ for E3}$$

where  $E_Y$  is the  $\gamma$ -ray energy in MeV and  $A$  is the mass number of the nucleus.

The probability of detecting prompt coincidence events between  $\gamma$ -rays feeding and de-exciting a state depends upon the lifetime of the fed state. The Weisskopf estimates of the transition probabilities show that the lower order multipoles are expected to dominate  $\gamma$ - $\gamma$  coincidence events since these multipoles usually have larger transition probabilities. However, transition probabilities may be enhanced or retarded from the Weisskopf estimates allowing higher order multipoles to compete with lower order multipoles. The mean life of a state is the inverse of the sum of the transition probabilities, so prompt coincidence events are fewer

for states with longer mean lives. Essentially no prompt coincidence events are detected for states with mean lives of the order of the coincidence resolving time since they are masked by the chance coincidence events.

Selection rules which govern the multipolarities of electromagnetic transitions between states are:

i) conservation of parity:

$$(\pi_i \pi_f) = (-)^L \text{ for electric transitions,}$$

$$(\pi_i \pi_f) = (-)^{L+1} \text{ for magnetic transitions,}$$

ii) conservation of angular momentum:

$$|J_i - J_f| \leq L \leq J_i + J_f .$$

These selection rules prevent electric and magnetic multipoles of the same order from competing with each other in a given transition. Additional selection rules arise from the application of different nuclear models.

Transition multipolarities are determined from internal conversion electron and  $\gamma$ -ray angular distribution measurements. The internal conversion coefficient is the ratio of the probability of electron emission to the probability of  $\gamma$ -ray emission. The conversion coefficient depends upon the multipolarity and the energy of the transition. In the  $A = 134$  mass region, the internal K-conversion coefficients for M1 and E2 transitions are similar for  $\gamma$ -ray energies between about 150 and 400 keV.

The angular distribution of the  $\gamma$ -ray transition is given by:

$$W(\theta) = A_0 + A_2 P_2(\cos \theta) + A_4 P_4(\cos \theta)$$

where  $W(\theta)$  is the detected yield of the  $\gamma$ -ray,

$P_{2,4}(\cos \theta)$  are Legendre polynomials,

$A_0, A_2, A_4$  are coefficients characterized by  $J_i, J_f$

and the transition multipolarity and

$\theta$  is the angle between the detector and the beam direction. When a nuclear state decays soon enough after the formation of the state that the nucleus does not undergo re-orientation in random atomic magnetic fields,  $A_2/A_0$  and  $A_4/A_0$  are close to their full theoretical values. Since there is anisotropy in the  $\gamma$ -radiation pattern, singles  $\gamma$ -ray yields are usually measured near  $125^\circ$  to the beam direction because  $P_2(\cos 125^\circ)$  is zero and  $A_4$  is small compared to  $A_2$ .

## The $^{133}\text{Cs}(d,p)^{134}\text{Cs}$ Reaction

### 3.1 Introduction

The single particle transfer reaction is known to be a useful tool for probing the structure of the nucleus. Both the stripping and pick-up reactions are widely used and well understood. These reactions provide information on the low-lying energy level structure of the resultant nucleus, the orbital angular momenta,  $l$ -values, of the transferred nucleon, and the spectroscopic strengths of the energy levels.

An examination of the neighbouring  $N = 79$ , even  $Z$  nuclei provides information concerning the nature of the levels expected to be populated by the  $(d,p)$  reaction. Since  $^{133}\text{Xe}$ ,  $^{134}\text{Cs}$  and  $^{135}\text{Ba}$  have the same number of neutrons, the same neutron orbitals should be occupied for the low-lying states. The low-lying states of  $^{133}\text{Xe}$  and  $^{135}\text{Ba}$  should arise from the odd neutron occupying shell model orbitals.

The ground states of  $^{133}\text{Xe}$  and  $^{135}\text{Ba}$  have a spin of  $3/2^+$  (Lederer and Shirley, 1978). The  $^{134}\text{Xe}(d,t)$  and  $^{134}\text{Ba}(d,p)$  experiments show that both ground states are strongly populated by  $l_n = 2$  neutron transfers (Schneid and Rosner, 1966 and von Ehrenstein et al., 1970). A

level with spin  $11/2^-$  is observed in  $^{133}\text{Xe}$  at 0.233 MeV and in  $^{135}\text{Ba}$  at 0.269 MeV. The  $^{134}\text{Xe}(d,t)$  experiment populates this level with an  $i_n$ -value of 5. Also a level with spin  $1/2^+$  occurs at 0.263 MeV in  $^{133}\text{Xe}$  while in  $^{135}\text{Ba}$  this level has an energy of 0.221 MeV. This spin  $1/2^+$  level is populated by an  $i_n$ -value of 0 in the neutron transfer experiments.

This shows that the  $3/2^+$  state in  $^{133}\text{Xe}$  and  $^{135}\text{Ba}$  originates from a  $2d_{3/2}$  neutron orbital in the shell model scheme. The  $11/2^-$  state would be identified as the  $1h_{11/2}$  neutron orbital and the  $1/2^+$  state would be the  $3s_{1/2}$  neutron orbital. The orbitals that are expected to be populated in the  $^{133}\text{Cs}(d,p)$  reaction are thus the  $2d_{3/2}$ ,  $3s_{1/2}$  and  $1h_{11/2}$  orbitals, corresponding to  $i_n$ -values of 2, 0 and 5, respectively.

### 3.2. Experimental Set-up

The targets used in the  $^{133}\text{Cs}(d,p)^{134}\text{Cs}$  experiment were made from  $\text{CsNO}_3$  deposited on carbon. Cesium has only one stable isotope. A chemically very pure sample was purchased from Alpha Division of Ventron Corporation. Since cesium compounds are highly soluble in water and generally very hygroscopic, the thin carbon backings were floated off from their glass slides and mounted on aluminum frames prior to depositing the  $\text{CsNO}_3$  on the backings. The cesium nitrate was heated in a

tantalum crucible and deposited on the carbon backings by vacuum evaporation. The nominal thicknesses of the target and backing were  $30 \mu\text{g}/\text{cm}^2$  and  $20 \mu\text{g}/\text{cm}^2$ , respectively.

The odd-odd nuclei in this mass region have high energy level densities. It is important to have as good energy resolution as possible. This requires a very stable monoenergetic beam of deuterons. The McMaster van de Graaff accelerator was used to provide such a beam of deuterons. The deuteron beam energy was 12.0 MeV. This choice of beam energy gave the deuterons enough energy to overcome the Coulomb barrier of the  $^{133}\text{Cs}$  nucleus. The energy was chosen such that the peaks from the  $^{28}\text{Si}(d,p)$  reaction obscured parts of the spectrum at as few of the angles for which data were collected. The beam current on the target was typically 1.2 to 2.0  $\mu\text{A}$  during this experiment.

To further ensure that good energy resolution can be attained, it is necessary to have a well collimated and sharply focused beam on the target. There are surface irregularities inherent in the target. A well collimated beam prevents the beam from wandering very far across the surface of the target.

A set of collimating slits was placed at the entrance to the target chamber to define the position of the beam. The horizontal and vertical dimensions of the

aperture were 1 mm by 3.5 mm. This prevented the beam spot from moving very far across the target. A faraday cup was placed at  $0^\circ$  to the beam direction to act as a beam stop and to monitor the beam current incident on the target. A current digitizer was connected to the faraday cup so that the total accumulated charge on the cup could be determined. A solid state silicon surface barrier detector with a depletion depth of 1 mm was placed at  $-30^\circ$  to the beam direction. A tantalum aperture was placed in front of this detector to define the solid angle subtended at the detector. The detector subtended a solid angle of 0.13 msr.

This detector was used to count the deuterons that were elastically scattered from the cesium nuclei at  $-30^\circ$  to the beam direction. A TN 1710 multichannel analyzer was used to collect the counts from the surface barrier detector.

The protons were momentum analyzed in an Enge magnetic spectrograph. The entrance aperture of the magnet was adjusted to give a solid angle of 1.3 msr. The protons were detected on Ilford K5 nuclear emulsions which were mounted in the focal plane of the spectrograph. Aluminum absorbers of  $3/8$  mm thickness were placed in front of the emulsions. The absorbers were thin enough to allow the protons to penetrate to the emulsion but heavier particles with the same magnetic

rigidity,  $mv/q$ , as the protons would be stopped in the absorber. The exposures were taken for an integrated charge that varied from  $9000 \mu\text{C}$  at  $7.5^\circ$  to  $18000 \mu\text{C}$  at  $75^\circ$ . The emulsions were scanned in  $0.25 \text{ mm}$  strips with a microscope.

In addition, short duration elastic exposures were collected. For these exposures, the solid angle at the entrance to the spectrograph was reduced to  $0.104 \text{ msr}$ . Ilford K5 emulsions were used to detect the deuterons but no absorbers were used. The elastic scattering data were collected at a laboratory angle of  $30^\circ$ . The elastic exposures were collected for an integrated charge of about  $5 \mu\text{C}$ .

### 3.3 Data Analysis

The reaction and elastic cross-sections are related to the number of counts in a peak as follows:

$$N = \frac{Qf}{ZeW} \frac{N_0 t}{d\Omega} \frac{d\sigma}{d\Omega} \Delta\Omega \quad (1)$$

where:

$N$  is the number of counts in a peak

$Q$  is the total accumulated charge

$Z$  is the charge state of the incident particles

$e$  is the electronic charge

$N_0$  is Avogadro's number

$W$  is the atomic weight of the target

$\frac{d\sigma}{d\Omega}$  is the differential cross-section

$\Delta\Omega$  is the solid angle subtended at the detector

$f$  is the fractional abundance of the isotope and

$t$  is the target thickness (expressed as a surface density).

The absolute reaction cross-sections can be determined without the knowledge of the target thickness if data are also collected simultaneously for elastic scattering. The relative reaction cross-sections can be determined from the monitor counts as follows:

$$\frac{N_{\text{reac}}^{\text{emul}}}{N_{\text{el}}^{\text{mon}}} = \frac{\left(\frac{d\sigma}{d\Omega}\right)_{\text{reac}} (\Delta\Omega)_{\text{reac}}^{\text{emul}}}{\left(\frac{d\sigma}{d\Omega}\right)_{\text{el}} (\Delta\Omega)_{\text{mon}}} \quad (2)$$

where the superscripts and subscripts denote the reaction (reac) scattering yields on the emulsions (emul) and the elastic scattering (el) detected in the monitor (mon). Similarly the elastic scattering yields on the emulsions give:

$$\frac{N_{\text{el}}^{\text{emul}}}{N_{\text{el}}^{\text{mon}}} = \frac{\left(\frac{d\sigma}{d\Omega}\right)_{\text{el}} (\Delta\Omega)_{\text{el}}^{\text{emul}}}{\left(\frac{d\sigma}{d\Omega}\right)_{\text{el}} (\Delta\Omega)_{\text{mon}}} \quad (3)$$

Dividing equation (3) into equation (2) gives:

$$\frac{N_{\text{reac}}^{\text{emul}}}{N_{\text{el}}^{\text{emul}}} = \frac{N_{\text{el}}^{\text{mon}} \left(\frac{d\sigma}{d\Omega}\right)_{\text{reac}}}{N_{\text{el}}^{\text{mon}} \left(\frac{d\sigma}{d\Omega}\right)_{\text{el}}} \quad (4),$$

from which the absolute reaction cross-sections can be calculated. The elastic scattering cross-section is obtained from optical model calculations with the computer code DWUCK4 (Kunz, 1974). The elastic cross-section given by DWUCK4 differs from the Rutherford scattering cross-section by about 2% at  $30^\circ$  for 12-MeV deuterons on  $^{133}\text{Cs}$ .

The automatic peak-fitting computer code SPECTR (O'Neil, 1970) was used to extract the peak areas and peak positions from the experimental data. The computer code utilizes a skewed gaussian function consisting of the sum of a gaussian function and an exponential function. The purpose of the exponential function is to provide a "tail" on one side of the gaussian function. There are two main contributors to this "tail": Improper location of the detector with respect to the focal plane can cause a "tail" on either side of the peak. This is usually less important than the other source of the "tail", straggling.

The width of the peak and hence the energy resolution are also affected by the aforementioned contributors to the "tail". The energy variation due to the different stopping power,  $dE/dx$ , curves of the proton

and deuteron also affects the energy resolution. The energy of the outgoing protons in the (d,p) reaction varies because the depth in the target at which the reaction occurs varies.

The form of the function used by the computer code is as follows:

$$y(x) = H \left( e^{-\frac{(x-x_0)^2}{G^2}} + s e^{-\frac{(x-x_0-GG)/A}{1-e^{-\frac{(x-x_0)^2}{GG}}}} \right)$$

where:

H is the height of the peak

$x_0$  is the position of the gaussian centroid

G, GG are gaussian width parameters

s is the parameter specifying the contribution of the exponential tail and,

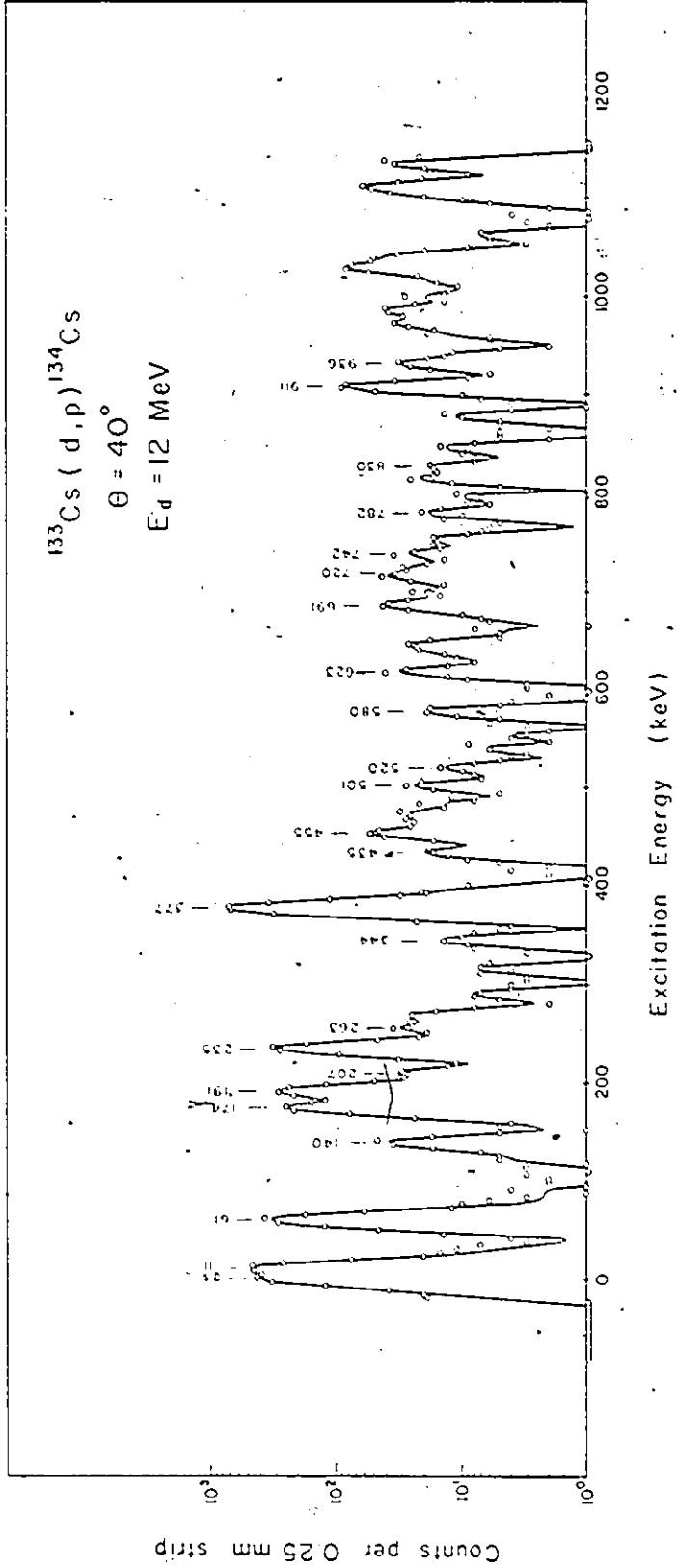
A is the exponential decay constant.

The exponential term is only calculated for  $(x-x_0) > 0$  or  $< 0$ , depending on which side of the peak the "tail" is located.

These parameters are selected to best fit a chosen sample peak. Then, with the shape fixed, the computer code performs a non-linear least squares fit over the spectrum. A spectrum taken at  $40^\circ$  is shown in Figure 3.1. The energy resolution of the spectrum was = 13 keV. The typical errors in the experimental cross-sections were about 10%. The error estimates account

Figure 3.1

The  $^{133}\text{Cs}(d,p)$  spectrum was taken at a laboratory angle of  $40^\circ$  with a beam energy of 12 MeV.



for the error in extracting the areas of the peaks and uncertainties in the normalization for the absolute cross-section.

To extract the  $l$ -values and the spectroscopic factors from the experimental angular distributions, DWBA calculations were needed. These calculations were performed with the computer code DWUCK4 (Kunz, 1974). The optical model parameters used are shown in table 3.1. The deuteron optical model parameters were extracted from a systematic study of elastic scattering differential cross sections and polarizations (Lohr and Haerberli, 1974). The proton parameters were obtained in a similar manner from the systematic analysis by Becchetti and Greenlees (1969). The neutron parameters are also from an analysis by Becchetti and Greenlees. The neutron well depth was a free parameter adjusted to reproduce the neutron binding energy. Non-local range corrections were made to the calculations. The nonlocal range parameters of 0.84 fm for the proton (Perey and Buck, 1962) and 0.54 fm for the deuteron (Bassel, 1966) were used. The normalization factor which appears in the expression relating the experimental to the DWBA differential cross-section in section 2.4.1 was adopted as 1.55 from Kunz (1974).

Differential cross-section calculations were performed for  $l_n = 0, 2$  and  $5$  corresponding to  $3s_{1/2}$ .

Table 3.1

Optical Model Parameters for the  $^{133}\text{Cs}(d,p)^{134}\text{Cs}$  Reaction at 12 Mev

Particle	V (MeV)	$r_{oc}$ (fm)	$r_{OR}$ (fm)	$a_R$ (fm)	W (MeV)	$W_D$ (MeV)	$r_{OI}$ (fm)	$a_I$ (fm)	$V_{so}$ (MeV)	$r_{so}$ (fm)	$a_{so}$ (fm)	Non Local Correction
d	-119.8	1.3	1.05	0.80	32.5	0	1.43	0.84	14.0	0.75	0.75	0.54
p	-57.8	1.3	1.17	0.75	39.4	-0.9	1.32	0.64	25.0	1.01	0.75	0.84
n	*	1.3	1.17	0.75	0	0	0.0	0.0	25.0			

\* adjusted to match neutron binding energy

$2d_{3/2}$  and  $1h_{11/2}$  neutron transfers, respectively since it was seen earlier that these were the  $l_n$ -values expected in the  $^{133}\text{Cs}(d,p)$  reaction.  $l_n$ -values of 1, 3 and 4 were not considered for these low-lying states because no neutron holes in p, f or g orbitals were expected from shell model considerations. The discussion in section 3.1 indicated that  $l_n = 0, 2$  and  $5$  are the  $l$ -values that are expected for the low-lying levels in  $^{134}\text{Cs}$ . Angular distributions were generated for centre of mass angles between  $0^\circ$  and  $90^\circ$  in increments of  $2.5^\circ$ . The calculations were performed for three excitation energies, 0, 500 and 1000 keV. The change in the differential cross-sections over this range of excitation energies was less than 5%.

The calculated angular distributions for  $l_n = 0, 2$  and  $5$  show characteristically different shapes. This allows unambiguous assignments of  $l_n$ -values to states displaying these shapes. The experimental angular distributions were least squares fitted with the DWBA calculations and the  $l_n$ -values and the spectroscopic factors were extracted. None of the levels were successfully fitted with incoherent mixtures of  $l = 0 + 2$ , which indicates an absence of significant mixing. The angular distributions and their DWBA fits are displayed in figure 3.2. A summary of the  $l_n$ -values and the

Figure 3.2

The angular distributions and their DWBA fits (solid curves) for the levels populated in the  $^{133}\text{Cs}(d,p)$  reaction with 12 MeV deuterons.

$^{133}\text{Cs}(d,p)^{134}\text{Cs}$   
 $E_d = 12.0 \text{ MeV}$

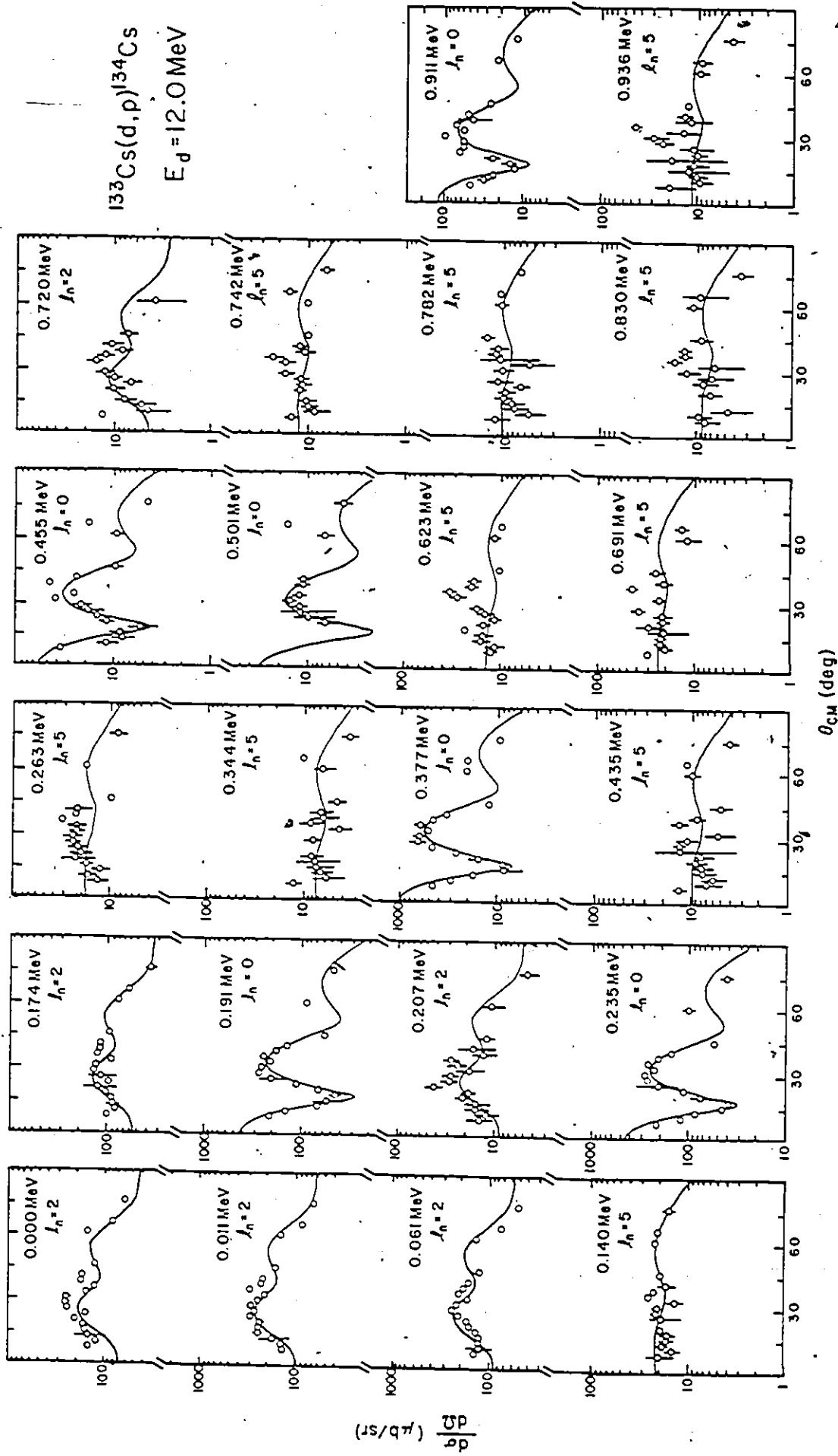


Table 3.2

Energy levels,  $t_n$ -values, and Spectroscopic Factors for  
the  $^{133}\text{Cs}(d,p)^{134}\text{Cs}$  Reaction

Energy (keV)	$t_n$	$\frac{[2J_f+1]}{[2J_i+1]}$	S
0 <u>+2</u>	2	0.46	<u>+ 0.06</u>
11 <u>+2</u>	2	0.69	<u>+ 0.11</u>
60	2	0.61	<u>+ 0.08</u>
140 <u>+2</u>	5	0.47	<u>+ 0.09</u>
174 <u>+3</u>	2	0.35	<u>+ 0.06</u>
191 <u>+3</u>	0	0.13	<u>+ 0.02</u>
207 <u>+3</u>	2	0.057	<u>+ 0.018</u>
235 <u>+2</u>	0	0.14	<u>+ 0.02</u>
263 <u>+3<sup>a</sup></u>	5	0.37	<u>+ 0.16</u>
344 <u>+2</u>	5	0.16	<u>+ 0.06</u>
377 <u>+2</u>	0	0.32	<u>+ 0.05</u>
435 <u>+2</u>	5	0.21	<u>+ 0.07</u>
455 <u>+2<sup>b</sup></u>	0	0.019	<u>+ 0.008</u>
501 <u>+3</u>	0	0.009	<u>+ 0.004</u>
520 <u>+3</u>			
580 <u>+3</u>			
623 <u>+2</u>	5	0.29	<u>+ 0.09</u>
691 <u>+2</u>	5	0.50	<u>+ 0.16</u>
720 <u>+3</u>	2	0.020	<u>+ 0.012</u>
742 <u>+3</u>	5	0.27	<u>+ 0.07</u>
782 <u>+3</u>	5	0.21	<u>+ 0.06</u>
830 <u>+3</u>	5	0.18	<u>+ 0.07</u>
911 <u>+2</u>	0	0.038	<u>+ 0.012</u>
936 <u>+2</u>	5	0.24	<u>+ 0.10</u>

<sup>a</sup> unresolved 257 and 267 keV doublet

<sup>b</sup> possibly doublet

spectroscopic factors are presented in table 3.2. The differential cross-sections for each of the energy levels identified are tabulated in appendix A.

Four prominent  $\lambda_n = 2$  and eleven (since the 263 keV peak listed in table 3.2 is a doublet) significant  $\lambda_n = 5$  states were observed in the (d,p) reaction. The presence of three rather than two strong  $\lambda_n = 0$  states indicate that some fragmentation of the spectroscopic strength may have occurred. In addition, there are a number of weaker states. The nature of these states is quite uncertain, given data from the (d,p) reaction alone. The only significant impurity peak in the spectra was from  $^{28}\text{Si}(d,p)$ . The emulsions were scanned up to about 1300 keV excitation for about 1/2 of the angles. Many peaks appear above 936 keV but none were positively identified as belonging to  $^{134}\text{Cs}$ . The total observed  $\lambda_n = 2$  strength in the  $^{133}\text{Cs}(d,p)$  reaction is 2.2 while the total  $\lambda_n = 2$  strength in the  $^{134}\text{Ba}(d,p)$  reaction was 1.73 (von Ehrenstein et al., 1970). The  $\lambda_n = 0$  strength in the  $^{133}\text{Cs}(d,p)$  reaction is 0.66 which is comparable to the value of 0.46 found by von Ehrenstein et al. (1970) in the  $^{134}\text{Ba}(d,p)$  reaction. The total observed  $\lambda_n = 5$  strength in the  $^{133}\text{Cs}(d,p)$  reaction is 2.9 but no comparison with the  $^{134}\text{Ba}(d,p)$  reaction can be made because the  $\lambda_n = 5$  level was not identified in that reaction.

The sum over all  $l_n$ -values of the spectroscopic strengths is 5.8 for the  $^{133}\text{Cs}(d,p)$  reaction. The sum rules predict that this should be equal to the number of neutron holes in the  $^{133}\text{Cs}$  target, which is four. The disagreement suggests that the DWBA cross-sections are too small or that the experimental cross-sections are too large.

Comparisons of the centroid energies of  $^{133}\text{Xe}$ ,  $^{135}\text{Ba}$  and in  $^{134}\text{Cs}$  for  $l_n = 0, 2$  and  $5$  are shown in table 3.3. Qualitative agreement is found for the locations of the centroids for each  $l_n$ -value.

Table 3.3

Centroid Energies of  $^{133}\text{Xe}$ ,  $^{135}\text{Ba}$  and  $^{134}\text{Cs}$  for  $l_n = 0, 2$  and  $5$ .

$J^\pi$	$^{133}\text{Xe}$ 1)		$^{134}\text{Cs}$ 2)		$^{135}\text{Ba}$ 3)	
	$l_n$	Energy (keV)	$l_n$	Energy (keV)	$l_n$	Energy (keV)
$3/2^+$	2	0	2	57	2	198
$11/2^-$	5	233	5	543	a	269
$1/2^+$	0	263	0	344	0	292

1) Schneid and Rosner (1966).

2) this study.

3) von Ehrenstein et al. (1970).

a The 269 keV level in  $^{135}\text{Ba}$  has spin  $11/2^-$  (Lederer and Shirley, 1978).

## The $^{135}\text{Ba}(t,\alpha)^{134}\text{Cs}$ Reaction

### 4.1 Introduction

Another approach to the study of the low-lying levels of  $^{134}\text{Cs}$  is provided by the  $^{135}\text{Ba}(t,\alpha)^{134}\text{Cs}$  reaction. The low-lying states of  $^{134}\text{Cs}$  are populated by the removal of one of the six protons beyond the  $Z=50$  closed shell. The ground state of  $^{135}\text{Ba}$  has spin  $3/2^+$  (Lederer and Shirley, 1978) and was observed in the  $^{134}\text{Ba}(d,p)^{135}\text{Ba}$  reaction to be populated by an  $i_n = 2$  neutron transfer. The ground state of  $^{135}\text{Ba}$  conforms to a neutron hole in the  $2d_{3/2}$  orbital.

The shell model orbitals occupied by the six valence protons can be ascertained by examining the neighboring odd  $Z$ , even  $N$  nuclei,  $^{133}\text{Cs}$ ,  $^{135}\text{Cs}$ ,  $^{137}\text{Cs}$ ,  $^{135}\text{La}$ ,  $^{137}\text{La}$  and  $^{139}\text{La}$ . The ground states of all but  $^{135}\text{La}$  have spin  $7/2^+$  and their first excited states have spin  $5/2^+$  (Lederer and Shirley, 1978). However, the first excited state of  $^{137}\text{La}$  is only at about 10 keV, so the  $1g_{7/2}$  and  $2d_{5/2}$  proton orbitals are very close together. The ground state of  $^{135}\text{La}$  is  $5/2^+$  but its first excited state at 119 keV is  $7/2^+$ . Proton transfer data is available for two  $N=82$  nuclei,  $^{137}\text{Cs}$  and  $^{139}\text{La}$  (Wildenthal et al., 1971). The ground states of  $^{137}\text{Cs}$

and  $^{139}\text{La}$  are populated by  $\lambda_p = 4$  proton transfers in the  $^{138}\text{Ba}(d, ^3\text{He})$  and  $^{138}\text{Ba}(^3\text{He}, d)$  reactions with strengths of 3.57 and 0.54 respectively. The first excited states of these two nuclei,  $^{137}\text{Cs}$  and  $^{139}\text{La}$ , are  $\lambda_p = 2$  with strengths of 0.71 and 0.90 respectively.

#### 4.2 Experimental Set-Up

In the discussion on the (d,p) reaction it was noted that the odd-odd nuclei in the  $A=134$  mass region have high level densities. This necessitates the use of a stable monoenergetic beam of particles which is well collimated and sharply focussed on the target. Negatively charged tritons were produced in a Middleton type sputter source and accelerated to 15 MeV by the McMaster tandem van de Graaff accelerator for this purpose.

This beam energy gave the tritons enough energy to overcome the Coulomb barrier for  $^{135}\text{Ba}$  kept to a minimum the number of angles at which peaks from the  $^{16}\text{O}(t,d)$  reaction obscured parts of the spectrum.

Isotopically enriched  $^{135}\text{BaO}$  deposited on a carbon foil backing was used as a target. The isotopic compositions of the target, given in table 4.1, are those stated by the supplier (Union Carbide Corporation). The target material was obtained in the form of  $^{135}\text{Ba}(\text{NO}_3)_2$ . The barium nitrate was heated in a tantalum crucible to form  $\text{BaO}$ . The barium oxide was then

Table 4.1

Isotopic Composition of  $^{135}\text{BaO}$  Target

Isotope	Atomic Percent	Precision
$^{130}\text{Ba}$	< 0.01	
$^{132}\text{Ba}$	< 0.01	
$^{134}\text{Ba}$	0.36	$\pm 0.05$
$^{135}\text{Ba}$	93.60	0.01
$^{136}\text{Ba}$	1.61	0.05
$^{137}\text{Ba}$	0.87	0.05
$^{138}\text{Ba}$	3.56	0.05

vacuum evaporated and condensed on the carbon backing mounted on aluminum frames suitable for use in the target chamber of the spectrograph. The  $^{135}\text{BaO}$  target was nominally  $50 \mu\text{g}/\text{cm}^2$  on a  $30 \mu\text{g}/\text{cm}^2$  carbon backing. From table 4.1, it is seen that the  $^{135}\text{Ba}$  is not 100% pure. The prominent impurities are  $^{136}\text{Ba}$  and  $^{138}\text{Ba}$ . The (t, $\alpha$ ) reactions on these impurities lead to  $^{135}\text{Cs}$  and  $^{137}\text{Cs}$ , respectively.

The Enge magnetic spectrograph was used to momentum analyze the  $\alpha$ -particles from the reaction. Two focal plane detection systems were employed to collect the data, Ilford K-1 nuclear emulsions, and a delay line counter constructed after the Michigan State University design (Markham and Robertson, 1975 and Wilkin, 1976). A number of complications occurred during the experiment which indicated that an alternative to the nuclear emulsions might be useful. Very intense groups of deuterons from the  $^{12}\text{C}(t,d)^{13}\text{C}$  and  $^{16}\text{O}(t,d)^{17}\text{O}$  reactions occurred at the same locations along the focal plane as some  $\alpha$ -particle groups of interest. Since the focal plane had been adjusted for the kinematics of the  $^{135}\text{Ba}(t,\alpha)$  reaction, the focal plane was not correct for the (t,d) reactions on the lighter nuclei. Hence, the peaks were very broad and portions of the (t, $\alpha$ ) reaction spectrum were uncountable. The K-1 nuclear emulsions were used since they are less sensitive to ionizing radiation than

K5 emulsions. The deuterons and tritons make very much lighter tracks in the K-1 emulsions than the  $\alpha$ -particles. However, the deuteron groups were so intense that portions of the K-1 emulsions were bleached. The tracks appeared very indistinctly and out of focus, so that it was not possible to count the tracks in these regions.

In addition, at a number of angles there was a continuum background from tritons scattered from the collimating slits. For  $\alpha$ -particles and tritons with the same magnetic rigidity,  $mv/q$ , the tritons have one-third of the  $\alpha$ -particle energy. These tritons have very nearly the same range in aluminum as the  $\alpha$ -particles. To ensure that the  $\alpha$ -particle groups would all penetrate the absorber while the tritons would stop, the absorber thickness was varied along the focal plane. A graded aluminum absorber was used to stop the tritons and allow the  $\alpha$ -particles to penetrate to the emulsion. The absorber was 0.18 mm thick for the first 80 mm of the plate, 0.165 mm for the next 30 mm, and 0.15 mm for the rest of the plate. Since the ground state  $\alpha$ -group was expected about 50 mm from the end of the plate and the dispersion was about 26 keV/mm, the thickest part of the absorber covered the first 780 keV of excitation and the 0.165 mm thick aluminum covered the next 780 keV of excitation.

The delay line counter was tried because it had two advantages over the nuclear emulsions, the spectra could be viewed immediately and particle discrimination was possible. The  $\Delta E$  signal from the back counter provided a means of identifying the particles since the rate of energy loss per distance travelled,  $dE/dx$ , differs for deuterons, tritons, and  $\alpha$ -particles. By setting gates on the  $\Delta E$  signal and requiring coincidences between the position sensitive front counter and the  $\Delta E$  back counter, spectra, with the deuteron peaks and triton background absent, could be collected.

Difficulties in the operation of the counter led to it not being used. It was necessary to have energy resolution which was at least as good as that attained with the nuclear emulsions since the level density in  $^{134}\text{Cs}$  is high. It was found that the energy resolution was not easily optimized without seriously affecting the counting efficiency. Problems were encountered in setting up and adjusting the counter and its associated electronics to count with the same efficiency across the length of the counter. A slow long term drift in the flow rate of the gas through the counter led to difficulties originating from the change in the signal gain for the back counter and a corresponding change in the resolution and counting efficiency in the front counter. Since there was not sufficient time to overcome the

shortcomings of the delay-line counter while the triton beam was available, it was decided to collect the data with the Ilford K-1 nuclear emulsions.

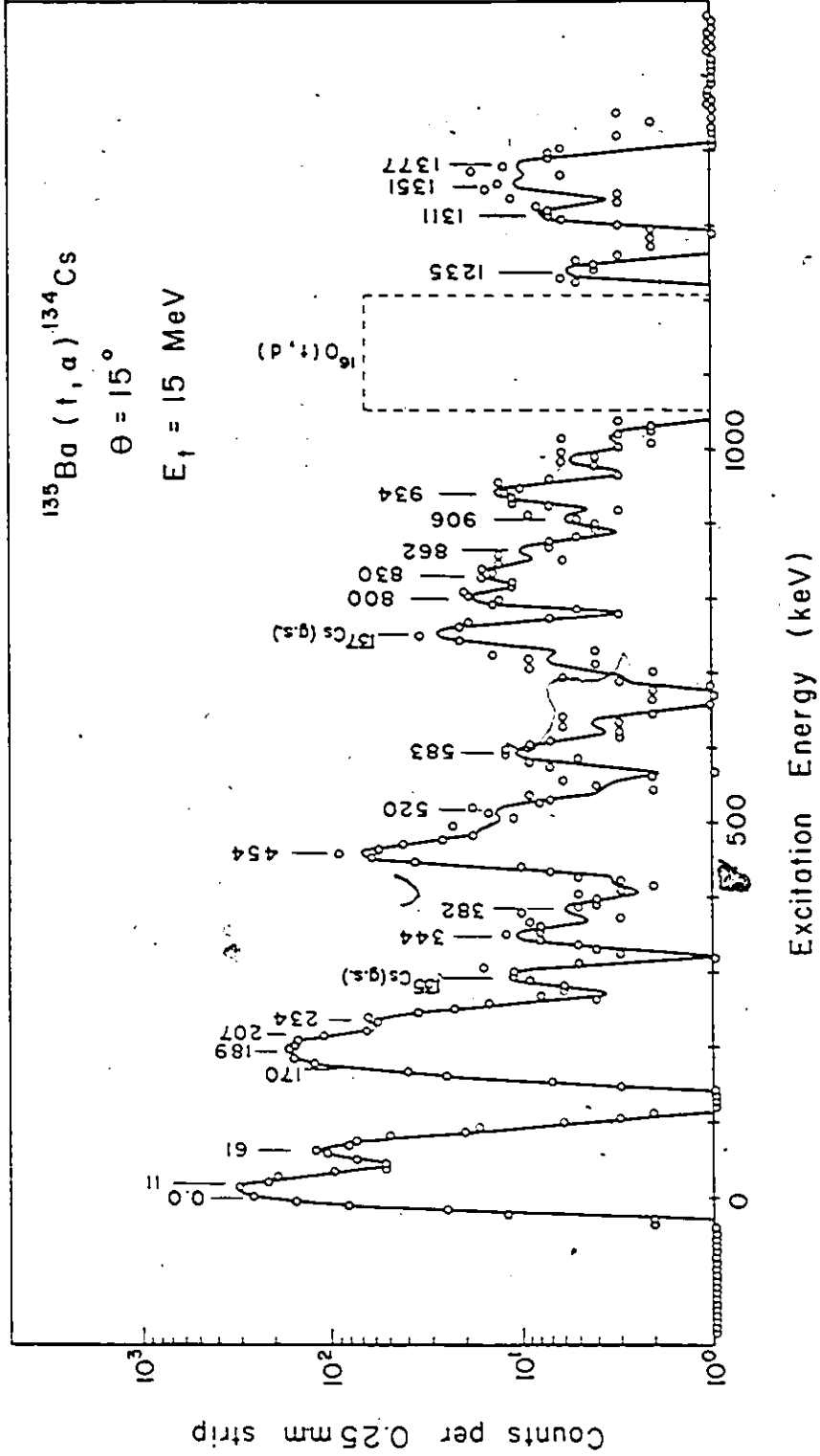
Angular distributions were collected for laboratory angles between  $7.5^\circ$  and  $40^\circ$ . The triton beam current on the target was between 120 and 160 nA. The spectrograph solid angle was 1.3 msr. The integrated charge on the faraday cup varied from 1000  $\mu\text{C}$  at forward angles to 3000  $\mu\text{C}$  at the backward angles. A silicon surface barrier detector at  $-30^\circ$  to the beam direction was used to count the elastically scattered tritons. The total number of tritons, elastically scattered from the barium nuclei, was used to normalize the exposures.

Absolute cross-sections were determined by normalizing the reaction yield to the elastic scattering yield. The elastic scattering yield was collected in short duration exposures on K5 nuclear emulsions. For these exposures, the solid angle of the spectrograph was reduced to 0.104 msr.

The spectra were obtained by scanning the emulsions in 0.25 mm strips. The data were fitted with the peak search computer code, SPECTR (O'Neil, 1970). An example of the  $(t, \alpha)$  reaction spectrum and the computer generated fit is shown in figure 4.1. The spectrum was obtained at a laboratory angle of  $15^\circ$ . The energy resolution was about 21 keV. The total accumulated

Figure 4.1

The  $^{135}\text{Ba}(t,\alpha)$  spectrum was taken at a laboratory angle of  $15^\circ$  with a beam energy of 15 MeV.



charge for the exposure was 1000  $\mu\text{C}$ .

### 4.3 Data Analysis

The experimental differential cross-sections were obtained from the data in the manner described in chapter 3. The 60 keV peak was used as the reference for the energies since the ground and 11 keV states were not resolved. The typical errors in the differential cross-sections were about 10%.

To obtain the  $a_p$ -values for the transferred proton and the spectroscopic factors for the energy levels, DWBA calculations were performed with the computer code, DWUCK4 (Kunz, 1974). The optical model parameters employed in these calculations are shown in table 4.2. The triton parameters were obtained from Conjeaud et al. (1973). The alpha particle parameters were obtained from Perey and Perey (1976), however, the radii for the real and imaginary wells were increased from 1.4 fm to 1.5 fm to give better fits to the experimental angular distributions. The calculated elastic scattering differential cross-section at  $30^\circ$  differed from the Rutherford cross-section by about 3% for 15 MeV tritons on  $^{135}\text{Ba}$ .

The experimental angular distributions and their DWBA fits are shown in figure 4.2. A summary of the observed levels and the corresponding  $a_p$ -values and

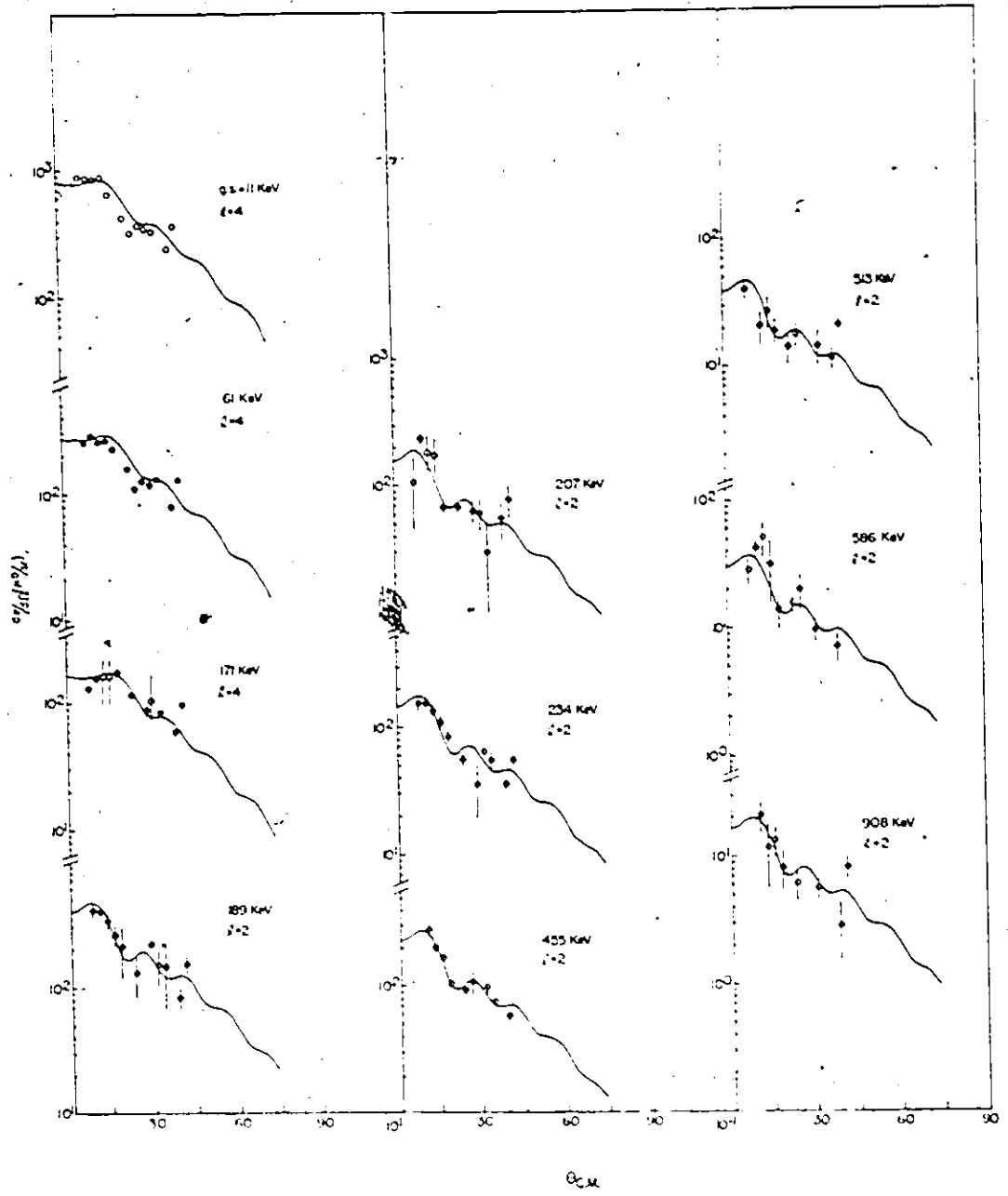
Table 4.2  
 Optical Model Parameters for the  $^{135}\text{Ba}(t, \alpha)^{134}\text{Cs}$  Reaction at 15 MeV

particle	V (MeV)	$r_{OR}$ (fm)	$a_R$ (fm)	W (MeV)	$W_D$ (MeV)	$V_{SO}$ (MeV)	$r_{OI}$ (fm)	$a_I$ (fm)	$r_{OC}$ (fm)
t	-153.0	1.35	.889	20.8	0	0	1.42	.889	1.3
$\alpha$	-172.8	1.5	.589	60.6	0	0	1.5	.589	1.3
p	*	1.25	.65	0	0	0			1.3

\* adjusted to fit binding energy

Figure 4.2.

The angular distributions and the DWBA fits (solid curves) for the levels populated in the  $^{135}\text{Ba}(t,\alpha)$  reaction with 15 MeV tritons.



spectroscopic factors are shown in table 4.3. The differential cross-sections for each energy level at each angle are tabulated in appendix B. These results were obtained by least squares fitting the DWBA calculations to the experimental angular distributions.

Table 4.3 lists nineteen levels which were identified and assigned to  $^{134}\text{Cs}$  from the (t, $\alpha$ ) reaction. There are eleven levels with assigned spectroscopic factors and  $l_p$ -values. Four levels were assigned  $l_p = 4$  and seven levels were assigned  $l_p = 2$ . The  $l_p = 4$  levels are among the most strongly populated levels in the (t, $\alpha$ ) reaction.

There is some uncertainty in the absolute values of the spectroscopic factors since the normalization factor for the (t, $\alpha$ ) reaction is not well known. A value of 23 was adopted (Flynn et al., 1977). This normalization factor results in the sum of the spectroscopic factors for the assigned  $l_p = 4$  states being 3.47 and for the assigned  $l_p = 2$  states being 0.70. From sum rule considerations, the sum of the spectroscopic factors for the proton pickup reaction equals the number of protons in a particular orbital beyond the nearest closed proton shell. The nearest closed shell for  $^{135}\text{Ba}$  is at  $Z=50$ . There should be six protons distributed among the  $1g_{7/2}$  and  $2d_{5/2}$  orbitals. A look at the spectroscopic strengths in the  $^{138}\text{Ba}(d, ^3\text{He})^{137}\text{Cs}$  provides an

Table 4.3

Energy,  $l_p$ -values, and Spectroscopic Factors for the  
 $^{135}\text{Ba}(t, \alpha)^{134}\text{Cs}$  Reaction.

Energy (keV)	$l_p$	S
g.s. + 11 $\pm$ 3	4	2.23 $\pm$ 0.16
60	4	0.77 $\pm$ 0.15
173 $\pm$ 2	4	0.46 $\pm$ 0.05
189 $\pm$ 2	2	0.27 $\pm$ 0.06
207 $\pm$ 2	2	0.11 $\pm$ 0.04
234 $\pm$ 2	2	0.10 $\pm$ 0.02
344 $\pm$ 2		
377 $\pm$ 3		
455 $\pm$ 2 <sup>a</sup>	2	0.16 $\pm$ 0.02
513 $\pm$ 2	2	0.027 $\pm$ 0.010
586 $\pm$ 2	2	0.021 $\pm$ 0.005
723 $\pm$ 3		
802 $\pm$ 3		
849 $\pm$ 3		
908 $\pm$ 3	2	0.012 $\pm$ 0.004
936 $\pm$ 3		
1282 $\pm$ 3		
1319 $\pm$ 3		

<sup>a</sup> possibly doublet

indication on how the protons are divided among the  $1g_{7/2}$  and  $2d_{5/2}$  orbitals. The ground state of  $^{137}\text{Cs}$  was populated with  $l_p = 4$  with a spectroscopic strength of 3.57 and the first excited state carried 0.71 units of  $l_p = 2$  strength (Wildenthal et al., 1971). The total strength for  $l_p = 4$  was 3.47 in the  $^{135}\text{Ba}(t,\alpha)$  reaction which agrees well with Wildenthal's value of 3.57 and the total strength for  $l_p = 2$  of 0.70 also agrees well with the value found by Wildenthal et al. (1971). Thus, the agreement appears to be good when a normalization factor of 23 is used.

The sum of the spectroscopic strengths over all of the  $l_p$ -values is 4.2 but a value of 6 is expected since there are a total of 6 valence protons in the  $^{135}\text{Ba}$  target. This suggests that the DWBA calculations are predicting cross-sections that are too large or that the experimental cross-sections are subject to an undetected systematic error.

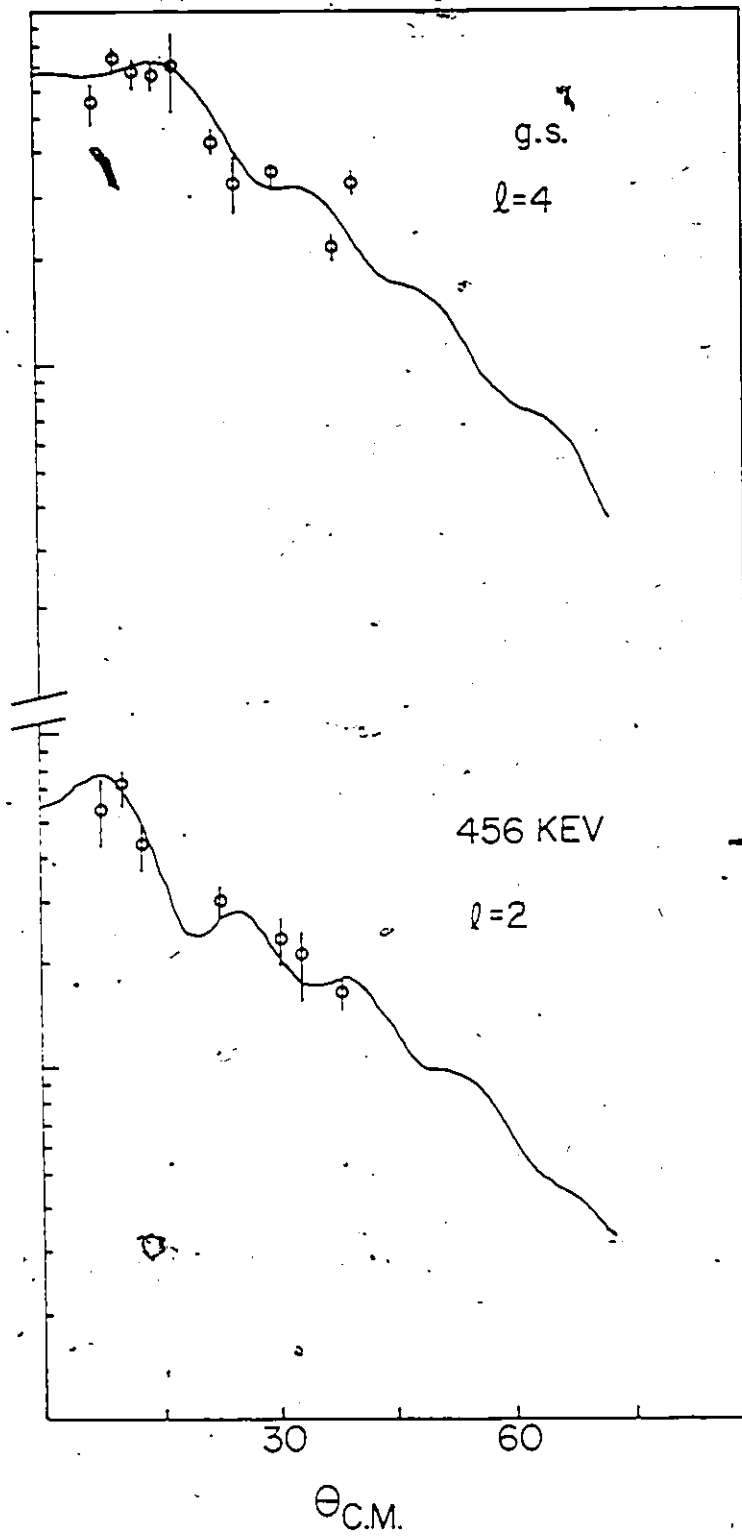
Alpha particle groups from reactions on the  $^{136}\text{Ba}$  and  $^{138}\text{Ba}$  impurities also appear in the spectra. The Q-values for the  $^{135}\text{Ba}(t,\alpha)$ ,  $^{136}\text{Ba}(t,\alpha)$  and  $^{138}\text{Ba}(t,\alpha)$  reactions are 11.563, 11.281 and 10.812 MeV (Gove and Wapstra, 1972), respectively. The  $\alpha$ -particles from the ground state of  $^{135}\text{Cs}$  are expected to appear at about 282 keV with respect to the ground state of  $^{134}\text{Cs}$ . The excited states of  $^{135}\text{Cs}$  are expected to appear at

about 530, 688, 888, 1067, 1261, and 1342 keV with respect to the ground state of  $^{134}\text{Cs}$ . These states would be very weakly populated if they appear. There is a peak at 288 keV which has the strength expected for the ground state of  $^{135}\text{Cs}$ . This is based on the abundance of  $^{136}\text{Ba}$  listed in table 4.1 and an estimate of the  $l_p = 4$  strength from the total observed  $l_p = 4$  strength in the  $^{135}\text{Ba}(t, \alpha)$  reaction. No peaks are identified at the energies corresponding to the excited states of  $^{135}\text{Cs}$ . The  $\alpha$ -particles corresponding to the ground state of  $^{137}\text{Cs}$  would occur at about 750 keV with respect to the ground state of  $^{134}\text{Cs}$ . The first excited state would occur at about 1210 keV and the second excited state would appear about 1600 keV with respect to the ground state of  $^{134}\text{Cs}$ . The spectra do indeed show peaks at 750 and 1210 keV. Since the plates were not scanned past about 1400 keV it is not known whether the peak at 1600 keV appears. The cross-section for the ground state of  $^{137}\text{Cs}$  is comparable to the total cross-sections for the corresponding  $l_p = 4$  states in  $^{134}\text{Cs}$ . Similarly, the first excited state of  $^{137}\text{Cs}$  has a cross-section which is comparable to the total observed cross-sections of the  $l_p = 2$  states in  $^{134}\text{Cs}$ .

The two levels of  $^{137}\text{Cs}$  that were present provide a further check on the normalization and on the DWBA calculations. The ground state of  $^{137}\text{Cs}$  is known to be

Figure 4.3

The angular distributions and the DWBA fits (solid curves) for the first two states of  $^{137}\text{Cs}$  in the  $^{138}\text{Ba}(t,n)$  reaction with 15 MeV tritons.



populated by  $\lambda_p = 4$  proton transfers (Wildenthal et al., 1971). The first excited state is similarly known to be populated by  $\lambda_p = 2$  proton transfers. The angular distributions for these levels are shown in figure 4.3. The ground state was found to have a spectroscopic factor of 5.2 and the first excited state had a spectroscopic factor of 1.2 when a normalization of 23 was used. These spectroscopic factors are in qualitative agreement with what is expected from the  $(d, {}^3\text{He})$  results of Wildenthal et al (1971). Hence, the normalization factor of 23 seems to be reasonable.

The centroid energies for the  $\lambda_p = 2$  and 4 strengths in  ${}^{134}\text{Cs}$ ,  ${}^{137}\text{Cs}$  and  ${}^{139}\text{La}$  are presented in table 4.4. The locations of the centroids are similar in all three nuclei.

The interpretation of these results in terms of shell model configurations and the assignment of the spins and parities are left for a later chapter. These results are combined with the results of the  $(d,p)$  particle work, the  $\gamma$ -ray studies described in the next chapter, and the published data of Alexeev et al. (1975) to give a proposed energy level scheme.

Table 4.4

Centroid Energies of  $^{134}\text{Cs}$ ,  $^{137}\text{Cs}$  and  $^{139}\text{La}$  for  $t_p = 2$   
and 4.

$^{137}\text{Cs}$ 1)			$^{134}\text{Cs}$ 2)			$^{139}\text{La}$ 1)		
$J^\pi$	$t_p$	Energy (keV)	$J^\pi$	$t_p$	Energy (keV)	$J^\pi$	$t_p$	Energy (keV)
$7/2^+$	4	0	$7/2^+$	4	42	$7/2^+$	4	0
$5/2^+$	2	488	$5/2^+$	2	295	$5/2^+$	2	166

1) Wildenthal et al. (1971).

2) this study.

## $\gamma$ -ray Studies

### 5.1 Introduction

The preceding chapters have described the use of single particle transfer reactions to study the low-lying levels in  $^{134}\text{Cs}$ . Further studies were conducted in which the electromagnetic transitions from the de-excitation of the excited states were examined. The  $\gamma$ -ray transitions in the  $^{133}\text{Cs}(d,p\gamma)$  and  $^{130}\text{Te}(^7\text{Li},3n\gamma)$  reactions were studied.

The use of  $\gamma$ -ray spectroscopy provides one advantage over charged particle spectroscopy. The energy resolution of the germanium  $\gamma$ -ray detectors is superior to the energy resolution attainable in charged particle spectroscopy. This is highly desirable when the nucleus under study has a high energy level density as in the case of  $^{134}\text{Cs}$ . The  $\gamma$ -ray transitions in the  $^{133}\text{Cs}(d,p\gamma)$  reaction were examined to gain a better understanding of the levels observed to be populated in the particle spectroscopy experiment.

The  $(d,p)$  and  $(t,\alpha)$  reactions did not populate levels of high spin. Energy levels involving the  $1h_{11/2}$  neutron hole were not populated at all in the  $(t,\alpha)$  reaction. In the  $(d,p)$  reaction, the  $l_n = 5$  levels are

not among the strongest peaks in the spectra. The  $(n, \gamma)$  reaction (Alexeev et al., 1975) populated some levels of modest spin but generally did not populate levels of high spin. The  $^{130}\text{Te}(^7\text{Li}, 3n)$  reaction was used in the hope of gaining information on levels with higher spins. This heavy ion reaction is less selective in the levels populated than the single particle transfer reactions.

The heavy ion reaction proceeds via the compound nucleus reaction mechanism rather than the direct reaction process. The formation of the compound nucleus through the fusion of the heavy ion projectile and the target nucleus generally imparts large amounts of angular momentum and energy to the compound nucleus. The highly excited compound nucleus initially de-excites by the emission of particles, but eventually, the total energy is not sufficient to permit particle emission and  $\gamma$ -ray emission takes over.

Excitation functions can provide a means of identifying  $\gamma$ -rays with their nuclei of origin. The yields of the  $\gamma$ -rays are well defined functions of the bombarding energy. The cross-sections for the heavy ion reactions rise from a value of zero to some maximum value, then decrease as the bombarding energy is increased. The threshold energy and the energy for maximum yield depend upon the Q-value and the Coulomb barrier for the reaction.

Complications in the use of excitation functions arise when thick targets are used. The beam particles slow down and stop in the target. The measured yield at each bombarding energy represents the integrated yield from that bombarding energy down to zero energy. For bombarding energies well beyond the maximum cross-section of a given reaction, the measured yield approaches a constant value.

Gamma-gamma coincidence measurements provide additional information for identifying  $\gamma$ -rays with their nuclei of origin. These measurements identify coincidence relationships between the transitions. These relationships collect the  $\gamma$ -ray transitions together into small groups. Identifying one or more elements in the group usually provides an identification of the nucleus to which the group belongs.

## 5.2 Experimental Set-Up

### 5.2.1 $^{133}\text{Cs}(d,p)^{134}\text{Cs}$ Reaction

A thick metallic cesium target was used for the  $\gamma$ -ray investigation of the  $^{133}\text{Cs}(d,p)^{134}\text{Cs}$  reaction. A number of cesium compounds,  $\text{Cs}_2\text{O}$ ,  $\text{CsOH}$ ,  $\text{CsCl}$ , were tried initially as target material. The  $\text{Cs}_2\text{O}$  and  $\text{CsOH}$  targets decomposed under vacuum and while being bombarded with the ion beam. The  $\text{CsCl}$  target produced a number of  $^{38}\text{Cl}$

$\gamma$ -rays which were undesirable.

A long thin-walled plastic tube was used for a target chamber. Two tantalum apertures were mounted in the tube to act as collimators for the ion beam. Absorption of the  $\gamma$ -rays in the walls of the target chamber was minimal since the plastic consisted of low-Z materials and the walls were thin.

An aluminum target holder was constructed to serve as the end plug sealing the plastic tube. During the preparation of the target, a glove bag was connected to this tube. The glove bag containing the end section of the beam line and a sealed vial of cesium was filled with argon. The vial of cesium was warmed to body temperature to melt the cesium. The vial was broken open and molten cesium was poured into a recess in the target holder to make a target about 0.3 cm thick and 2.2 cm in diameter. An ice pack, outside the glove bag, was placed next to the wall of the glove bag. The target holder was held against the ice pack from within the glove bag to cool the cesium. When the cesium solidified, the target holder was inserted into the end of the plastic tube and the beam line was evacuated. The glove bag was then removed. The target was kept cold by placing an ice pack around the end of target holder. This ensured that the target remained solid during the experiment.

A  $1 \text{ cm}^3$  Ge(Li) detector and a  $15 \text{ cm}^3$  intrinsic germanium detector were used to collect the singles  $\gamma$ -ray data. The detectors were placed facing the front of the target, at about  $150^\circ$ . The detectors were between 10 and 15 cm. from target. Lead bricks were placed around the tube to shield the two detectors from  $\gamma$ -rays originating from the tantalum apertures.

The deuteron beam energy was 12.0 MeV, the same as the bombarding energy for the (d,p) particle spectroscopy experiment. The current on the target could not be monitored reliably. The presence of the ice against the target holder caused the electrometer to act erratically. The beam current (5-10 nA) was adjusted to provide an adequate count rate which gave about 10% dead time on the ADC's.

The detector signals were amplified in linear amplifiers and passed through linear gate and stretcher modules. The outputs of the linear gate and stretcher modules were used as the energy signals to the ADC's.

A  $^{152}\text{Eu}$  source was placed near the target and the spectra containing both the reaction  $\gamma$ -rays and the  $^{152}\text{Eu}$  source lines were collected. The well known  $\gamma$ -ray energies of the  $^{152}\text{Eu}$  source (Lederer and Shirley, 1978) were used to calibrate the spectra. The derived energies for the strongest reaction lines were then used to internally calibrate the singles spectra.

A standard three parameter coincidence set-up was used for the coincidence data collection. Two planar detectors, a 15 cm<sup>3</sup> intrinsic germanium and a 14 cm<sup>3</sup> Ge(Li), were used for the coincidence experiment. The detectors were placed facing the front of the target, at 150°. The distance to the target was less than 10 cm. Thin cadmium and copper absorbers were placed in front of the detectors to prevent low energy x-rays from reaching the detectors since the high count rate from the x-rays would overload the electronics.

Timing filter amplifiers amplified and shaped the detector signals for constant fraction timing discriminator (CFTD) modules. The CFTD modules provided fast negative signals for a time-to-amplitude converter (TAC). The discriminator thresholds were set to 0.50 volts. The 15 cm<sup>3</sup> detector supplied the start signal and the 14 cm<sup>3</sup> detector supplied the stop signal for the TAC whose resolving time was set to 100 nsec. The time peak was about 10 nsec (FWHM). The valid stop signal from the TAC was used to gate three ADC's, one for the time spectrum and one for each of the two energy spectra.

The output of the linear amplifier for the 15 cm<sup>3</sup> detector was connected to a second linear gate and stretcher module. This energy signal was put into a fourth ADC to accumulate a singles monitor spectrum.

At the end of the coincidence experiment, energy and efficiency calibrations were performed for the 14 cm<sup>3</sup> and 15 cm<sup>3</sup> detectors. The data acquisition was switched from the coincidence mode to a singles mode to obtain the calibration data. The energy calibration was done as described earlier for the singles experiment. For the efficiency calibration, two sources, <sup>182</sup>Ta and <sup>152</sup>Eu, were placed in the target chamber in place of the target and their spectra accumulated. The efficiencies of the detectors were determined from a comparison of the measured energies and relative intensities with those listed in the Table of Isotopes, 7th ed. (Lederer and Shirley, 1978).

Data acquisition was performed by a PDP-9 computer. The coincidence data were written as address recorded events on 2400 foot magnetic tapes. The total projections for each ADC were also collected. These were later used to set the energy and time gates.

The address recorded events were replayed on a PDP-15 computer and the coincidence spectra were accumulated. In this sorting process, gates were set on the time spectrum and on each of the energy spectra. Two time gates were set, one on the time peak, for the true plus chance events, and one on the time background, for chance events. The energy gates consisted of a gate on the  $\gamma$ -ray photopeak and two gates on the Compton back-

ground, one on each side of the photopeak. Counts were added to the appropriate spectrum when events occurred in the photopeak and time peak gates. When events occurred in a background gate, either time or energy, counts were subtracted from the appropriate spectrum. Thus, the resultant spectra represented the true events with the Compton background removed.

### 5.2.2 $^{130}\text{Te}(^7\text{Li},3n)^{134}\text{Cs}$ Reaction

The target was a pellet of isotopically enriched  $^{130}\text{Te}$  in the oxide form,  $^{130}\text{TeO}$ . The isotopic composition of the material as stated by the supplier (Union Carbide Corporation) is listed in Table 5.1. The  $^{130}\text{TeO}$  pellet was mounted on a tantalum backing. The pellet was sufficiently thick that the ion beam was stopped in the target.

The target chamber that was used in the (d,p) experiment was used in this experiment but a slightly different target holder was used. The pellet and its backing were mounted in the tube, perpendicular to the beam direction with an end plug to seal the chamber.

A  $15\text{ cm}^3$  planar intrinsic germanium and a  $37\text{ cm}^3$  coaxial Ge(Li) detector were used. The detectors were placed facing the target at approximately  $135^\circ$  to the beam direction and less than 10 cm from the target. Lead bricks were placed on either side of the beam pipe

Table 5.1

Isotopic Composition of the Enriched  $^{130}\text{TeO}$  Target

Isotope	Atomic Percent	Precision
$^{120}\text{Te}$	< .02	----
$^{122}\text{Te}$	0.04	$\pm 0.01$
$^{123}\text{Te}$	0.02	0.01
$^{124}\text{Te}$	0.02	0.01
$^{125}\text{Te}$	0.03	0.01
$^{126}\text{Te}$	0.10	0.02
$^{128}\text{Te}$	0.30	0.05
$^{130}\text{Te}$	99.49	0.05

to reduce the chance of  $\gamma$ -rays scattering directly from one detector into the other. Thin cadmium and copper absorbers were placed in front of the detectors to eliminate the counting of low-energy x-rays.

A beam of  ${}^7\text{Li}$  ions was produced in a Middleton type negative ion source and accelerated to energies of 27 to 34 MeV with the McMaster van de Graaff accelerator. A beam current of 0.06 nA, measured on the target provided an adequate count rate for the experiment.

To obtain excitation functions,  $\gamma$ -ray spectra were collected for a series of bombarding energies from 27 MeV to 34 MeV. The total charge deposited in the target was used to normalize the  $\gamma$ -ray yields. The  $\gamma$ -ray spectra were collected in singles mode with a PDP-9 computer. The areas of the photopeaks of the  $\gamma$ -rays were extracted from the spectra with the computer program SOFT on the PDP-15 computer. After normalizing the yield, plots of the  $\gamma$ -ray yields versus the incident beam energies were made.

Beam energies of 32 and 34 MeV were selected for the coincidence experiment. Since the yield for several  $\gamma$ -rays which matched in energy with  $\gamma$ -rays reported in the (n, $\gamma$ ) work of Alexeev et al. (1975) appeared to still be increasing up to 34 MeV, it was decided to run at 34 MeV. During the experiment, the stability of the accelerator deteriorated, high voltage sparking

occurred, and the energy was lowered to 32 MeV.

The  $\gamma$ - $\gamma$  coincidence electronics were set-up similarly to the set-up described for the  $^{133}\text{Cs}(d,p\gamma\gamma)$  experiment. Unlike the (d,p $\gamma$ ) experiment, no singles experiment was conducted separately. Singles  $\gamma$ -ray data were obtained from the monitor spectrum. This was accumulated from the 15 cm<sup>3</sup> detector with the  $\gamma$ - $\gamma$  coincidence data collection proceeding simultaneously. Hence the count rate was not ideally suited for the singles data acquisition and the energy resolution in the singles spectra was not as good as it could be.

Energy and efficiency calibrations were also performed as described for the  $^{133}\text{Cs}(d,p\gamma)$  experiment. The same radioactive sources were used in this experiment.

### 5.3 Data Analysis

#### 5.3.1 $^{133}\text{Cs}(d,p\gamma)^{134}\text{Cs}$ Reaction

The ( $^{133}\text{Cs} + d$ ) reaction produced several final nuclei. The  $\gamma$ -ray spectra contained lines from  $^{133}\text{Cs}$ ,  $^{134}\text{Cs}$ ,  $^{133}\text{Ba}$ , and  $^{134}\text{Ba}$ . The  $\gamma$ -rays associated with the  $^{133}\text{Cs}(d,p\gamma)$  reaction were identified on the following basis:

- i) their energies agreed with  $\gamma$ -ray transitions assigned to  $^{134}\text{Cs}$  by Alexeev et al. in the (n, $\gamma$ ) study,

ii) their energies fitted the transition energies between levels in  $^{134}\text{Cs}$  known from the (d,p) particle spectroscopy study to  $\pm 5$  keV,

iii) the  $\gamma$ -rays were observed to have coincidence relationships with  $\gamma$ -rays already identified with  $^{134}\text{Cs}$ .

The lines not specifically identified with competing reactions in the target, from reactions in the slits, or from reactions on impurities such as O, F, C, Na, etc. are also considered, at least provisionally, to belong to  $^{134}\text{Cs}$ .

#### 5.3.1.1 Singles $\gamma$ -ray Measurements

The earlier singles experiment collected data for about 10 hours. Some weak lines which did not appear in this earlier singles experiment were seen in the monitor spectrum. The singles data from the monitor spectrum were collected for about thirty hours with the  $15\text{ cm}^3$  detector and the spectrum is shown in figure 5.1. The energy resolution is about 1.1 keV at 121.8 keV.

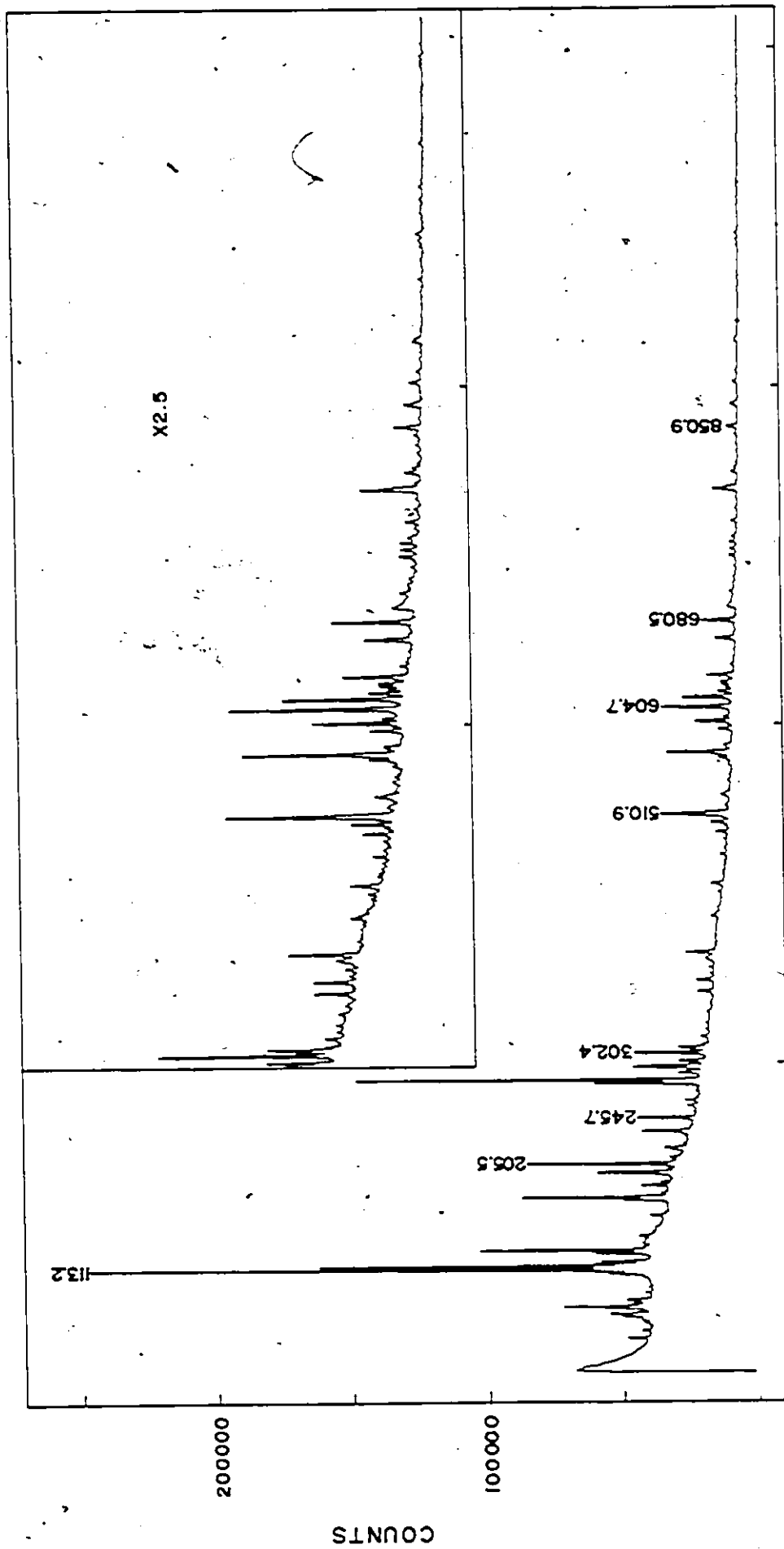
The relative yields of the  $\gamma$ -rays are presented in table 5.2. The yields were corrected for detector efficiency and target absorption, and then normalized to the yield of the 116.2 keV line. The detector efficiency corrections were made with the efficiency calibration described earlier.

Target absorption corrections were more diffi-

---

Figure 5.1  
Singles  $\gamma$ -ray spectrum for ( $^{133}\text{Cs} + d$ ) with 12 MeV  
deuterons.

Sample



cult to make. The fraction of  $\gamma$ -rays that are detected is given by:

$$f_{\gamma} = \frac{\int_0^R \sigma(E) e^{-\mu x / \cos \theta} dx}{\int_0^R \sigma(E) dx}$$

where  $\sigma(E)$  is the reaction cross-section at beam energy,  $E$ ,  $\mu$  is the mass attenuation coefficient,  $\theta$  is the angle between the detector and the normal to the target, and  $R$  is the range of the deuteron in the target. The mass attenuation coefficients for  $\gamma$ -ray energies from 60 to 200 keV were obtained from the compilation by Storm and Israel (1970). The depth-energy relationship was estimated from the stopping power tabulation of Northcliffe and Schilling (1970). Stopping power data are not given for cesium, so data for silver and europium were interpolated to obtain the stopping power for cesium.

The reaction cross-section as a function of energy was estimated from the excitation functions for the  $^{116}\text{Cd}(d,p)$  (Padalko et al., 1974) and  $\text{Sn}(d,p)$  (Madueme et al., 1976) reactions. These excitation functions provided estimates for the relative cross-sections for deuteron energies from 7 to 12 MeV. The excitation functions show that the cross-section at 7 MeV is about 8 times smaller than the cross-section at 12 MeV. The contributions to the integral become very small for deuteron energies less than 7 MeV, so the

calculation was cut off at 7 MeV.

A 5 MeV loss in the beam energy corresponds to penetrating to a depth of  $239 \text{ mg/cm}^2$ .  $f_\gamma$  is calculated to be 36% for 60 keV  $\gamma$ -rays, 76% for 100 keV  $\gamma$ -rays and 96% for 200 keV  $\gamma$ -rays. The correction becomes negligible for  $\gamma$ -ray energies greater than 200 keV. Uncertainties in the corrections come from the difficulties encountered in estimating the cross-sections, the depth of penetration, and the finite solid angle of the detector. These uncertainties amount to about 10% of the correction.

Low energy singles data were obtained with the  $1 \text{ cm}^3$  detector. Lines were found at 38.5, 60.1, 67.2, 74.0 and 86.9 keV. All but the 38.5 keV line were also observed in the  $15 \text{ cm}^3$  detector. A weak peak was observed at 38.5 keV in the  $1 \text{ cm}^3$  detector. No relative yield is given for this line because the detector efficiency is not known. Detector efficiency corrections were not made for the  $1 \text{ cm}^3$  detector since an efficiency calibration was not obtained. The low energy 37.0 keV transition suggested by Alexeev et al. (1975) to explain a coincidence relationship was not found. The 44.1 keV transition suggested by Alexeev et al. (1975) and reported by them in a later publication (Alexeev et al., 1978) was also not observed in the (d,p $\gamma$ ) spectrum.

Table 5.2

$\gamma$ -ray Energies and Relative Yields in the ( $^{133}\text{Cs} + d$ )  
Reactions at  $E_d = 12 \text{ MeV}$

Energy (keV)	Relative Yield*
59.8(1)	30.6 (4.0)
66.9(1)	14.6 (1.0)
69.4(2)	42.0 (4.8)
72.8(2) <sup>e</sup>	48.5 (5.3)
74.6(2) <sup>d,e</sup>	64.0 (6.0)
79.4(2) <sup>a</sup>	30.4 (1.0)
80.7(1) <sup>a</sup>	64.0 (6.1)
84.6(1) <sup>e</sup>	6.8 (0.7)
86.9(1) <sup>d,e</sup>	14.2 (1.4)
92.9(1)	2.2 (0.3)
97.3(1)	1.3 (0.3)
109.7(1)	11.5 (0.4)
113.2(3) <sup>c,d</sup>	178.0 (4.6)
116.2(1)	100.0
118.2(1)	15.6 (0.5)
120.5(1)	13.7 (0.5)
127.4(1)	20.3 (0.9)
130.0(1)	57.0 (1.8)
139.8(1)	2.8 (0.2)
142.5(1)	5.3 (0.5)
149.4(1)	1.1 (0.2)
160.4(1) <sup>a</sup>	4.7 (0.4)
174.2(1)	13.9 (0.7)
176.2(1)	56.0 (3.5)

Table 5.2 (continued)

Energy (keV)	Relative Yield
179.8(1)	2.8 (0.6)
186.7(1)	10.0 (0.8)
189.8(1)	3.7 (0.4)
197.4(2)	16.0 (2.0)
198.3(2)	28.0 (3.3)
200.6(1)	2.8 (0.7)
205.5(1)	54.3 (2.5)
207.7(1)	2.1 (0.1)
209.4(1)	2.0 (0.1)
211.2(1)	4.1 (0.2)
218.3(2)	4.9 (0.2)
219.8(2)	8.2 (0.3)
229.0(1)	1.5 (0.1)
232.1(3)	4.8 (0.2)
234.0(1)	28.0 (1.0)
245.7(1)	37.0 (1.2)
251.2(1)	0.8 (0.1)
254.8(1)	1.8 (0.1)
256.2(1)	6.0 (0.3)
260.9(1)	8.6 (0.3)
263.6(1)	2.3 (0.1)
268.9(1)	1.8 (0.1)
271.6(1)	2.2 (0.1)
276.0(1) <sup>a</sup>	92.0 (4.0)
278.8(3) <sup>b,d</sup>	242.0 (8.0)
285.7(1) <sup>c</sup>	13.5 (0.6)
287.0(1)	8.4 (0.3)
290.5(2) <sup>b</sup>	43.0 (3.0)
291.6(2) <sup>b</sup>	41.2 (2.7)
293.3(3)	3.4 (0.2)

Table 5.2 (continued)

Energy (keV)	Relative Yield
295.5(1)	23.6 (0.8)
302.4(3) <sup>a,b,d</sup>	74.2 (5.0)
306.4(3)	9.4 (0.4)
307.8(3)	21.2 (0.7)
309.6(2) <sup>b,d</sup>	5.0 (0.2)
316.2(2)	2.1 (0.1)
317.6(2)	5.3 (0.3)
322.9(1)	2.6 (0.2)
328.7(1)	3.1 (0.2)
338.6(1)	5.4 (0.3)
345.1(1)	2.2 (0.2)
347.2(1)	1.8 (0.2)
353.4(1)	2.1 (0.2)
356.1(1) <sup>a,d</sup>	19.7 (0.7)
366.6(1)	16.1 (0.6)
368.0(1)	2.4 (0.2)
371.7(1)	3.8 (0.3)
377.0(1)	6.1 (0.3)
381.9(1)	0.9 (0.1)
384.5(1)	6.5 (0.3)
385.9(1) <sup>b</sup>	8.5 (0.3)
387.4(1)	3.3 (0.2)
390.3(1) <sup>c</sup>	45.8 (1.6)
393.7(1)	1.2 (0.2)
401.8(1)	1.9 (0.2)
405.3(1)	1.1 (0.2)
407.6(1)	1.3 (0.2)
412.6(1)	1.9 (0.2)
417.3(1)	2.1 (0.2)
421.6(1)	14.7 (0.6)

Table 5.2 (continued)

Energy (keV)	Relative Yield
424.3(1)	7.3 (0.4)
427.8(1)	3.9 (0.4)
439.0(1)	2.4 (0.2)
442.7(1)	5.9 (0.3)
449.4(3)	5.2 (0.3)
450.6(3)	13.6 (1.8)
451.4(3)	8.5 (1.1)
454.4(3)	0.7 (0.1)
458.1(1)	4.8 (0.3)
461.0(1)	4.0 (0.3)
464.9(1)	2.8 (0.2)
469.6(1)	3.0 (0.2)
475.3(1) <sup>c</sup>	9.7 (0.4)
480.9(2)	2.8 (0.3)
482.1(3) <sup>b</sup>	2.7 (0.3)
488.2(3)	1.7 (0.2)
489.8(3)	3.5 (0.2)
492.1(3)	4.0 (0.3)
495.2(1)	25.8 (1.0)
500.1(1)	7.0 (0.4)
503.6(2)	40.0 (1.4)
510.9(2)	420.0(18.0)
518.8(3)	3.8 (0.7)
519.7(3)	3.8 (0.7)
525.7(3)	2.3 (0.6)
527.3(3) <sup>b</sup>	7.6 (0.8)
528.2(3)	10.1 (0.8)
529.6(2)	6.8 (0.5)
539.8(3)	4.8 (0.7)
540.6(3)	4.4 (0.7)

Table 5.2 (continued)

Energy (keV)	Relative Yield
544.7(2) <sup>c</sup>	4.3 (0.3)
554.5(2)	8.3 (0.5)
560.4(2) <sup>a,b</sup>	34.4 (1.2)
563.3(4) <sup>c</sup>	38.0 (1.3)
565.2(4) <sup>b</sup>	162.0 (5.0)
570.2(3)	6.6 (0.3)
572.1(3) <sup>b</sup>	10.7 (0.4)
585.3(2) <sup>b,c</sup>	28.6 (1.1)
589.0(2)	3.9 (0.3)
592.1(2) <sup>b,c,d</sup>	87.5 (9.0)
595.9(2) <sup>b</sup>	14.4 (0.6)
604.7(2) <sup>c</sup>	191.0 (16.0)
610.9(2)	7.9 (0.4)
613.3(2)	145.0 (5.0)
618.2(2) <sup>b</sup>	40.0 (1.4)
621.8(2) <sup>b</sup>	19.2 (0.8)
624.5(2) <sup>a,c</sup>	30.7 (1.1)
626.9(2)	32.0 (1.2)
632.7(2) <sup>a,b</sup>	72.6 (3.0)
638.0(2) <sup>b</sup>	0.6 (0.2)
641.8(2)	10.1 (0.5)
645.7(2)	4.8 (0.3)
649.2(2)	4.3 (0.3)
654.3(2)	3.3 (0.3)
658.6(2)	1.7 (0.2)
664.9(2) <sup>b</sup>	84.0 (3.0)
668.6(2)	6.3 (0.4)
676.0(2) <sup>b</sup>	7.7 (0.5)
680.5(2)	126.0 (5.0)
705.8(2) <sup>a</sup>	17.5 (1.0)

Table 5.2 (continued)

Energy (keV)	Relative Yield
713.0(2)	3.8 (0.3)
714.5(2)	4.2 (0.3)
718.2(2)	9.2 (0.5)
722.8(2)	2.7 (0.3)
728.3(2)	9.0 (0.6)
733.6(2)	5.0 (0.4)
737.4(2)	33.0 (1.3)
743.5(2)	33.0 (1.3)
750.2(2)	19.0 (1.0)
752.8(2)	3.8 (0.3)
754.8(2)	11.0 (0.5)
768.0(2)	28.7 (1.2)
775.5(2)	4.0 (0.3)
779.0(2)	11.2 (0.6)
788.6(2)	14.2 (0.7)
795.2(2) <sup>c</sup>	243.0(12.0)
797.9(3)	112.0 (6.0)
802.1(3)	9.7 (0.6)
811.1(3) <sup>b,c</sup>	41.3 (1.7)
815.1(3)	23.0 (1.0)
819.4(3)	6.3 (1.0)
826.4(3)	3.0 (0.3)
828.9(3)	5.4 (0.4)
835.5(3)	10.2 (0.6)
839.3(3)	2.1 (0.3)
850.9(3) <sup>b</sup>	70.0 (3.0)
859.1(3) <sup>b</sup>	5.2 (0.4)
890.1(3)	28.0 (1.1)
899.7(3) <sup>c</sup>	10.7 (0.5)
916.5(3)	2.8 (0.3)

Table 5.2 (continued)

Energy (keV)	Relative Yield
920.7(3)	3.2 (0.3)
926.6(3)	13.3 (0.7)
929.0(3)	11.6 (0.7)
962.7(3)	2.7 (0.3)
969.7(3)	5.0 (0.4)
980.8(3)	8.8 (0.5)
994.5(3)	3.6 (0.4)
997.7(3)	8.3 (0.5)
1009.6(3) <sup>b</sup>	12.4 (0.7)
1014.7(3)	25.0 (1.1)
1020.4(3)	31.0 (1.3)
1034.4(3)	4.3 (0.4)
1039.3(3) <sup>c</sup>	17.0 (1.5)
1051.1(3)	17.0 (1.5)
1061.9(3)	16.0 (1.4)
1067.4(3)	7.7 (0.6)
1100.6(3) <sup>b</sup>	10.7 (1.1)
1105.0(3)	4.0 (0.4)
1128.1(3)	3.6 (0.4)
1134.1(3)	3.8 (0.4)
1140.7(3)	2.2 (0.2)
1145.3(3)	4.0 (0.4)
1176.6(3)	12.0 (1.2)
1188.1(3)	8.0 (0.8)

a  $^{133}\text{Cs}$ b  $^{133}\text{Ba}$ c  $^{134}\text{Ba}$ d  $^{134}\text{Cs}$  contributes part of the line

e lead x-rays

\* Yields are normalized to the 116 keV line and corrected for target absorption and detector efficiency.

### 5.3.1.2 Coincidence Measurements

The coincidence data established relationships between the  $\gamma$ -rays and helped to identify the  $\gamma$ -rays observed in the singles spectra. A selection of the coincidence spectra is shown in figures 5.2 (a and (b). A summary of the gates and the coincident  $\gamma$ -rays is given in table 5.3.

The total projected time spectrum showed a slightly asymmetric peak. There was a longer tail on the right-hand side of the peak. A close examination of the time spectra for individual  $\gamma$ -rays revealed a time "walk" problem. The time peaks for the low energy  $\gamma$ -rays were displaced from the locations of the time peaks for the higher energy lines. The time peaks for the low energy lines were also highly asymmetric, with long tails on one side. Long tails on time peaks are usually indicative of some delayed coincidence events. However, this did not appear to be the case in this experiment. These low energy lines were already known from the  $(n,\gamma)$  reaction (Alexeev et al., 1975). Some of these lines were reported to be in delayed coincidence, but not all of the lines. As a result, no statements concerning the lifetimes of the levels can be made on the basis of the  $(d,p)$   $\gamma$ - $\gamma$  data.

The large amount of time "walk" made it difficult to collect coincidence information between high and low energy  $\gamma$ -rays. Low energy lines which might otherwise appear in some high energy gates are very weak or absent. The 60 keV gate listed in table 5.3 was seen only weakly for the 15 cm<sup>3</sup> detector. The 14 cm<sup>3</sup> detector did not show a 60 keV line at all.

A doublet, at 218.3 and 219.8 keV, appears in the singles spectrum (table 5.2). In the projections a wide peak appears at 219 keV which is probably the two lines, poorly resolved.

In addition to the coincident lines listed in table 5.3, the 113 keV gated spectrum contains lines at 390, 604 and 812 keV which are identified with <sup>134</sup>Ba (Morek et al., 1980 and Lederer and Shirley, 1978). The 390, 604 and 812 keV lines do not appear in coincidence with the 277, 589, 737 or 929 keV lines.

The 278 keV line is the strongest line in the singles spectrum. The 278 keV line belongs to <sup>133</sup>Ba since  $\gamma$ -rays identified with <sup>133</sup>Ba appear in coincidence with the 278 keV line as expected from Lederer and Shirley (1978). However, the coincident lines listed in table 5.3 for the 277+279 keV gate do not appear in coincidence with  $\gamma$ -rays identified with <sup>133</sup>Ba.

Table 5.3

$\gamma$ -ray Gates and the Coincident  $\gamma$ -rays for  $^{134}\text{Cs}$

Gate Energy (keV)	Coincident Lines (keV)
60	113, 130
87	118, 279
113	(277), 589, 737, (929)*
116	200, 218, (256), 307, (356)
118	87, (177), 279
120	205, 256, 269, (450)
130	186, 261, 263
142	(174), 234
174	219
186	130
189	295
198	293, 309
200	307
205	120, 269, 279, 295, (554), 593
218 + 219	116, 174, 176, 234, 307
234	142, 219
245	(87), (120)
256	120
261	130
269	120, 205
277 + 279	113, 118, 205, (589)
295	189, 295
307	(176), 200, 218, (232)
450	(120)
554	(205)
593	(205)
737	(113)

\* ( ) denotes doubtful coincidences. \*

The 593 keV line is observed to be in coincidence with several lines from  $^{133}\text{Ba}$  as well as with a 205 keV line which is tentatively identified with  $^{134}\text{Cs}$ . No 205 keV line is known to exist in  $^{133}\text{Ba}$ .

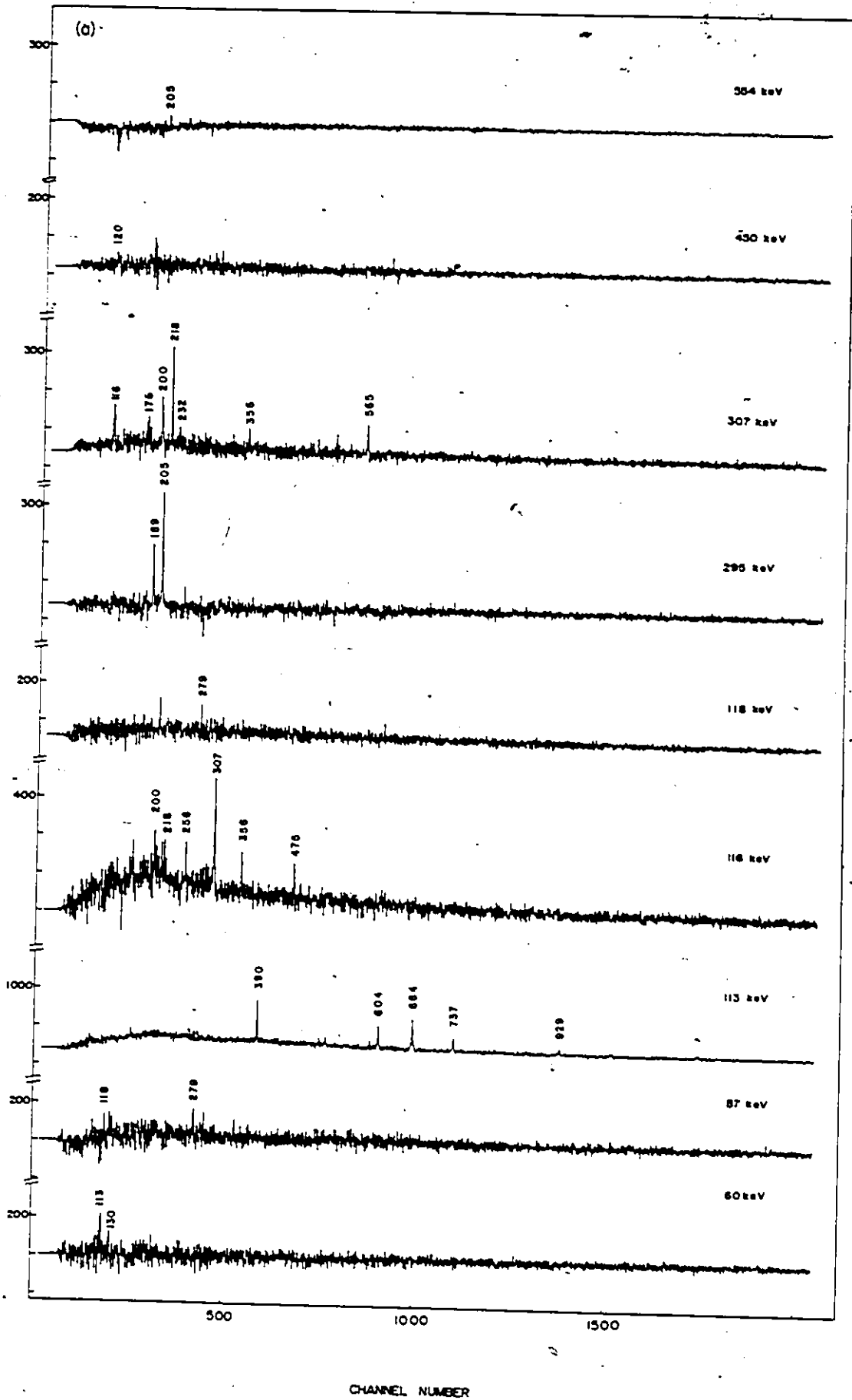
A detailed discussion of the coincidence data for  $^{134}\text{Cs}$  and the placement of these lines in the level scheme is presented in the next chapter.

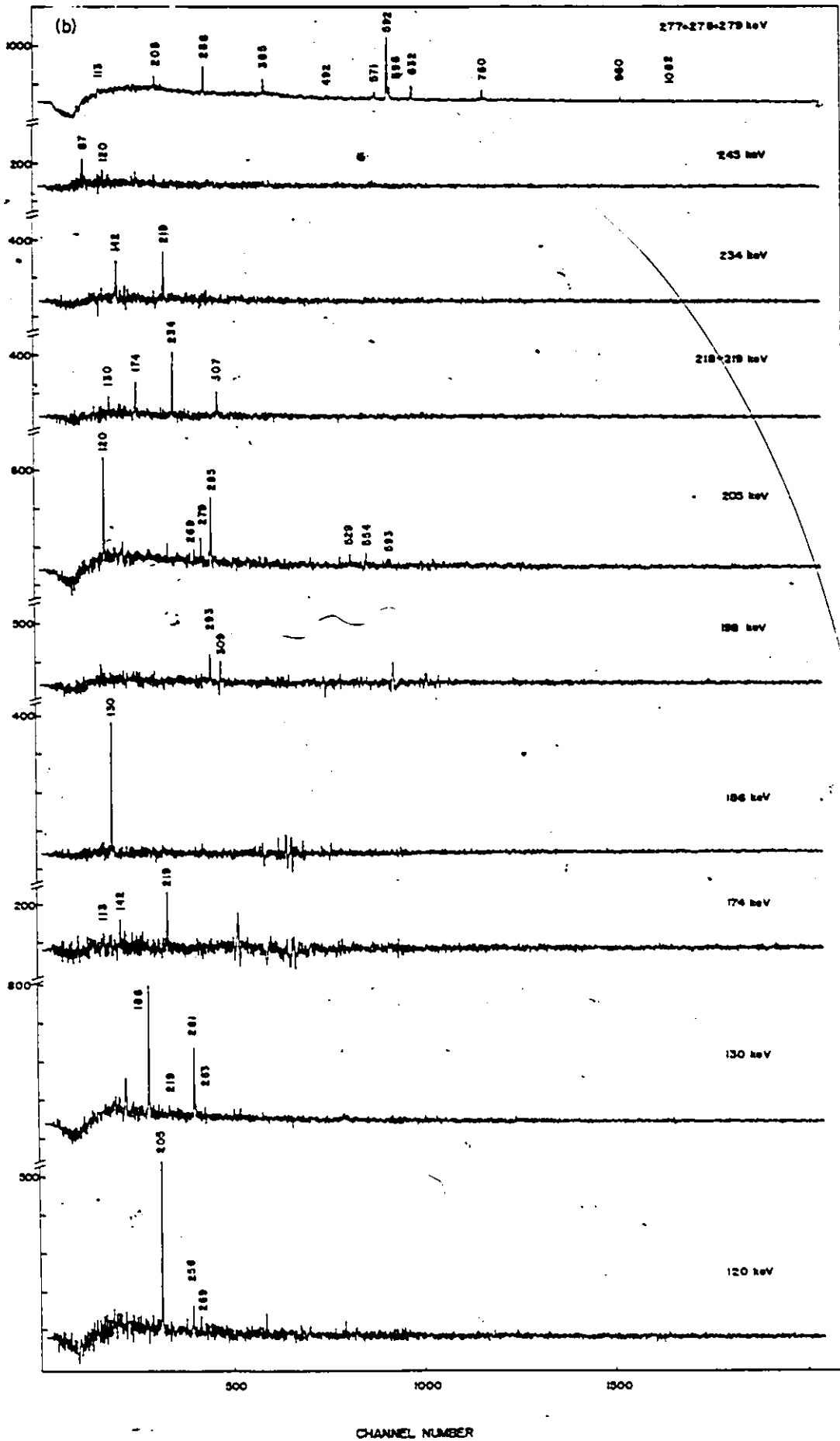
### 5.3.2 $^{130}\text{Te}(^7\text{Li},3n)^{134}\text{Cs}$ Reaction

The  $^{130}\text{Te}(^7\text{Li},3n)$  reaction was expected to populate levels in  $^{134}\text{Cs}$  which were not observed in the other studies. A major difficulty with heavy ion reactions, like ( $^{130}\text{Te} + ^7\text{Li}$ ), is that many reaction channels are open. This results in  $\gamma$ -rays from many nuclei being detected. It is not easy to identify the observed  $\gamma$ -rays with their nuclei of origin, especially when the transitions have not been reported in other studies. Also, many of the  $\gamma$ -ray energies may be close together, giving doublet and sometimes multiplet lines in the  $\gamma$ -ray spectra.

Figure 5.2

Coincidence spectra from the ( $^{133}\text{Cs} + d$ ) reactions: a) gates were set on the 15 cm<sup>3</sup> detector, b) gates were set on the 14 cm<sup>3</sup> detector. The 277+278+279 keV gate is triplet with 277 and 279 keV from  $^{134}\text{Cs}$  and 278 keV from  $^{133}\text{Ba}$ .





### 5.3.2.1 Decay Spectrum

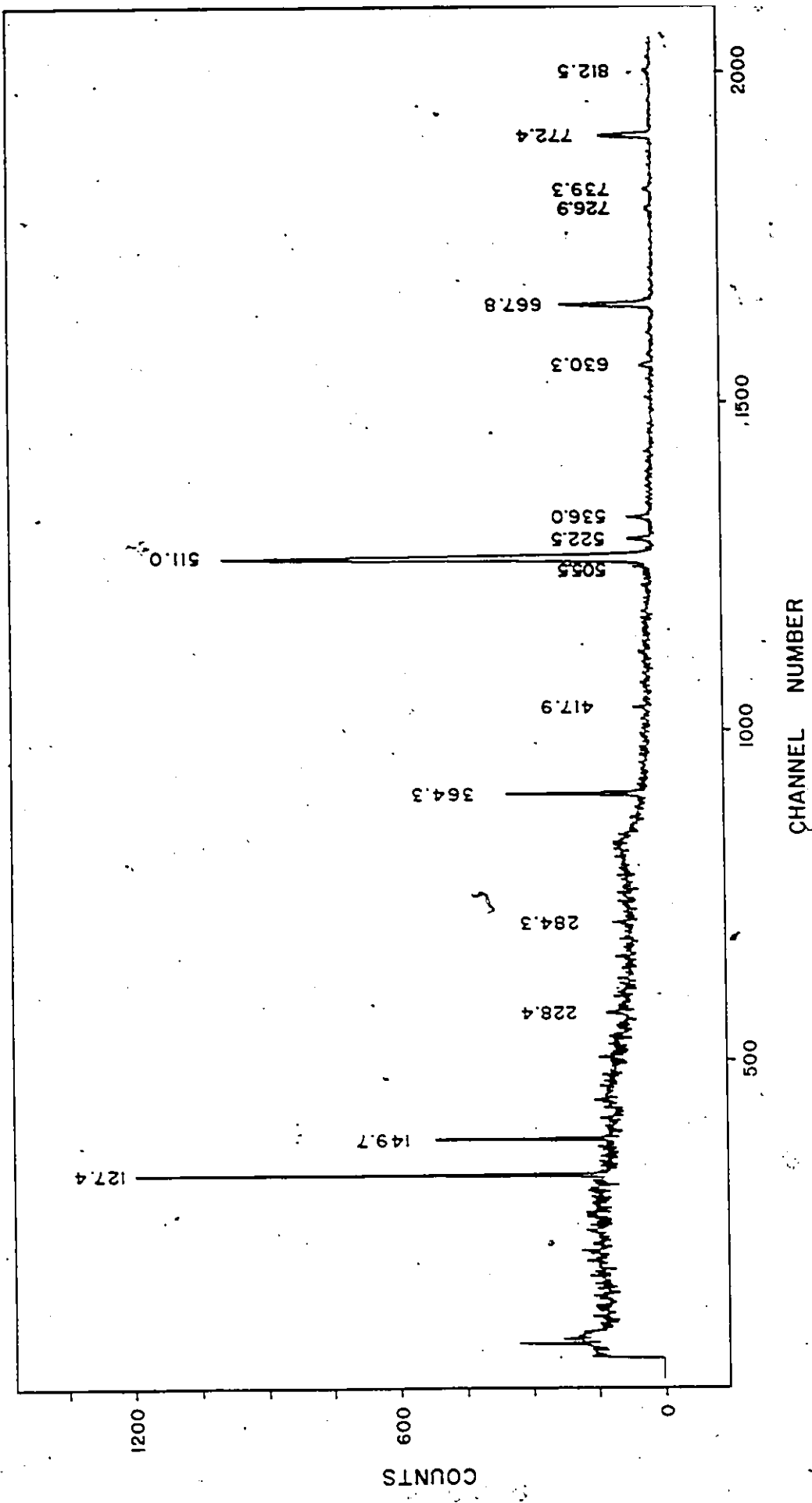
Some of the nuclei produced in the ( $^{130}\text{Te} + ^7\text{Li}$ ) reaction were identified from the decay spectrum. After the target had been irradiated for about 30 hours with 34 MeV  $^7\text{Li}$  ions, the beam was turned off and a  $\gamma$ -ray spectrum was collected for about 20 minutes. The lines in the spectrum originate from long lived isomers and the beta decay of unstable nuclei produced in the irradiation. A list of the decay lines is shown in table 5.4 and the decay spectrum is shown in figure 5.3. The 127.5 keV line indicates that  $^{134}\text{Cs}$  was produced in the 138 keV isomer state. There was no evidence for ground state production but this is not surprising since the ground state of  $^{134}\text{Cs}$  has a half-life of 2.06 years. Other reactions that were identified from this spectrum are  $^{130}\text{Te}(^7\text{Li}, \alpha n)^{132}\text{I}$ ,  $^{130}\text{Te}(^7\text{Li}, \alpha 2n)^{131}\text{I}$  and  $^{130}\text{Te}(^7\text{Li}, \alpha 3n)^{130}\text{I}$ . The half-lives of the reaction products are 2.9 hr for  $^{134m}\text{Cs}$ , 12.36 hr for  $^{130}\text{I}$ , 9.2 min for  $^{130m}\text{I}$ , 8.04 days for  $^{131}\text{I}$  and 2.28 hr. for  $^{132}\text{I}$ . The stable  $^{133}\text{Cs}$  could not be identified in this manner nor could  $^{135}\text{Cs}$  because of its very long half-life ( $2.3 \times 10^6$  years).

Table 5.4  
Residual Activity in  $^{130}\text{Te}$  Target

Energy (keV)	Relative Yield	Source
127.4 $\pm$ 0.1	100	$^{134\text{m}}\text{Cs}$
149.7 $\pm$ 0.1	49 (1)	$^{131\text{m}}\text{Te}$
228.4 $\pm$ 0.1	13 (2)	
284.3 $\pm$ 0.1	14 (3)	$^{132}\text{I}$
364.3 $\pm$ 0.1	190(13)	$^{131}\text{I}$
417.9 $\pm$ 0.2	17 (3)	$^{130}\text{I}$
505.5 $\pm$ 0.2	23 (4)	$^{132}\text{I}$
522.5 $\pm$ 0.2	60 (7)	$^{132}\text{I}$
536.0 $\pm$ 0.2	50 (6)	$^{130}\text{I}$
630.3 $\pm$ 0.2	52 (6)	$^{132}\text{I}$
636.5 $\pm$ 0.2	12 (3)	$^{131}\text{I}$
667.8 $\pm$ 0.2	439(26)	$^{130}\text{I}, ^{132}\text{I}$
726.9 $\pm$ 0.3	25 (5)	$^{131}\text{Te}$
739.3 $\pm$ 0.3	37 (5)	$^{130}\text{I}$
772.4 $\pm$ 0.3	322(22)	$^{132}\text{I}$
812.5 $\pm$ 0.3	29 (5)	$^{132}\text{I}$

Figure 5.3

The decay spectrum of the  $^{130}\text{Te}$  target following the  $(^{130}\text{Te} + ^7\text{Li})$  reaction at 34 MeV. The spectrum was collected for 20 minutes following about 30 hours of irradiation.



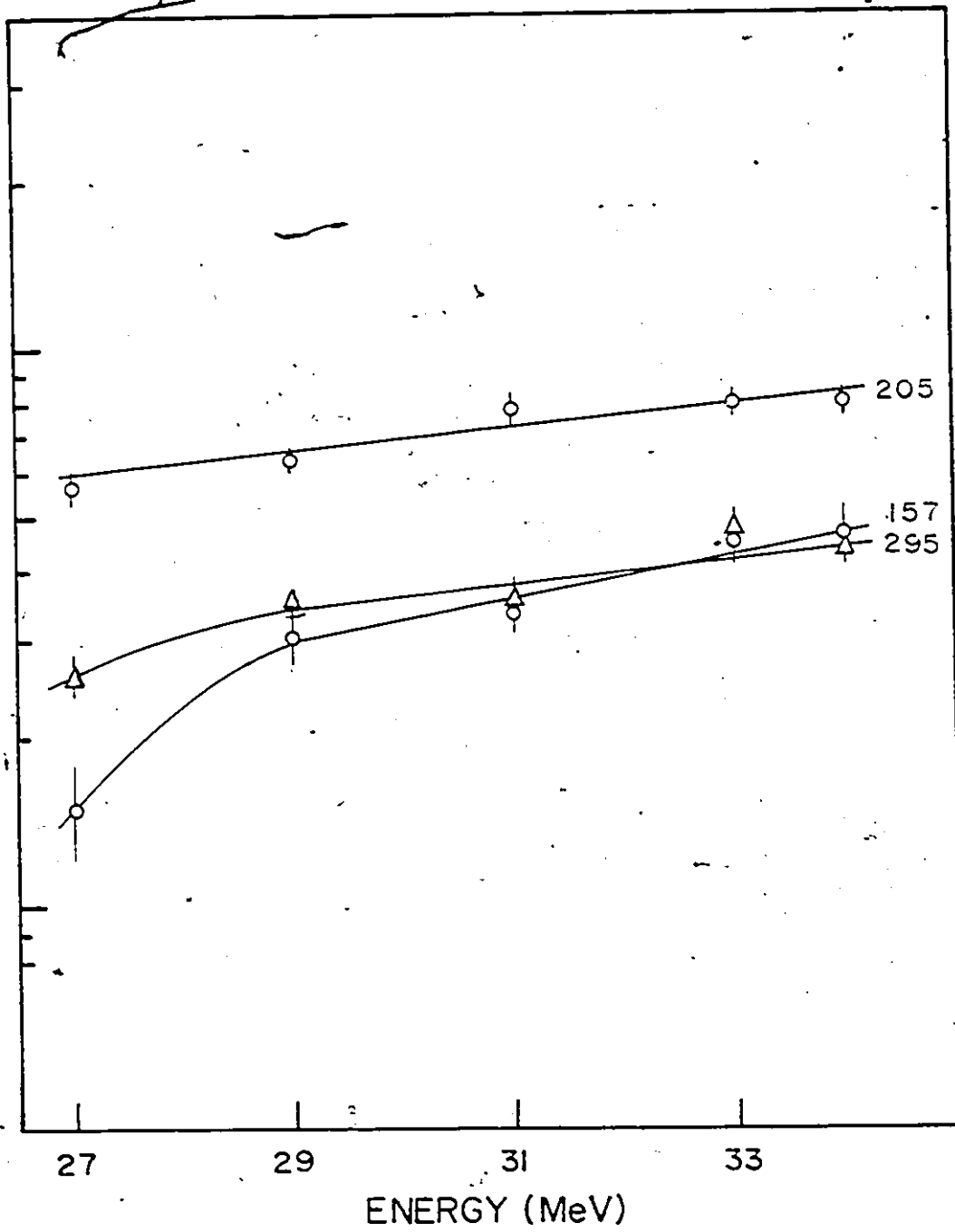
### 5.3.2.2 Excitation Functions

The lines attributed to the  $^{133}\text{Cs}$  nucleus were very strong in the singles measurements and showed very steeply rising excitation functions. This suggested that the bombarding energies at which the experiment was conducted were too high. The  $(^7\text{Li},4n)$  reaction being very strong meant that the bombarding energy was well past the energy at which the cross-section for the  $(^7\text{Li},3n)$  reaction would be greatest. The 32 and 34 MeV bombarding energies were above the 24.6 MeV Coulomb barrier for  $^7\text{Li}^{3+}$  ions on  $^{130}\text{Te}$ . Since the Q-value for the  $(^7\text{Li},4n)$  reaction is -16.637 MeV and the Q-value for the  $(^7\text{Li},3n)$  reaction is -9.746 MeV (Gove and Wapstra, 1972), the bombarding energies are also beyond the thresholds for the  $(^7\text{Li},4n)$  and the  $(^7\text{Li},3n)$  reactions. At these bombarding energies the  $(^7\text{Li},3n)$  cross-section would be small so very little  $^{134}\text{Cs}$  is expected to be produced. The excitation functions for the  $(^7\text{Li},3n)$  reaction are expected to be nearly constant at the higher bombarding energies.

One group of lines, 157, 205 and 295 keV, were observed to display this behaviour. Their excitation functions are shown in figure 5.4. The 205 keV and 295 keV lines were also found in the  $^{133}\text{Cs}(d,p)$   $\gamma$ -ray study

Figure 5.4

Excitation functions for the 157, 205 and 295 keV lines in the ( $^{130}\text{Te} + ^7\text{Li}$ ) reaction. The solid curves are intended as a guide for the eye.



and are reported by Alexeev et al. (1975) so there seems to be little doubt that these lines belong to  $^{134}\text{Cs}$ .

#### 5.3.2.3 Coincidence Measurements

There were some difficulties in identifying the lines belonging to  $^{134}\text{Cs}$ . The 157, 205, 295 and 418 keV lines were found in coincidence and are assumed to belong to  $^{134}\text{Cs}$  from the  $^{130}\text{Te}(^7\text{Li},3n)$  reaction. The coincidence spectra for gates on 157, 205, 295 and 418 keV are shown in figure 5.5. The gates and the coincident  $\gamma$ -rays are tabulated in table 5.5.

The discussion of the placement of these transitions in the level scheme is presented in section 6.2.

#### 5.3.2.4 Singles Measurements

Table 5.6 give the relative yields for the lines identified as belonging to  $^{134}\text{Cs}$  in the  $(^7\text{Li},3n)$  reaction at 34 MeV. The 205.6 keV yield was used for the normalization since it was positively identified as belonging to  $^{134}\text{Cs}$ . The 295 keV line is stronger than the 205 keV line in the  $(^7\text{Li},3n)$  reaction while the reverse is true in the  $(d,p\gamma)$  reaction. Representative lines from other reactions which occurred in the  $^{130}\text{Te}$  target are included for comparison.

Figure 5.5

Coincidence spectra for the  $^{130}\text{Te}(^7\text{Li},3n)$  reaction with 34 MeV  $^7\text{Li}$  ions. Gates are set on  $\gamma$ -ray energies of 157, 205, 295 and 418 keV.

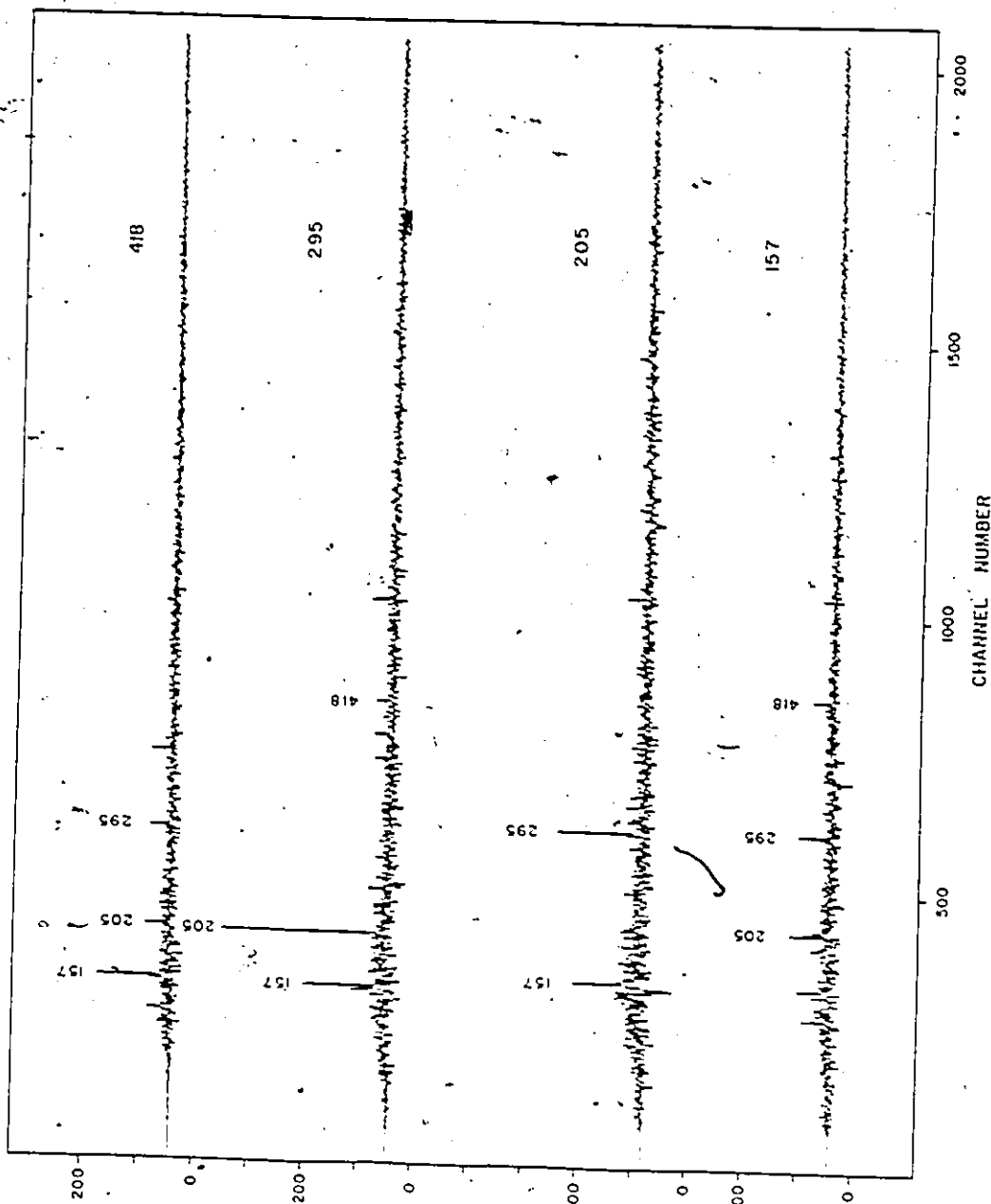


Table 5.5  
 $\gamma$ -ray Gates and the Coincident  $\gamma$ -rays for  $^{134}\text{Cs}$

Gate Energy (keV)	Coincident Lines (keV)
157	205, 295, 418
205	157, 295, (418)*
295	157, 205, (418)
418	157, 205, 295

\* ( ) denotes doubtful coincidences.

Table 5.6  
 $\gamma$ -ray Energies and Relative Yields from ( $^{130}\text{Te}+^7\text{Li}$ )  
 Reaction at 34 MeV

Energy (keV)	Relative Yield
127.5(1)	
149.7(1) <sup>a</sup>	196(10)
157.5(1)	32 (2)
205.6(1)	100
295.8(1)	128 (7)
418.5(2)	36 (3)
632.5(2) <sup>c</sup>	417(23)
667.8(2) <sup>b</sup>	201(11)

<sup>a</sup>  $^{131}\text{I}$

<sup>b</sup>  $^{132}\text{I}$

<sup>c</sup>  $^{133}\text{Cs}$

## Discussion and Interpretation

### 6.1 Introduction

The preceding three chapters have described the present experimental studies and presented the data from these studies. An energy level scheme is given in this chapter, based on the present studies and the published data.

The spins of the ground state and 138 keV isomer were measured by atomic beam studies (Fuller, 1976) to be 4 and 8 respectively. Sunyar et al. (1954) established the spin of the 11 keV state to be  $5^+$  in the study of the decay of  $^{134m}\text{Cs}$ .

Archer et al. (1966) studied the high energy  $\gamma$ -radiation following thermal neutron capture by  $^{133}\text{Cs}$ . This was followed by a study of the low energy transitions of  $^{134}\text{Cs}$  in an  $(n,\gamma)$  reaction by Alexeev et al. (1975, 1978). To assist the reader in understanding the discussion which follows, the level scheme of Alexeev et al., shown in figure 1.1, has been redrawn in figure 6.1. Additional data from a later publication (Alexeev et al., 1978) have been included in figure 6.1. The conventions employed by the Nuclear Data Sheets have been used and the branching ratios for the transitions

are included. For readability, the energies are quoted to only one decimal place. Transitions which were shown in figure 1.1 as M1, E2 have had their multipolarities omitted. One may refer to figure 1.1 for the greater detail.

## 6.2 Energy Level Scheme

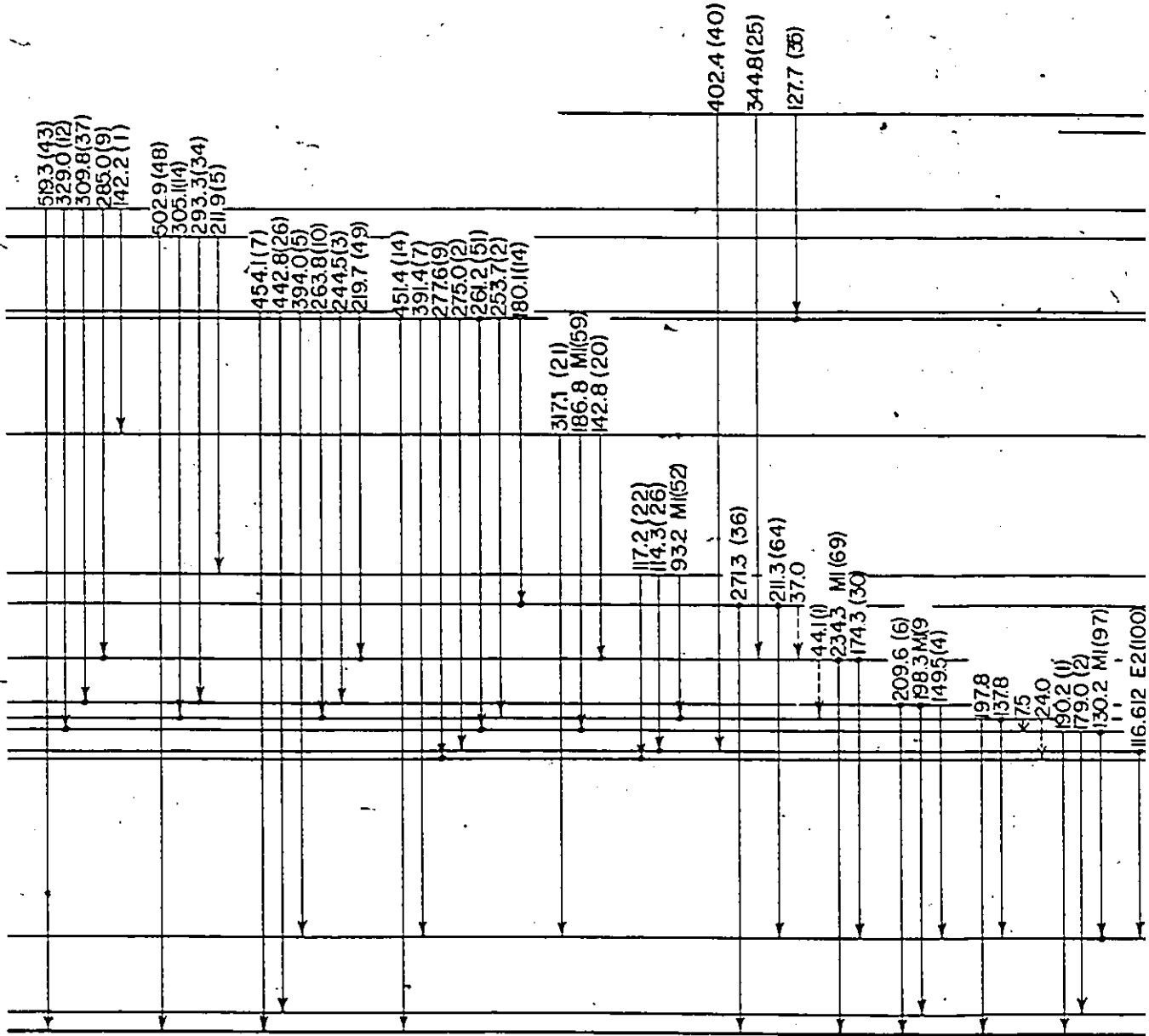
The proposed level scheme in figure 6.2 was constructed from the data collected in the experimental studies described in chapters 3, 4 and 5. The published data from the  $^{133}\text{Cs}(n,\gamma)$  studies also provided information for the construction of the level scheme in figure 6.2. The (d,p) and (t, $\alpha$ ) reactions identified many levels that were directly populated. The singles and coincidence  $\gamma$ -ray data (tables 5.2, 5.3 and 5.5) provided information on the decay modes of the levels. The level energies shown in figure 6.2 were obtained from the transition energies given in table 5.2.

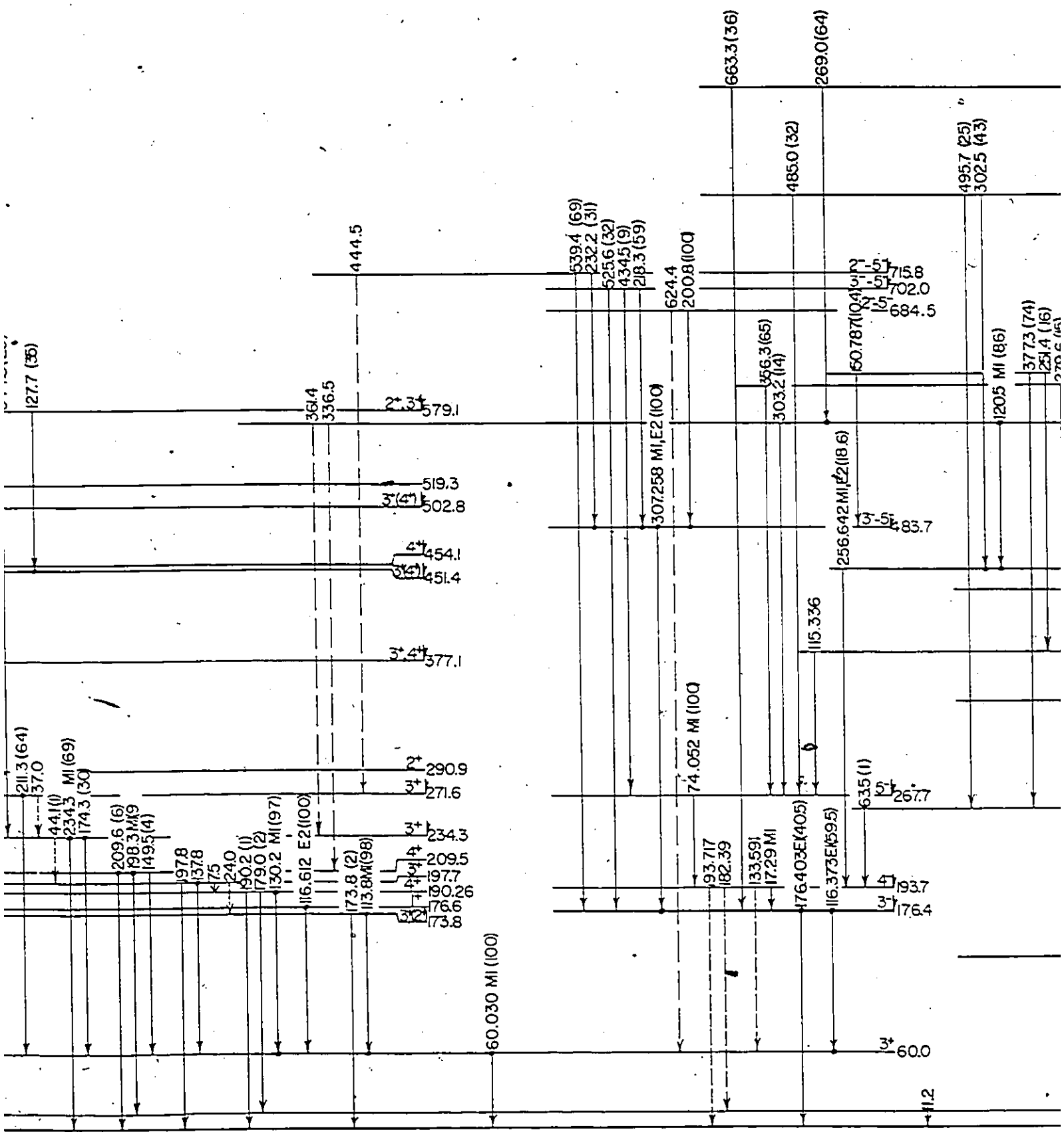
A detailed discussion of the levels shown in figure 6.2 follows. The data from the present study are used to deduce the p-n multiplet structure for some of the levels and to assign spins to them.

Ground State: The spin of the ground state was previously known from atomic beam experiments to be 4 and the parity is known to be even from the measured magnetic moment (Fuller, 1976). The ground state was populated

### Figure 6.1

The level scheme of Alexeev et al. This level scheme has been redrawn and branching ratios deduced from the Alexeev's  $(n,\gamma)$  data are included. Energies are only quoted to one decimal place. All multipolarities which were determined to be mixed M1, E2 are omitted. These additional details can be found in figure 1.1. This figure is provided to assist in understanding the discussion of the level scheme in sections 6.2 and 6.3. The additional data from Alexeev et al. (1978) is included in this figure but is missing from figure 1.1.





127.7 (36)  
 211.3 (64)  
 37.0  
 441 (1)  
 234.3 MI (69)  
 174.3 (30)  
 209.6 (6)  
 98.3 MI (9)  
 149.5 (4)  
 197.8  
 137.8  
 175  
 240  
 90.2 (1)  
 79.0 (2)  
 130.2 MI (97)  
 116.612 E2 (100)  
 173.8 (2)  
 113.8 MI (98)  
 234.3  
 209.5  
 197.7  
 190.26  
 176.6  
 173.8  
 60.030 MI (100)  
 74.052 MI (100)  
 93.717  
 182.39  
 133.591  
 17.29 MI  
 176.403E(405)  
 116.373E(59.5)  
 63.5 (1)  
 5.4  
 267.7  
 4.4  
 193.7  
 3.4  
 176.4  
 3.4  
 600  
 112  
 307.258 MI E2 (100)  
 624.4  
 200.8 (100)  
 356.3 (65)  
 303.2 (14)  
 74.052 MI (100)  
 115.336  
 256.642 MI E2 (18.6)  
 13.5  
 83.7  
 60.787 (104)  
 2.5  
 715.8  
 2.5  
 702.0  
 2.5  
 684.5  
 1205 MI (86)  
 37.73 (74)  
 25.4 (16)  
 370.6 (15)  
 539.4 (69)  
 232.2 (31)  
 525.6 (32)  
 434.5 (9)  
 218.3 (59)  
 624.4  
 200.8 (100)  
 663.3 (36)  
 485.0 (32)  
 269.0 (64)  
 495.7 (25)  
 302.5 (43)



in the (d,p) reaction, with an  $i_n = 2$  strength of  $0.46 \pm 0.06$  which is weaker than what is expected from the (2J+1) rule for the  $4^+$  member of the  $[\pi g_{7/2}, (\nu d_{3/2})^{-1}]$  multiplet. It was also part of an unresolved 0 + 11 keV doublet in the (t, $\alpha$ ) reaction. The angular distribution of the doublet is well fitted with  $i_p = 4$  and carries a strength of  $2.23 \pm 0.16$ . The strength is consistent with the expected combined strength of the  $4^+$  and  $5^+$  members of the  $[\pi g_{7/2}, (\nu d_{3/2})^{-1}]$  multiplet. It is probable that both the ground state and the 11 keV state have  $i_p = 4$  angular distributions.

11 keV State: This state was reported by Sunyar et al. (1954) in the study of the decay of  $^{134m}\text{Cs}$ . The 127.5 keV E3 transition from the isomer to the 11 keV state was used to assign  $5^+$  to the 11 keV level. The present studies are consistent with this spin assignment since the 11 keV state carries an  $i_n = 2$  strength which is very close to the strength predicted by the (2J+1) rule for the  $5^+$  member of the  $[\pi g_{7/2}, (\nu d_{3/2})^{-1}]$  multiplet.

60 keV State: A 60 keV  $\gamma$ -ray was reported in the (n, $\gamma$ ) reaction and Alexeev et al. (1975) determined the transition multipolarity to be M1. They assigned the 60 keV  $\gamma$ -ray to be the transition from a 60 keV level to the ground state. They deduced the spin of this level to be  $3^+$  on the basis of the observed transition to the ground state and the lack of a transition to the 11 keV level.

However, the  $4^+$  and  $5^+$  possibilities can not be ruled out completely on the basis of the absence of an otherwise allowed M1 transition.

The 60 keV level was populated by  $l_n = 2$  with a strength of  $0.61 \pm 0.11$  in the (d,p) reaction and by  $l_p = 4$  with a strength of  $0.77 \pm 0.15$  in the (t, $\alpha$ ) reaction. The (2J+1) rule predicts the 60 keV level should carry an  $l_n = 2$  strength of 0.48 and an  $l_p = 4$  strength of 0.76 if it were the  $3^+$  member of the [ $^{\infty}g_{7/2}, (vd_{3/2})^{-1}$ ] multiplet.

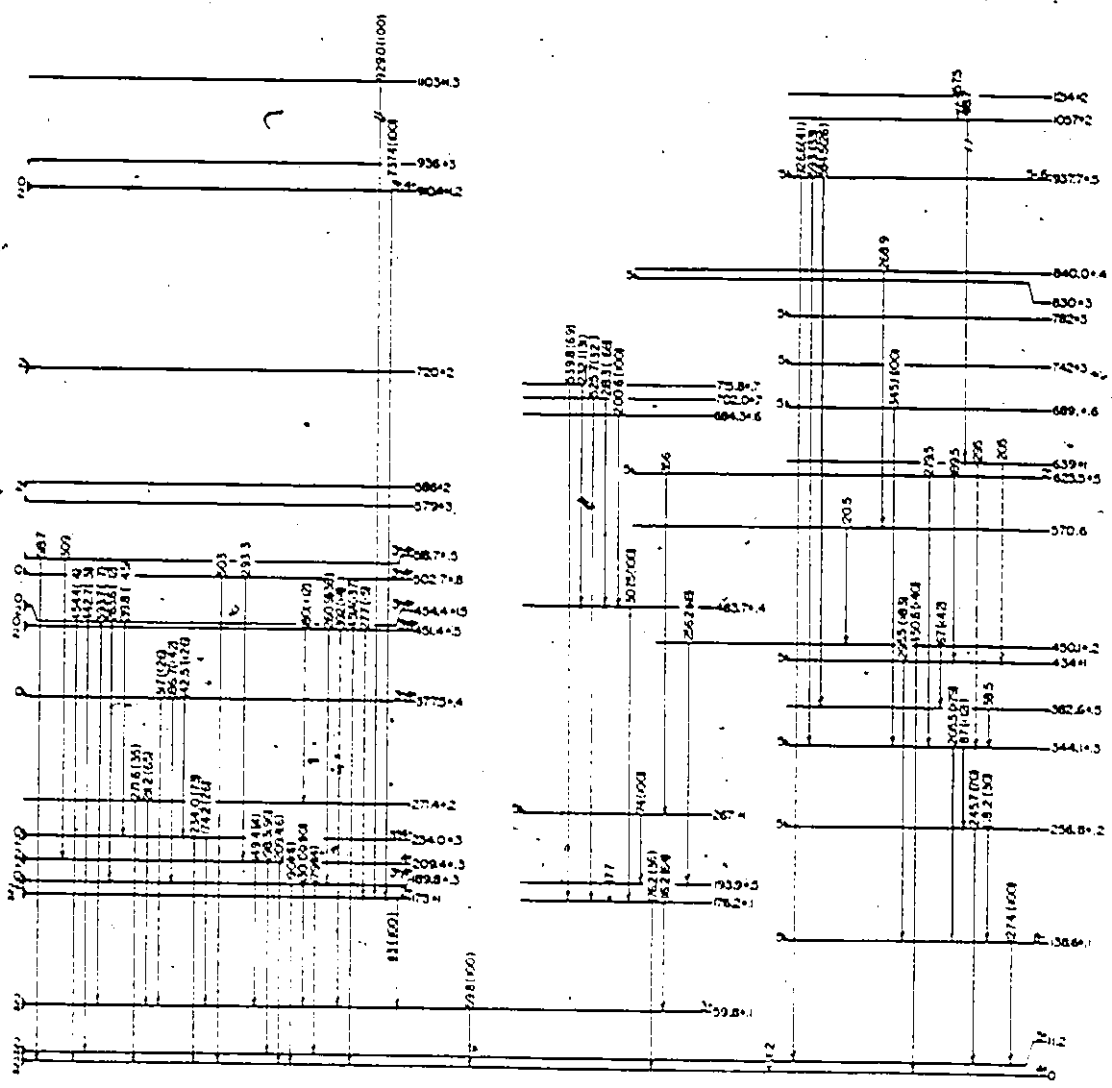
The  $\gamma$ -ray studies show a 60 keV  $\gamma$ -ray in the singles spectrum of the (d,p $\gamma$ ) experiment corresponding to the transition from the 60 keV state to the ground state. No transition to the 11 keV state is observed.

138 keV State: This is the well known 2.9-hour isomer in  $^{34}\text{Cs}$ . It has spin  $8^-$  (Sunyaev et al., 1954 and Fuller, 1976). The isomer decays via a 127.5 keV (99.97%) E3 transition to the 11 keV level and a 138.7 keV (0.03%) M4 transition to the ground state, where the branching ratios are obtained from the data of Alexeev et al. (1975).

Table 5.2 shows the 127.5 keV  $\gamma$ -ray but the 138.7 keV  $\gamma$ -ray was too weak to appear in the singles spectrum of the (d,p $\gamma$ ) reaction. The 138 keV level carries an  $l_n = 5$  strength of  $0.47 \pm 0.09$ , consistent with the predicted strength of 0.51 for the  $8^-$  member of

Figure 6.2

The energy level scheme of  $^{134}\text{Cs}$ , constructed from the data obtained in this study. The notation of the Nuclear Data Sheets has been used. The  $\blacktriangle$  symbol is used to denote that the level was found in the (d,p) reaction and the  $\nabla$  symbol denotes that the level was populated in the (t, $\alpha$ ) reaction. The dashed lines represent transitions whose placement are in doubt.



the  $[\pi g_{7/2}, (\nu h_{11/2})^{-1}]$  spin multiplet. No 138 keV level appeared in the (t,  $\alpha$ ) reaction.

173 keV State: Alexeev et al. observed coincidences between  $\gamma$ -rays of 60 and 113 keV. They also reported a very weak 173 keV  $\gamma$ -ray which fitted well in energy as the cross over transition to the ground state. The branching ratios for the 113 and 173 keV transitions are listed in table 6.1. In the (n,  $\gamma$ ) work, the 113 keV branch carried 98% of the strength. The M1 transition multipolarity of the 113 keV transition to the 60 keV level was used to assign  $J^\pi = 2^+$  or  $3^+$  to the level. Alexeev et al. (1975) assumed the 60 keV level was  $3^+$ . Since the  $4^+$  and  $5^+$  possibilities for the 60 keV level could not be excluded by Alexeev's data,  $4^+$ ,  $5^+$  and  $6^+$  have to be considered as possibilities for the 173 keV level.

The 173 keV level carries an  $\lambda_p = 4$  strength of  $0.46 \pm 0.05$  in the (t,  $\alpha$ ) reaction and an  $\lambda_n = 2$  strength  $0.35 \pm 0.06$  in the (d, p) reaction. The (2J+1) rule shows that these results are consistent with the interpretation of the 173 keV level as the  $2^+$  member of  $[\pi g_{7/2}, (\nu d_{3/2})^{-1}]$  with the 60 keV state, the ground state and the 11 keV state representing the  $3^+$ ,  $4^+$  and  $5^+$  members of the multiplet.

The  $\gamma$ -ray data in tables 5.2 and 5.3 show a 113 keV transition which connects the 173 and 60 keV levels.

The 60-113 keV coincidences support this  $\gamma$ -ray placement. No transition from the 173 keV level to the ground state was observed. The energy for the 113 keV transition, listed in table 5.2, is in poor agreement with the energy found by Alexeev et al. (differs by 0.6 keV). The 113 keV line is identified as a doublet with one component assigned to  $^{134}\text{Ba}$ . The present study assigned 100% of the strength to the 113 keV transition since the 173 keV-branch was not observed.

176.4 keV State: Alexeev et al. (1975) reported transitions of 116 and 176 keV which they assigned to the decay of a 176.4 keV level. They assigned the 6716 keV primary transition reported by Archer et al. (1966) to feed the level. However, it is not clear how they decided that the  $6716 \pm 5$  keV primary  $\gamma$ -ray fed the 176.4 keV level rather than the 173 or 176.6 keV level. From their conversion electron measurements, Alexeev et al. concluded that the 176.4 keV  $\gamma$ -ray has E1 multipolarity. The spin and parity of the 176.4 keV level is restricted to  $3^-$ ,  $4^-$  or  $5^-$ . If the 60 keV level is adopted as  $3^+$ , then the existence of the 116 keV transition to it eliminates the  $5^-$  possibility since an M2 transition would never compete with an E1.

The  $\gamma$ -ray data from the (d,p $\gamma$ ) experiment show transitions of 116 and 176 keV which agree with transitions assigned by Alexeev et al. (1975). The  $\gamma$ -ray coin-

cidence data also supports the assignment of this level by Alexeev et al. The same coincidences for the 116 keV transition are found in both reactions. The 176.4 keV level was found in the  $(n,\gamma)$  reaction to have a half-life of 49 nsec. The 116 keV coincidences were obtained from delayed coincidence measurements. The problems encountered with the time spectrum in the  $(d,p\gamma)$  experiment were described in the previous chapter. Wide gates on the time spectrum were set due to the "walk" problem. These gates overlapped part of the delayed time peak for the 116 keV transition. This allowed the coincidences for this  $\gamma$ -rays to be collected. Table 6.1 shows good agreement for the branching ratios of the 116 and 176 keV  $\gamma$ -rays between the  $(n,\gamma)$  and  $(d,p\gamma)$  reactions.

The 176.4 keV level was not identified in the  $(d,p)$  and  $(t,\alpha)$  particle spectra. If the negative parity assignment of Alexeev et al. is adopted, the 176.4 keV level would not be populated in the  $(t,\alpha)$  reaction. The 176.4 keV level is fed from the 193 keV level by a 17 keV  $\gamma$ -ray. The 193 keV level is in turn fed by a 74 keV  $\gamma$ -ray. About 2/3 of the yield for the 74 keV line in table 5.2 is attributed to this transition, the remainder belonging to Pb x-rays. The total yield feeding the 176.4 keV level from the 193 keV level is 128, where the  $\gamma$ -ray yield of the 74 keV transition has been adjusted for the conversion electron yield

( $\alpha_{TOT} = 2.16$ ). The 176.4 keV level is also fed by  $\gamma$ -rays of 256, 307 and 539 keV. The total yield feeding the 176.4 keV level is 160, while the total yield of the 116 and 176 keV  $\gamma$ -rays is 156. So there is no reason to believe that there is any direct feed to the 176 and 193 keV levels in the (d,p) reaction.

190 keV State: Alexeev et al. (1975) reported three transitions, 130, 179 and 190 keV, in the decay of the 190 keV level to the 60, 11 and 0 keV levels. The multipolarity of the 130 keV transition was deduced from their conversion electron data to be M1. Their conversion electron data result for the 179 keV  $\gamma$ -ray was ambiguous, nevertheless Alexeev et al. assigned M1, E2 multipolarity to that transition. No electron data were available for the 190 keV transition. Alexeev et al. (1975) assigned  $4^+$  to the level on the basis of the transitions. The 179 keV transition is very weak compared to the 130 keV transition so the possibility that the state is  $3^+$  should not be ruled out completely.

The 190 keV level carries an  $\lambda_n = 0$  strength of  $0.13 \pm 0.02$  in the (d,p) reaction and an  $\lambda_p = 2$  strength of  $0.27 \pm 0.06$  in the (t, $\alpha$ ) reaction. The spin of the state is therefore restricted to  $3^+$  or  $4^+$ . In terms of the shell model, the 190 keV level is interpreted as an admixture of the [ $\pi g_{7/2}, (\nu s_{1/2})^{-1}$ ] and the [ $\pi d_{5/2}, (\nu d_{3/2})^{-1}$ ] configurations. The (d,p) reaction selec-

tively populated [ $\pi g_{7/2}, (\nu s_{1/2})^{-1}$ ] and the (t,  $\alpha$ ) reaction selected the other configuration.

A 130 keV transition was found in the (d, p)  $\gamma$ -ray data, connecting the 190 keV level to the 60 keV level, but the 179 and 190 keV transitions reported by Alexeev et al. (1975) are not resolved from nearby lines that also belong to  $^{134}\text{Cs}$ .

193 keV State: Alexeev et al. (1975) placed the 193 keV level by the 6701  $\pm$  5 keV primary transition (Archer et al., 1966) from the capture state and the 17 keV transition to the 176.4 keV negative parity state. It is not clear how they decided that the primary  $\gamma$ -ray fed the 193 keV level rather than the 190 keV level. An observed 63 keV  $\gamma$ -ray from the 257 keV ( $6^-$ ) level to the 193 keV level was later placed by Alexeev et al. (1978). The M1 nature of the 17 keV transition (Alexeev et al., 1975) requires that the 193 keV level also have negative parity. The primary transition would be E1 since the capture state is  $3^+$  or  $4^+$ . Alexeev et al. reported that the 193 keV level was fed by a 256 keV  $M1, E2$  transition from the 450 keV  $5^-$  (to be justified below) level. The possible spins are  $3^-$  or  $4^-$  but Alexeev et al. (1975) assigned  $4^-$  to the level.

The 17 keV transition was of course not seen in the (d, p $\gamma$ ) experiment. A weak 256-116 keV coincidence was seen in the (d, p $\gamma$ ) data consistent with the level

scheme of Alexeev et al. (1975). The 193 keV level was not observed in either the (d,p) or the (t, $\alpha$ ) particle spectra.

209 keV State: Alexeev et al. (1975) placed a level at 209 keV from  $\gamma$ -ray transitions of 149, 198 and 209 keV which feed the 60, 11 and 0 keV levels. They deduced the multipolarity of the 198 keV transition to be M1 from the experimental L-conversion coefficient. The 209 keV transition was assigned M1, E2 multipolarity. Their conversion electron data for the 209 keV transition showed poor agreement between the experimental and theoretical K-conversion coefficients for M1 and E2 multipolarities, their experimental value being larger than either theoretical value. The error in the L-conversion coefficient was too large to make an unambiguous assignment. Alexeev et al. assigned  $4^+$  to the level, but the  $5^+$  possibility can not be excluded by their data.

The 209 keV level was very weakly populated by  $\ell_n = 2$  in the (d,p) reaction but carries an  $\ell_p = 2$  strength of  $0.11 \pm 0.04$  in the (t, $\alpha$ ) reaction. The level appears to contain a small component of the [ $g_{7/2}, (vd_{3/2})^{-1}$ ] configuration since it was weak in the (d,p) reaction and a large component of the [ $d_{5/2}, (vd_{3/2})^{-1}$ ] configuration since it was strong in the (t, $\alpha$ ) reaction.  $2^+$ ,  $3^+$  or  $4^+$  are the allowed possibi-

lities for this level.

Three  $\gamma$ -rays at 149, 198 and 209 keV were also observed to depopulate the 209 keV level in the (d,p $\gamma$ ) experiment. Since the transition multipolarities are expected to be M1, E2 or a mixture of M1 and E2, the  $2^+$  possibility is eliminated.  $3^+$  or  $4^+$  remain as possibilities, but  $3^+$  is not allowed by Alexeev's measured M1 multipolarity for the 198 keV  $\gamma$ -ray. Therefore, the level is  $4^+$ . The branching ratios from the (d,p $\gamma$ ) data show remarkably good agreement with the branching ratios from Alexeev et al. (1975).

234 keV State: Transitions of 174 keV to the 60 keV level and 234 keV to the ground state were reported by Alexeev et al. (1975) for this level. No transition to the 11 keV state was reported. This level was also fed by a primary  $\gamma$ -ray transition in the (n, $\gamma$ ) work of Archer et al. (1966). Alexeev et al. (1975) determined the transition multipolarity for the 174 keV  $\gamma$ -ray to be M1. Their K-conversion measurements for the 234 keV agreed well with an M1 assignment but was close to the theoretical value for E2. Their L-conversion coefficient gave ambiguous results so a mixed M1, E2 multipolarity was assigned. Alexeev et al. assigned  $3^+$  to the level. The  $4^+$  and  $5^+$  possibilities should not be ruled out on the basis of the reported data of Alexeev et al.

The 234 keV level carries an  $\lambda_n = 0$  strength of

0.14  $\pm$  0.02 (the same strength as the 190 keV level) in the (d,p) reaction and also carries an  $i_p = 2$  strength of 0.10  $\pm$  0.02 (tied with the 209 keV level) in the (t, $\alpha$ ) reaction. Like the 190 keV level, this state is interpreted as an admixture of the [ $\pi g_{7/2}, (\nu s_{1/2})^{-1}$ ] and the [ $\pi d_{5/2}, (\nu d_{3/2})^{-1}$ ] configurations. The allowed spins are 3<sup>+</sup> or 4<sup>+</sup>.

The 174 and 234 keV transitions that were reported by Alexeev et al. were observed in the (d,p $\gamma$ ) experiment. The  $\gamma$ -ray branching ratios from the (d,p $\gamma$ ) data are in good agreement with the branching ratios of Alexeev et al.

257 keV State: Alexeev et al. (1975) postulated this level to account for an observed 118 keV transition (to the 138 keV isomer) and a 245 keV transition (to the 11 keV state). They also reported a very weak 63 keV  $\gamma$ -ray (Alexeev et al., 1978) which was placed to feed the 193 keV level, to account for observed 87-116 keV coincidences. Alexeev et al. measured the transition multipolarities to be E2 for the 118 keV  $\gamma$ -ray and E1 for the 245 keV  $\gamma$ -ray. Since the 118 keV transition feeds the 8<sup>-</sup> isomer and the 245 keV transition feeds the 11 keV 5<sup>+</sup> state the spin and parity were uniquely determined to be 6<sup>-</sup>.

A peak with  $i_n = 5$  appeared at 263 keV in the (d,p) spectra. This peak is really an unresolved

doublet, consistent with the 257 and 267 keV levels of Alexeev et al. (1975). The counting statistics were poor, making it difficult to reliably extract two peaks from the spectra. The  $l_n = 5$  angular distribution establishes the parity of at least one member of the doublet as negative. There is a possibility that the overall angular distribution contains components of an even and an odd  $l$ -value. If Alexeev's parity assignments for the 257 and 267 keV levels are accepted, then both levels must have  $l_n = 5$ . These levels were absent from the  $(t, \alpha)$  spectra as expected for negative parity states involving the  $1h_{11/2}$  neutron hole in the configuration.

$\gamma$ -rays of 118 and 245 keV were found in the  $(d, p\gamma)$  experiment, in agreement with the findings of Alexeev et al. (1975). The 63 keV transition reported by Alexeev et al. (1978) was not seen in the  $(d, p\gamma)$  spectrum. The  $(d, p)$  coincidence data, listed in table 5.3, show the same coincidences that were seen in the  $(n, \gamma)$  reaction. The coincidences in the  $(d, p\gamma)$  experiment were very weak for the 245 keV gate. The branching ratios for the 118 and 245 keV transitions were in good agreement with the values from the  $(n, \gamma)$  work.

267 keV State: The 267 keV level was placed by Alexeev et al. from the 6626 keV primary transition reported by Archer et al. (1966). Alexeev et al. (1975) placed the 74 keV  $\gamma$ -ray to depopulate the 267 keV level from the

coincidence relationships with the 116 and 176 keV transitions. The M1 nature of the 74 keV transition to the assumed  $4^-$  level at 193 keV requires negative parity for the 267 keV level. The 6626 keV primary transition must be E1 since the capture state is  $3^+$  or  $4^+$ . Alexeev et al. assigned  $5^-$  to this level but  $3^-$  and  $4^-$  should not be excluded as possibilities.

This is the other level in the unresolved 263 keV doublet in the (d,p) spectra. The  $l_n = 5$  angular distribution requires either this level or the 257 keV level or both levels to have negative parity.

A 74 keV  $\gamma$ -ray was also observed in the (d,p $\gamma$ ) experiment. The presence of lines at 72, 74, 84 and 87 keV are indicative of the presence of lead x-rays in the (d,p $\gamma$ ) singles spectrum. The lead x-ray at 74 keV overlaps the 74 keV line from  $^{134}\text{Cs}$ . This accounts for the poor energy match with the (n, $\gamma$ ) data. Coincidences between the 74, 116 and 176 keV transitions were not observed.

271 keV State: This level was placed by Alexeev et al. on the basis of 180-211 and 180-271 keV coincidences. Alexeev et al. also identified this as a level fed by a primary  $\gamma$ -ray from the capture state. The 211 and 271 keV transitions were deduced to be M1, E2 by Alexeev et al. They assigned  $3^+$  to the level but  $2^+$ ,  $4^+$  and  $5^+$  can not be excluded from consideration on the basis of their

data.

The 180-211 and 180-271 keV coincidences were not observed in the (d,p $\gamma$ ) experiment but weak singles  $\gamma$ -rays corresponding to these transition energies were observed. The branching ratios for these lines agreed with the branching ratios from the (n, $\gamma$ ) data. This level was not observed in either the (d,p) or the (t, $\alpha$ ) particle spectra. The differential cross-section that would be expected for this level in the (d,p) particle data can be estimated by comparing the total ( $\gamma$ -ray plus electron) yield of this level with the total yield of another positive parity level that is seen in the particle data. The 271 keV level is predicted to have a differential cross-section of 26  $\mu$ b/sr at 30 $^\circ$  (near the second maximum of the  $l_n = 0$  angular distribution) if it is an  $l_n = 0$  level and a differential cross-section of 4  $\mu$ b/sr at 22.5 $^\circ$  (near the maximum of the  $l_n = 2$  angular distribution) if it is an  $l_n = 2$  level. An  $l_n = 0$  level of that strength would have been seen but such a weak  $l_n = 2$  level would not have been noticed in the analysis of the plate data.

344 keV State: This level was placed by Alexeev et al. (1975) with transitions of 87 keV to the 257 keV level and 205 keV to the 138 keV isomer. Alexeev et al. assigned M1 multipolarity to the 87 keV transition. Their conversion electron data shows an anomaly for the

87 keV transition. Their measured K-conversion coefficient does not agree with the theoretical values for E1, M1 or E2 multipolarities. No L-conversion coefficient was measured. From their K-conversion coefficient they assigned M1, E2 multipolarity to the 205 keV transition, the L-conversion coefficient measurement favored the M1 choice. The 205 keV transition feeds the  $8^-$  isomer, while the 87 keV transition feeds the 257 keV  $6^-$  level. The only spin that is consistent with both transitions being M1 multipolarities is  $7^-$ .

The 344 keV level was one of the weakest  $J_n = 5$  levels ( $0.16 \pm 0.06$ ) in the (d,p) particle spectra. A very weak 344 keV level also appeared in the (t, $\alpha$ ) reaction. It is presumably not the same 344 keV level since the negative parity states would not be populated in the (t, $\alpha$ ) reaction. The spectroscopic strength of the 344 keV level in the (d,p) reaction does not account for the strength needed for a spin  $7^-$  assignment. If the spin assignment is accepted, then the shell model strength must be fragmented and at least one other  $7^-$  level must exist to carry the missing 65% of the strength.

Two  $\gamma$ -rays, 87 and 205 keV, were observed in the (d,p) reaction which corresponded to the transitions placed by Alexeev et al. The coincidence data from the (d,p $\gamma$ ) reaction were consistent with the data from the (n, $\gamma$ ) reaction. The branching ratios from the (d,p $\gamma$ )

Table 6.1

Branching Ratios for the  $\gamma$ -ray Transitions

Energy (keV)	(n, $\gamma$ ) study		present study	
	Transition (keV)	Branching Ratio (%)	Transition <sup>a</sup> (keV)	Branching Ratio (%)
11.2	11.2	100		
60.0	60.0	100	59.8	100
138.7	127.5	100	127.4	100
173.8	113.8	98	113	100
	173.8	2		
176.4	116.4	60	116.2	64
	176.4	40	176.2	36
176.6	116.6	100		
190.3	130.2	97	130.0	>90
	179.0	2	a	< 4
	190.3	1	b	< 6
193.7	17.3	100		
197.8	(7.5)			
	-(24.0)			
	137.8			
	197.8			
209.6	149.5	4	149.4	4
	198.3	90	198.3	90
	209.6	6	209.4	6
234.3	44.1	1		
	174.3	30	174.2	27
	234.3	69	234.0	73
257.1	63.5	1		
	118.4	32	118.2	30
	245.9	67	245.7	70

Table 6.1 (continued)

Energy (keV)	(n, $\gamma$ ) study		present study	
	Transition (keV)	Branching Ratio (%)	Transition (keV)	Branching Ratio (%)
267.7	74.1	100	74	100
271.4	(37.0)			
	211.3	64	211.2	65
	271.4	36	271.6	35
291.0	93.2	52		
	114.3	26		
	117.2	22		
344.4	87.3	16	c	21
	205.6	84	205.5	79
377.1	142.8	20	142.5	<26
	186.8	59	186.7	>48
	317.1	21	d	<26
383.1	38.6	91	38.5	
	115.3	9		
434.2	177.0	7		<17
	295.4	93	295.5	>83
450.3	67.2	31	e	<42
	256.6	19	256.2	>18
	450.3	50	450.6	>40
451.4	180.1	14	f	<12
	253.7	2		< 3
	261.2	51	260.9	>38
	275.0	2		< 2
	277.6	9		< 5
	391.5	7		< 4
	451.4	14	451.4	<37
454.1	219.8	49	219.8	45
	244.5	3		< 3
	263.8	10	263.6	12
	394.0	5	393.7	7
	442.8	26	442.7	31
	454.1	7	454.4	4
483.7	307.2	100	307.5	100
502.8	211.9	5		
	293.3	34	293.3	
	305.1	14		
	502.9	48	g	

Table 6.1 (continued)

Energy (keV)	(n, $\gamma$ ) study		present study	
	Transition (keV)	Branching Ratio (%)	Transition (keV)	Branching Ratio (%)
519.3	142.2	1		
	285.0	9		
	309.8	37	h	
	329.0	12	i	
570.9	519.3	43	518.8	
	120.6	86	120.5	
579.1	303.2	14	j	
	127.7	35		
	344.8	25		
624.0	402.4	40		
	189.8	20	k	
	279.7	15	l	
634.4	356.3	65	m	
	150.8	10		
	251.4	16		
684.5	377.3	74		
	200.8	100	200.6	100
689.3	345.4	100	345.1	100
702.0	218.3	59	218.3	68
	434.5	9		
715.8	525.6	32	525.7	32
	232.2	31	232.1	31
	539.4	69	539.8	69
752.8	302.5	43		
	485.1	32		
	495.7	25		
839.9	269.0	64	268.9	
	663.3	36	n	
910.4			737.4	100
937.8			554.5	26
			593	33
			926.6	41
			929.0	100
1103				

<sup>a</sup> Part of the yield of the 179.8 keV line may belong to the 451 keV level.

- b Part of the yield of the 189.8 keV line may belong to the 624 keV level.
- c Part of the 86.9 keV yield belongs to a Pb x-ray.
- d Part of the 317.6 keV yield may belong to an unidentified source.
- e Part of the 66.9 keV yield may belong to an unidentified source.
- f Part of the 179.8 keV line may belong to the 190 keV level.
- g Part of the 503.6 keV yield may belong to an unidentified source.
- h Part of the 309.6 keV line belongs to  $^{133}\text{Ba}$ .
- i Part of the 329.3 keV yield may belong to an unidentified source.
- j The 303 keV line is obscured by a very strong doublet from  $^{133}\text{Cs}$  and  $^{133}\text{Ba}$ .
- k Part of the 189.8 keV line may belong to the 190 keV level.
- l The 279 keV line is obscured by the very strong 278.8 keV line from  $^{133}\text{Ba}$ .
- m Part of the 356.1 keV line belongs to  $^{133}\text{Cs}$ .
- n There is a very strong line at 664.9 keV from  $^{133}\text{Ba}$  which obscures the 663.3 keV line.

data were also in agreement with the  $(n,\gamma)$  data, even though part of the 87 keV yield in the  $(d,p\gamma)$  spectrum was attributed to Pb x-rays. The Pb x-ray intensities from Lederer and Shirley (1978) were used to estimate what fraction of the 87 keV yield belonged to the Pb x-ray. The estimated fraction was 1/7 of the yield shown in table 5.2. A 205 keV  $\gamma$ -ray, observed in the  $(^{130}\text{Te} + ^7\text{Li})$  reaction, may not be the same transition placed by Alexeev et al. (1975).

377 keV State: Three  $\gamma$ -rays at 142, 186 and 317 keV were reported by Alexeev et al. (1975) to depopulate the 377 keV level. Their 142-174, 142-234 and 186-130 keV coincidences provided the evidence for placement of the  $\gamma$ -rays. The 317 keV  $\gamma$ -ray was placed by the very good energy fit in the  $(n,\gamma)$  work. The 377 keV level is fed by the 6512 keV primary  $\gamma$ -ray reported by Archer et al. (1966). Alexeev et al. assigned  $3^+$  or  $4^+$  to the level. This assignment was based on the M1 nature of the 186 keV transition and the 317 keV M1, E2 transition to the 190 keV  $4^+$  level and the 60 keV  $3^+$  level, respectively. Since the spin of the 60 keV level was not firmly established by Alexeev et al.,  $5^+$  should not be ruled out completely as a possibility.

The 377 keV level is the strongest of the  $i_n = 0$  levels in the  $(d,p)$  reaction with a spectroscopic strength of  $0.32 \pm 0.05$ , but it is very weakly populated

in the  $(t, \alpha)$  reaction. These results are consistent with the 377 keV level being a member of the  $[\pi g_{7/2}, (\nu s_{1/2})^{-1}]$  configuration. The  $a_n = 0$  strength requires that the spin of the level be either  $3^+$  or  $4^+$  since the spin of the  $^{133}\text{Cs}$  target ground state is  $7/2^+$ . The  $(2J+1)$  rule allows either assignment.

The 142-174, 142-234 and 186-130 keV coincidences were found in the  $(d, p\gamma)$  experiment. A 317 keV line appears in the  $(d, p)$  singles data but it differs in energy from Alexeev's 317 keV line by 0.5 keV. The ratio of the yields of the 142 to 186 keV lines in the  $(d, p)$  data is 1/2 but in the  $(n, \gamma)$  data it is 1/3. The poor agreement suggests that the 142 and 317 keV lines have components which do not belong to  $^{134}\text{Cs}$ .

383 keV State: Alexeev et al. placed this level to account for 67-205 and 67-87 keV coincidences. The 38 and 115 keV  $\gamma$ -rays were placed by their energy fits to depopulate this level. They deduced the 38 keV transition multipolarity to be M1 from their conversion electron data. The 38 keV transition feeds the  $7^-$  level at 344 keV. The 383 keV level is in turn fed by a 67 keV M1 transition from the 450 keV  $5^-$  level. Alexeev et al. assigned  $6^-$  to the 383 keV state which is the only possibility if the spins and parities of the 344 and 450 keV levels are accepted.

This level does not appear in the particle spec-

tra. In the (d,p) particle spectra it would not have been resolved from the 377 keV level. Also, it would be an  $l_n = 5$  state since Alexeev et al. determined the state to have negative parity. These states appeared much more weakly than the  $l_n = 0$  states at the angles for which data were collected. So it would have been obscured by the very intense peak nearby (see figure 3.1).

The 38 keV transition was seen in the  $1 \text{ cm}^3$  detector in singles mode in the (d,p $\gamma$ ) spectrum. No definite evidence for the 115 keV transition was found in the (d,p $\gamma$ ) data. The 87-120 and 120-205 keV coincidences were observed in the (d,p $\gamma$ ) reaction. Additional 554-205 and 593-205 keV coincidences in the (d,p $\gamma$ ) data provide evidence for this level placement. The 554 and 593 keV transitions are placed to depopulate a level at 937 keV. The 554 keV transition feeds the 383 keV level and the 593 keV transition feeds the 344 keV level (see figure 6.2).

434 keV State: Alexeev et al. (1975) placed the 434 keV level on the basis of the 177 and 295 keV  $\gamma$ -rays and 189-295 keV coincidences. They placed the 177 keV  $\gamma$ -ray to feed the 257 keV state and the 295 keV  $\gamma$ -ray to feed the  $8^-$  isomer. From their K-conversion data they assigned M1, E2 multipolarity to the 295 keV  $\gamma$ -ray. Alexeev et al. assigned  $6^-$  to this level. The 434 keV

level is fed by the 189 keV M1 transition from the  $5^-$  level at 624 keV (justified below). Hence, the spin of the 434 keV level is not more than  $6^-$ . The 295 keV transition to the  $8^-$  isomer is at most E2, so the spin and parity must be  $6^-$ .

The 434 keV level was among the weaker  $l_n = 5$  levels populated in the (d,p) reaction, with an  $l_n = 5$  strength of  $0.21 \pm 0.07$ . The 434 keV level was absent from the (t, $\alpha$ ) spectra. Not all of the  $6^-$  strength expected by the (2J+1) rule (0.39) is accounted for by this level, but Alexeev et al. placed another  $6^-$  level at 257 keV which could account for the missing component of the  $6^-$  strength. If the observed strength of the 263 keV doublet were shared equally between the 257 and 267 keV levels, then the 257 keV level would account for the remainder of the  $6^-$  strength.

In the (d,p $\gamma$ ) data, a 189-295 keV coincidence was seen. A 295 keV  $\gamma$ -ray was also seen in the ( $^{130}\text{Te} + ^7\text{Li}$ ) reaction. The 177 keV line was not resolved from the strong line at 176 keV in the (d,p $\gamma$ ) spectrum. Alexeev's 177 keV line would be 0.8 keV away from the 176.2 keV line in the (d,p $\gamma$ ) spectrum. If a peak were located there it would represent about 10% of the yield of the 176.2 keV line. The branching ratios for the 177 and 295 keV lines were calculated and are given in table 6.1 with this estimate as the upper limit of the 177 keV

yield. The agreement with the branching ratios of Alexeev et al. is good.

450 keV State: Alexeev et al. (1975) placed the 450 keV level with 67-87, 67-205 and 120-256 keV coincidences, and energy fits for the 256 keV transition to the 193 keV level and for the 450 keV transition to the ground state. They determined the multipolarity of the 67 keV  $\gamma$ -ray to be M1 from their conversion electron data. Since a parity change is therefore involved for the 450 keV transition, the multipolarity was assumed to be E1, although they were not able to confirm it. They assigned  $5^-$  to the level.

Archer et al. (1966) reported a primary  $\gamma$ -ray of  $6443 \pm 5$  keV which Alexeev et al. (1975) have placed to feed the 451 and 454 keV levels. There is no evidence to exclude the 450 keV level as the level fed by the primary transition. Also there is no evidence to indicate whether the primary transition reported by Archer et al. is a singlet, doublet or triplet.

The (d,p)  $\gamma$ -ray data show transitions of 67, 256 and 450 keV. Moreover, coincidences between 256 and 120 keV and weak coincidences between 120 and 450 keV were observed in the (d,p $\gamma$ ) experiment. The 67 keV  $\gamma$ -ray is 0.3 keV lower and the 256 keV transition is 0.4 keV lower than the energies reported by Alexeev et al. (1975). The ratio of the 256 to the 450 keV lines in

the (d,p) reaction is 0.44 while the ratio of these lines in the (n, $\gamma$ ) data is 0.38. The agreement is not unreasonable. The ratio of the 67 keV to the 450 keV  $\gamma$ -ray yield in the (d,p $\gamma$ ) experiment is 1.1 while in the (n, $\gamma$ ) data it is 0.62. The agreement is poor, suggesting that there is a contaminant 67 keV line. The absence of the stronger Ta x-ray lines eliminates Ta as a source of the contaminant.

A peak appears in the (d,p) and (t, $\alpha$ ) particle spectra at 455 keV. The energy resolution was not good enough to separate three close lying levels of 450, 451 and 454 keV. The (t, $\alpha$ ) reaction can not populate the 450 keV level since this level has negative parity which involves the  $1h_{11/2}$  neutron hole in the configuration. The 455 keV peak in the (d,p) reaction may have a component belonging to the 450 keV level.

The yield expected for the 450 keV level in the (d,p) particle data can be estimated as follows. The total yield ( $\gamma$ -ray plus electron conversion) for this level, corrected for feeding from higher levels, is compared to the corresponding yield for another negative parity level which is populated in the particle spectra, such as 624 keV. The 450 keV is estimated to have a differential cross-section of 23  $\mu\text{b}/\text{sr}$  near the peak of the  $i_n = 5$  angular distribution, comparable to the observed differential cross-section of the  $8^-$  isomer.

Since the observed cross-sections for the 455 keV peak are as low as 5  $\mu\text{b}/\text{sr}$ , there is no contribution to the 455 keV peak from the 450 keV level.

451 keV State: Alexeev et al. (1975) assigned  $\gamma$ -ray transitions of 180, 254, 261, 275, 277, 391, and 451 keV to the 451 keV level. They reported 261-130 and 277-113 keV coincidences. Their electron conversion data provided the M1, E2 transition multipolarities for the 261 and 277 keV  $\gamma$ -rays. Alexeev et al. (1975) identified the 451 keV level as a level which is fed by a primary transition from the  $3^+$  or  $4^+$  capture state. They assigned  $3^+$  or  $4^+$  to the level from the observed transitions.

The 180, 261, and 451 keV transitions were found in the (d,p $\gamma$ ) data. 261-130 and 113-277 keV coincidences were seen in the (d,p $\gamma$ ) data but the 277 keV line was not resolved from the strong 278 keV line in the singles spectrum. The 254 and 275 keV lines do not appear in the (d,p $\gamma$ ) data.  $\gamma$ -rays with relative yields less than about 0.7 were not separated from the Compton background, so the 254 and 275 keV lines have yields less than 0.7. The ratio of the 254 keV to the 261 keV yield would be less than 0.07 while in Alexeev's data it is 0.04. The ratio of the 275 keV to the 261 keV yield would compare similarly. Relative to the 261 keV line the 451 keV line was much stronger in the (d,p $\gamma$ ) data

than the  $(n,\gamma)$  branching ratios led one to expect. This suggests that there is another 451 keV line in the  $(d,p\gamma)$  spectrum which does not belong to  $^{134}\text{Cs}$ .

454 keV State: Alexeev et al. (1975) placed the 454 keV level from  $\gamma$ -rays at 219, 244, 263, 394, 442, and 454 keV. They reported 219-174, 219-234, and 263-130 keV coincidences. They determined the transition multipolarities of the 219 and 263 keV  $\gamma$ -rays to be M1, E2. Alexeev et al. (1975) reported that the 454 keV level was populated by a primary  $\gamma$ -ray transition from the  $3^+$  or  $4^+$  capture state. They assigned  $4^+$  to the level. There is no evidence in the  $(n,\gamma)$  data to exclude  $3^+$  or  $5^+$  as possibilities for the 454 keV level.

All of the  $(n,\gamma)$  lines except 244 keV were observed in the  $(d,p\gamma)$   $\gamma$ -ray spectra. The yield for the 244 keV line is estimated to be not more than 0.6 in the  $(d,p\gamma)$  reaction. The branching ratios for the other lines depopulating the 454 keV level are in good agreement with the  $(n,\gamma)$  branching ratios. The coincidences reported by Alexeev et al. (1975) were also observed in the  $(d,p\gamma)$  experiment.

The 455 keV peak in the particle spectra must be attributed to the 451 and 454 keV levels. The  $\gamma$ -ray yields from the  $(d,p\gamma)$  spectrum for the two levels were compared to determine the contribution of each level to the  $(d,p)$  particle spectroscopy strength. This compari-

son showed the two levels were nearly equally populated. The 455 peak has a weak  $l_n = 0$  angular distribution in the (d,p) reaction but carries an  $l_p = 2$  strength of  $0.16 \pm 0.02$  in the (t, $\alpha$ ) reaction. These  $l$ -values restrict the allowed spins to  $3^+$  or  $4^+$  for the 451 and 454 keV levels. Interpretation of the particle data in terms of shell model configurations is difficult. It is possible that the peak in the (t, $\alpha$ ) particle spectra is due to either the 451 keV level or the 454 keV level or both. This result indicates that at least one of the levels, 451 or 454 keV, is an admixture of the [ $\pi g_{7/2}, (v s_{1/2})^{-1}$ ] and the [ $\pi d_{5/2}, (v d_{3/2})^{-1}$ ] configurations.

483 keV State: Alexeev et al. placed this level from the 307-116 and 307-176 keV coincidences and the direct feeding via a primary  $\gamma$ -ray (Archer et al., 1966). Their conversion electron data could not distinguish between M1 and E2 multipolarities for the 307 keV  $\gamma$ -ray, but the exclusion of E1 is sufficient to assign negative parity. Any spin from  $2^-$  to  $5^-$  is possible.

The 307-116 keV coincidences were seen in the (d,p $\gamma$ ) data but the 307-176 keV coincidences were not observed. These coincidences involved the 49 nsec isomer at 176.4 keV.

The 483 keV level does not appear in the particle spectra. Estimates of the expected yield in the particle spectra are made in the manner that was

described for the 450 keV level. The total yield of the 307 keV transition, corrected for the yield of lines feeding the 483 keV level, was compared with the yield of the lines depopulating the 624 keV level. The 483 keV level would require a differential cross-section of 5  $\mu\text{b/sr}$  near the peak of the  $\ell_n = 5$  angular distribution. Such a weak peak could easily be overlooked.

503 keV State: The level was established in the  $(n,\gamma)$  reaction by transitions of 212, 293, 305 and 503 keV and the direct feed from the capture state. The 293 keV transition was the only one with a multipolarity assignment. The multipolarity was M1, E2 since the K-conversion coefficient could not distinguish between the two (Alexeev et al., 1975).  $3^+$  or  $4^+$  was assigned by Alexeev et al., consistent with the level being fed from the capture state. However, they were not justified in excluding other possibilities.

This was the weakest  $\ell_n = 0$  level identified in the  $(d,p)$  spectra. This level was absent from the  $(t,\alpha)$  reaction. The  $\ell_n = 0$  angular distribution restricts the spin to  $3^+$  or  $4^+$ , consistent with the possibilities allowed by Alexeev et al.

The 293-198 keV coincidence relationship was found in the  $(d,p\gamma)$  reaction. Lines at 293 and 503 keV appear in the singles data for the  $(d,p\gamma)$  reaction. The ratio of the yields of the 293 to the 503 keV lines in

the (d,p $\gamma$ ) experiment is about 8 times smaller than the (n, $\gamma$ ) ratio. This suggests that there is at least one other 503 keV line which does not belong to  $^{134}\text{Cs}$ . Alexeev's 212 keV  $\gamma$ -ray would be next to the 211.2 keV  $\gamma$ -ray in the (d,p $\gamma$ ) spectrum. Most of the 211.2 keV yield is accounted for by the decay of the 271 keV level since the branching ratio for the 211.2 keV  $\gamma$ -ray agreed well with the branching ratio from the (n, $\gamma$ ) data. The ratio of the 212 keV yield to the 293 keV yield would be less than 0.12 while in Alexeev's data it is 0.15. The 305 keV line does not appear in the (d,p $\gamma$ ) spectrum, so it could not have more than 0.6 units of relative yield, since lines with less than this yield were not separated from the Compton background. The ratio of the 305 keV to the 293 keV yield would be less than 0.2 while in the (n, $\gamma$ ) data it is 0.41.

519 keV State: Alexeev et al. placed the level from the 142, 285, 309, 329 and 519 keV transitions. Coincidences were observed for 285-234, 309-198, and 329-130 keV. The spin was assigned as  $3^+$  or  $4^+$  from the M1, E2 multipolarities of the 285 and 309 keV transitions.

The 520 keV peak did not appear at enough angles in the (d,p) particle spectra for an angular distribution to be obtained.

Only the 309-198 keV coincidences were confirmed from the (d,p $\gamma$ ) data. A 142 keV transition appears in

the (d,p)  $\gamma$ -ray data, but it was identified principally as the transition between the 377 and 234 keV levels. One third of its yield may represent this other 142 keV line. The lines at 285, 309 and 329 keV were obscured by other strong lines within the energy resolution.

571 keV State: Alexeev et al. placed this level from the 120-205 keV coincidences and the direct population by a primary transition from the capture state. A 303 keV  $\gamma$ -ray was also placed to feed the 267 keV level. A 269 keV  $\gamma$ -ray was placed to feed the 571 keV level to account for 269-120 keV coincidences. The 571 keV state was assigned  $4^-$  or  $5^-$  from the 120 keV M1 and 303 keV M1, E2-multipolarities.

The 120-205 and 120-269 keV coincidences were seen in the (d,p $\gamma$ ) experiment. Weak 120-450 keV coincidences were observed in the (d,p)  $\gamma$ -ray data. The 303 keV line was obscured by a very strong doublet line at 302 keV which does not belong to  $^{134}\text{Cs}$ .

No 571 keV level was identified in the particle spectra. An estimate of the expected particle yield can be made by comparing the  $\gamma$ -ray yield, adjusted for the conversion electron yield, for this level in the (d,p $\gamma$ ) experiment with the corresponding yield for the 624 keV level. The 571 keV level would require a differential cross-section of about 15  $\mu\text{b}/\text{sr}$  near the maximum of the  $\mu_n = 5$  angular distribution, comparable to the 624 keV level. A level this strong would have been identified

from the (d,p) particle spectra. However, no peak at 571 keV is found. A peak does appear at about 579 keV (see figure 3.1), but this is primarily attributed to the 579 keV level. So there must be at least one other  $\gamma$ -ray feeding the 571 keV level which has not been identified to account for the extra yield.

579 keV State: The 579 keV level was ~~based~~ based on the 127-261 keV coincidences and energy fits for the 344 and 402 keV  $\gamma$ -rays (Alexeev et al., 1975) and the direct feed (6309 keV  $\gamma$ -ray) from the capture state (Archer et al., 1966). The 402 keV transition feeds the 176 keV level and the 344 keV transition feeds the 234 keV level. Alexeev et al. assigned  $2^+$  or  $3^+$  to the level. The M1 multipolarity of the primary transition allows  $2^+$ ,  $3^+$ ,  $4^+$  or  $5^+$ .  $4^+$  and  $5^+$  are excluded by the 402 keV transition to the assumed  $1^+$  level at 176.6 keV.

The 127-261 keV coincidences were not seen in the (d,p $\gamma$ ) spectrum. In the singles (d,p)  $\gamma$ -ray data there are lines at 127.4, 345.1 and 401.8 keV. The yield of the 127.4 keV line is associated with the decay of the isomer. The 345.1 keV line in the (d,p $\gamma$ ) spectrum differs from Alexeev's 344.8 keV line by 0.3 keV. The yield for the 345 keV line in the (d,p $\gamma$ ) data is associated with the 689 keV level. The 401.8 keV line in the (d,p $\gamma$ ) data disagrees with the 402.4 keV line reported by Alexeev et al. by 0.6 keV. This is a large

difference so the 401.8 keV line is not identified as the 402 keV transition reported by Alexeev et al. The (d,p $\gamma$ ) data do not agree with the  $\gamma$ -ray assignments of Alexeev et al. for this level.

This level was weakly populated in the (d,p) spectra but no  $\lambda$ -value could be extracted. A level was also weakly populated at 586 keV in the (t, $\alpha$ ) reaction and no  $\lambda$ -value was extracted. The 586 keV level does not agree well in energy so it is not identified as the 579 keV level reported by Alexeev et al.

624 keV State: Alexeev et al. placed this level from the 189-295, 279-87 and 279-205 keV coincidences and the direct population of the level via a 6267 keV primary  $\gamma$ -ray (Archer et al., 1966). A 356 keV  $\gamma$ -ray was placed by the good energy fit. They assigned  $5^-$  to the level on the basis of the 189 keV M1, 279 keV M1, E2 and 356 keV M1, E2 transitions (see figure 6.1) and the assumption that a parity changing primary  $\gamma$ -ray must be E1.

An  $\lambda_n = 5$  level was present in the (d,p) reaction with a strength of  $0.29 \pm 0.09$ . The observed strength for the 624 keV level is consistent with a  $5^-$  assignment since the (2J+1) rule predicts that the  $5^-$  member of the [ $\pi g_{7/2}, (\nu h_{11/2})^{-1}$ ] multiplet would carry strength of 0.33.

The 189-295, 279-87 and 279-205 keV coincidences were verified by the (d,p $\gamma$ ) data. Unfortunately, the

279 keV line is not resolved from a strong line at 278.8 keV from  $^{133}\text{Ba}$  and the 356 keV line is unresolved from the 356.1 keV line from  $^{133}\text{Cs}$ . The 189 keV line in the (d,p) singles data may also have a component which belongs to the 190 keV level in  $^{134}\text{Cs}$ .

639 keV State: This state is placed by observed 205-295 keV coincidences. These coincidences appeared in the (d,pr), ( $^7\text{Li}$ ,3n) and (n, $\gamma$ ) (Alexeev et al., 1975) reactions. The coincidence was not accounted for by Alexeev et al. Since there are already 205 and 295 keV transitions in the level scheme that cannot be in coincidence with one another, one must conclude that at least one of the two lines is in fact a doublet. One possibility is that the 205 keV  $\gamma$ -ray is a doublet, with one component feeding the 434 keV level from the 639 keV level. The other possibility is that the 295 keV  $\gamma$ -ray is doublet and connects the 639 keV level with the 344 keV level. It is also possible that both are doublet and both transitions exist. Since it was not decided which transition should be placed in the scheme, both transitions appear as dashed transitions in figure 6.2. No 639 keV level was observed in the (d,p) particle spectra and no estimates of its required strength can be made.

684 keV State: The (n, $\gamma$ ) work placed this level to explain the 200-307 keV coincidences. The 200 keV transition was assigned M1, E2 multipolarity. -Spins

from  $2^-$  to  $5^-$  are suggested by Alexeev et al. (1975). Their data do not exclude  $1^-$  or  $6^-$  as possibilities.

The 200-307 keV coincidence relationship was also found in the (d, $p\gamma$ ) data.

This is another level for which no particle spectroscopy data exists. The total ( $\gamma$ -ray plus electron) yield in the (d, $p\gamma$ ) experiment was used to estimate the expected particle yield in the (d,p) reaction. Comparison of the yield for the 684 keV level with the yield for the transitions depopulating the 624 keV level predict that the 684 keV level would require a differential cross-section of 3  $\mu\text{b/sr}$  near the maximum of the  $\lambda_n = -5$  angular distribution. This would be about 10-15% of the cross-sections listed in table A1 for the 689 keV level.

689 keV State: An  $\lambda_n = 5$  level carrying a strength of  $0.50 \pm 0.16$  was found in the (d,p) particle spectra. No 689 keV level appeared in the (t, $\alpha$ ) reaction. This level must have negative parity due to the  $1h_{11/2}$  neutron hole in the configuration for the level. If only a small part of the strength of the level is attributed to the 684 keV level, then the 689 keV level still carries a large amount of strength. This suggests that it must have a large spin.  $8^-$  is already assigned to the isomer so this level is a strong candidate for the  $9^-$  assignment.

A 345-205 keV coincidence was not placed by Alexeev et al. The 345 keV  $\gamma$ -ray was weak so coincidences with the 87 keV transition were not likely to be observed. A weak 345 keV line was also seen in the (d,p $\gamma$ ) spectrum but no coincidences were observed. Alexeev's observed coincidence suggests that there is a 345 keV transition feeding the 344 keV level from the proposed level at 689 keV. The energy for the 345 keV  $\gamma$ -ray in the (d,p $\gamma$ ) data differs from the (n, $\gamma$ ) value by about 0.3 keV. The energy fit is not very good, therefore. The level energy is adopted from the placement of the 345.1 keV  $\gamma$ -ray to the 344 keV level.

Levels with higher spins were expected to be populated in the ( $^7\text{Li},3n$ ) reaction but no 345 keV line appears in that reaction. Also, if the 689 keV level really is a  $9^-$  state then it is expected to decay to the isomer since that would involve an M1 transition of 550 keV. No 550 keV  $\gamma$ -ray was found in the (d,p $\gamma$ ) data.

702 keV State: The 702 keV level was placed in the (n, $\gamma$ ) work by three  $\gamma$ -rays at 218, 434 and 525 keV. A primary  $\gamma$ -ray of 6186 keV was found to feed this level (Archer et al., 1966). The 218 keV  $\gamma$ -ray was reported to be in coincidence with the 307 keV  $\gamma$ -ray. The 218 keV transition has M1, E2 multipolarity. Spins from  $3^-$  to  $5^-$  were suggested for this level by Alexeev et al. It is not clear how they excluded  $2^-$  as a possibility.

The 218 and 525 keV transitions were seen in the (d,p $\gamma$ ) data. Coincidences between the 218 and 307 keV lines were verified by the data. The 434 keV line was not seen, so it would have a yield that is less than 0.5 in the (d,p $\gamma$ ) experiment. The ratio of the 434 keV to the 218 keV yield would be less than 0.12, while in the (n, $\gamma$ ) data it is 0.15. The ratio of the yields of the 218 keV line to the 525 keV line in the (d,p $\gamma$ ) experiment is 2.2 and the same ratio in the (n, $\gamma$ ) data is 1.8. The agreement is reasonable.

This is another level for which no particle data exists. Estimates of the particle yield for this level were made by comparing the  $\gamma$ -ray yield, adjusted for the conversion electron yield, of the transitions depopulating the level in the (d,p $\gamma$ ) experiment with the corresponding yield for the 624 keV level. The 702 keV level would require a differential cross-section of 4  $\mu$ b/sr at 60 $^\circ$  (near the maximum for the  $l_n = 5$  angular distribution). Such a weak level would be easily overlooked during the analysis of the plate data.

715 and 720 keV States: Alexeev et al. placed the 715 keV level from the 232-307 keV coincidences and the energy fit for the 539 keV line. Archer et al. also observed a 6177 keV primary  $\gamma$ -ray which Alexeev et al.

assigned to feed this level. Alexeev et al. suggested spins from  $2^-$  to  $5^-$  for this level from the M1, E2 transition multipolarity of the 232 keV  $\gamma$ -ray.

In addition to 232-307 keV coincidences there is a 539 keV line in the  $\gamma$ -ray data from the (d,p $\gamma$ ) experiment. Good agreement is found with Alexeev's branching ratios.

This level does not appear in the (d,p) particle spectra, although a peak does appear near 720 keV. The peak at 720 keV has an  $l$ -value of 2 in the (d,p) reaction and is weakly populated in the (t, $\alpha$ ) reaction, so it does not have the right parity to be Alexeev's 715 keV level. If the 715 keV level were directly populated in the (d,p) reaction it could not be resolved from the 720 keV level. When the 232 keV yield was compared to the net yield of the 624 keV level, it was found that the 715 keV level would require a differential cross-section of 4  $\mu\text{b/sr}$  near the maximum of the  $l_n = 5$  angular distribution. This weak level could easily be overlooked during the analysis of the plate data.

840 keV State: Alexeev et al. placed this level from 269-120 and 269-205 keV coincidences and the energy fit for the 663 keV  $\gamma$ -ray. The 840 keV level was also fed by the 6052 keV primary  $\gamma$ -ray from the capture state (Archer et al., 1966). The level was assigned  $3^-$  or  $4^-$ , based on the M1, E2 multipolarity of the 269 keV transi-

tion. The  $2^-$  and  $5^-$  possibilities should not be excluded.

The 269-120 and 269-205 keV coincidences were also seen in the (d,p $\gamma$ ) data. The 663 keV line is completely obscured by a very strong line at 664.9 keV.

The 840 keV level was also not observed in the particle spectra. The particle yield was estimated from the yield of the 269 keV  $\gamma$ -ray. The 840 keV level would require a differential cross-section of 3  $\mu$ b/sr near the maximum of the  $l_n = 5$  angular distribution. Such a weak peak was easily overlooked during the analysis of the plate data.

910 keV State: The 910 keV level was weakly populated in the (d,p) reaction by  $l_n = 0$ . It was also the weakest level for which the  $l$ -value was obtained in the (t, $\alpha$ ) reactor. The level was assigned  $l_p = 2$ . The  $l_n = 0$  angular distribution limits the spin to  $3^+$  or  $4^+$  since the  $^{133}\text{Cs}$  target ground state spin is  $7/2^+$ .

Coincidences between  $\gamma$ -rays of 737 and 113 keV were seen in the (d,p $\gamma$ ) data. These are not reported in the (n, $\gamma$ ) work where the coincidence data do not extend beyond 345 keV.

936 and 937 keV States: The 937 keV state has an  $l_n = 5$  strength of  $0.24 \pm 0.10$  in the (d,p) reaction. The  $l_n$ -value requires that the parity be negative. The state at  $936 \pm 3$  keV in the (t, $\alpha$ ) reaction is presumably

another separate state since the (t, $\alpha$ ) reaction is not expected to populate negative parity states.

Two coincidences, 554-205 and 593-205 keV were found in the (d,p)  $\gamma$ -ray data. The 554 keV  $\gamma$ -ray has been placed to feed the 383 keV level and the 593 keV  $\gamma$ -ray has been placed to feed the 344 keV level. The branching ratios for the 593 and 554 keV lines were extracted from the 205 keV coincidence gate since, in singles, the 593 keV line is obscured by a strong line at 592 keV. A 926 keV transition was observed in the singles data which fits to within 0.5 keV as the transition to the 11 keV  $5^+$  state. The 593 keV transition feeds the 344 keV  $7^-$  level. If the 593 keV transition is at most E2, then the allowed spins for the 937 keV level are  $5^-$  or  $6^-$ . The spectroscopic strength of the 937 keV level is weaker than what is expected for either  $5^-$  or  $6^-$  spin assignments. It is quite probable that this is a level resulting from the fragmenting of the shell model strength.

1103 keV State: This state was suggested by a 113-929 keV coincidence in the (d,p $\gamma$ ) data. There was also a level at about 1102 keV, populated by a 5790 keV primary transition in the (n, $\gamma$ ) work of Archer et al. (1966). The 1103 keV level was not observed in the (d,p) or the (t, $\alpha$ ) particle spectra. Since the 929 keV  $\gamma$ -ray feeds a  $2^+$  state, the level is  $2^-$  or  $3^-$  if the 1103 keV state is

negative parity and  $1^+$ ,  $2^+$ ,  $3^+$  or  $4^+$  if the state is positive parity.

1057 and 1214 keV States: The  $^{130}\text{Te}(^7\text{Li},3n)$  reaction contained a  $\gamma$ -ray cascade, 157, 205, 295 and 418 keV. The 205-295 keV coincidence has already been explained by placing a level at 639 keV. The 418 keV line was stronger in the singles spectrum of the  $(^7\text{Li},3n)$  reaction than the 157 keV line, so it should be placed next. Placing this transition on top of the 639 keV level requires a level at 1057 keV. Then a level is needed at 1214 keV to feed the 1057 keV level by a 157 keV transition. The spins of these two levels are expected to be larger than those of levels populated in the (d,p) or (n, $\gamma$ ) reactions.

742, 782 and 830 keV Levels: Three additional  $i_n = 5$  levels were identified in the (d,p) particle spectra, but were absent from the (t, $\alpha$ ) reaction. These levels must have negative parity. The  $\gamma$ -ray transitions depopulating these levels could not be identified from the  $\gamma$ -ray data. Comparisons of the strengths of these levels to another  $i_n = 5$  level for which  $\gamma$ -ray decays were identified provide estimates on the  $\gamma$ -ray yields for these levels. If one assumes that each level de-excites by a single  $\gamma$ -ray, then the lines would require relative yields of 18, 14 and 12 for the 742, 782 and 830 keV levels, respectively. These  $\gamma$ -ray

yields are comparable to the 120 keV yield from the de-excitation of the 571 keV level in the (d,p $\gamma$ ) experiment.

### 6.3 Additional Levels in (n, $\gamma$ ) Scheme

Additional levels at 176.6, 197, 291, 634 and 752 keV were reported by Alexeev et al. (1975) (see figure 6.1) but are not included in figure 6.2, because these levels were not seen in the present study.

The 176.6 keV level was placed by Alexeev et al. by virtue of 114-116 keV coincidences and the energy fit for the 275 keV  $\gamma$ -ray between the 451 and 176.6 keV levels. They used the observed E2 multipolarity for the 116 keV transition to the assumed  $3^+$  level at 60 keV to assign  $1^+$  to the 176.6 keV level, although  $2^+$ ,  $3^+$ ,  $4^+$  and  $5^+$  can not be ruled out completely.

The 197 keV level was based on the 137-305 keV coincidences and the energy fit for the 197 keV transition to the ground state. Alexeev et al. assigned  $3^+$  to the level, but there is no evidence for excluding  $4^+$  or  $5^+$  as possibilities.

Alexeev et al. placed a level at 291 keV, based on the observation of 93-130, 114-116 and 117-113 keV coincidences. Their 93 keV transition is reported to have M1 multipolarity and their 114. Alexeev et al. (1975) assigned  $2^+$  to the level. However, the spin of

the 197 keV level is not well established so  $3^+$ ,  $4^+$ ,  $5^+$  or  $6^+$  should be considered as possibilities.

Alexeev et al. placed the 634 keV level by the energy fits for the 150, 251 and 377 keV  $\gamma$ -rays. It is not evident from the published data how Alexeev et al. decided upon  $5^-$  or  $6^-$  as the spin and parity for this level. There is a very weak 251 keV line in the (d,p $\gamma$ ) spectrum. There is also a 377 keV line in the (d,p $\gamma$ ) spectrum but it differs in energy from the (n, $\gamma$ ) data by 0.4 keV. The 377 keV line in the (d,p)  $\gamma$ -ray data is not the same line reported by Alexeev et al since the 377 keV line is 7.5 times stronger than the 251 keV line in the (d,p $\gamma$ ) data but only 4.5 times stronger in the (n, $\gamma$ ) data. No 150 keV line was observed in the (d,p $\gamma$ ) spectrum, but since Alexeev's data show this to be the weakest of the lines from the 634 keV level, the absence of the line from the (d,p $\gamma$ ) data is not surprising. It is not clear whether the 634 keV level is populated in the (d,p $\gamma$ ) experiment. No 634 keV level was identified from the (d,p) particle spectra.

The 752 keV level was placed by Alexeev et al. (1975) with 302-205 keV coincidences and energy fits for the 485 and 495 keV transitions. They placed the 302 keV transition to feed the 450 keV level rather than the 383 keV level. The M1, E2 multipolarity of the 302 keV  $\gamma$ -ray limited the spin possibilities to  $4^-$  or  $5^-$ .

Archer et al. (1966) reported a 6138 keV primary transition in their  $(n,\gamma)$  study which Alexeev et al. assigned to feed a 752 keV level. A very strong 302 keV doublet appeared in the  $(d,p\gamma)$  singles spectrum but no 302-205 keV coincidences were found. The 302 keV lines were primarily attributed to  $^{133}\text{Cs}$  and  $^{133}\text{Ba}$ . The 485 keV line does not appear at all. There is a 495 keV line which is very strong but it differs in energy from the  $(n,\gamma)$  value by 0.5 keV. Since the 495 keV line is weaker than the 485 keV line in the  $(n,\gamma)$  reaction, it should also be true here if the  $(n,\gamma)$  level scheme is to be believed. Thus one concludes that the 752 keV level is not populated in the  $(d,p\gamma)$  experiment.

#### 6.4 Shell Model Configurations in $^{134}\text{Cs}$

The four members of the  $[\pi g_{7/2}, (v d_{3/2})^{-1}]$  configuration are positively identified as the  $4^+$  ground state, the  $5^+$  11 keV level, the  $3^+$  60 keV level and the  $2^+$  173 keV level. In the  $(d,p)$  particle data the ground state is weaker than the predicted strength for the  $4^+$  member and the 60 keV level is stronger than the predicted strength for the  $3^+$  member. The 11 and 173 keV levels carry strengths which are appropriate to their respective spin assignments in the  $(d,p)$  particle data. In the  $(t,\alpha)$  experiment, the 60 and 173 keV levels carry strengths consistent with the  $(2J+1)$  sum rule predic-

tions for the  $3^+$  and  $2^+$  members of  $[\pi g_{7/2}, (\nu d_{3/2})^{-1}]$ . The combined strength of the ground state and 11 keV level in the (t, $\alpha$ ) experiment is also consistent with the sum of the predicted strengths for the  $4^+$  and  $5^+$  members.

Two strong  $\lambda_n = 0$  levels were expected in the (d,p) reaction, corresponding to the  $3^+$  and  $4^+$  members of the  $[\pi g_{7/2}, (\nu s_{1/2})^{-1}]$  configuration. The (2J+1) rule predicts strengths of 0.37 for the  $4^+$  member and 0.29 for the  $3^+$  member. Three strong  $\lambda_n = 0$  levels at 190, 234 and 377 keV were found in the (d,p) particle data. The 377 keV level carries all of the strength of one member of the configuration, while the 190 and 234 keV level equally share the strength of the other member. The (d,p) particle data suggest that the 190 and 234 keV levels have the same spin. However, the (t, $\alpha$ ) data do not support this.

The (t, $\alpha$ ) data are used to identify the four members of the  $[\pi d_{5/2}, (\nu d_{3/2})^{-1}]$  configuration which would not be populated in the (d,p) reaction. Four strong  $\lambda_p = 2$  levels at 190, 209, 234 and 455 keV were found in the (t, $\alpha$ ) reaction. The (d,p) data would require that the 190 and 234 keV levels have the same spin. However, the 190 keV level alone carries enough  $\lambda_p = 2$  strength to account for the  $4^+$  member, so the (t, $\alpha$ ) data would require that the 190 and 234 keV levels

have different spin. The 209 keV level is tentatively assigned  $4^+$  in the present study since it is the only spin which is consistent with data from this study and the  $(n,\gamma)$  work of Alexeev et al. (1975). The discussion on the 451 and 454 keV levels indicated that the 455 keV level in the  $(d,p)$  reaction is doublet. The same may be true in the  $(t,\alpha)$  reaction. The observed  $\lambda_p = 2$  strength for the 455 keV level could account for the remaining strength of the  $4^+$  member. One cannot conclude from the available data which spins should be assigned to the 190, 234 and 455 keV levels. The spins of the 190 and 234 keV levels can only be restricted to a choice of  $3^+$  or  $4^+$ . Since no other strong  $\lambda_p = 2$  levels remain, there are no candidates for the  $2^+$  and  $1^+$  members of the multiplet. In view of the resolution problems in the  $(t,\alpha)$  experiment, it is possible that there is another  $\lambda_p = 2$  level unresolved from the 190 keV level. This could explain the large  $\lambda_p = 2$  strength carried by the 190 keV level.

In summary, the positive parity states are identified as follows:

14 keV	$[\pi g_{7/2}, (v d_{3/2})^{-1}] 5^+$
0 keV	$[\pi g_{7/2}, (v d_{3/2})^{-1}] 4^+$
60 keV	$[\pi g_{7/2}, (v d_{3/2})^{-1}] 3^+$
173 keV	$[\pi g_{7/2}, (v d_{3/2})^{-1}] 2^+$
190 keV	$[\pi g_{7/2}, (v s_{1/2})^{-1}] + [\pi d_{5/2}, (v d_{3/2})^{-1}] 3^+, 4^+$

209 keV	$[\pi d_{5/2}, (v d_{3/2})^{-1}] 4^+$
234 keV	$[\pi g_{7/2}, (v s_{1/2})^{-1}] + [\pi d_{5/2}, (v d_{3/2})^{-1}] 3^+, 4^+$
377 keV	$[\pi g_{7/2}, (v s_{1/2})^{-1}] 3^+, 4^+$
455 keV	$[\pi d_{5/2}, (v d_{3/2})^{-1}]$

where the 455 keV level may be the 451 keV level, the 454 keV level or both in the (t,  $\alpha$ ) reaction.

Eight members of the  $[\pi g_{7/2}, (v h_{11/2})^{-1}]$  configuration are expected in the (d, p) reaction. None of these are expected to appear in the (t,  $\alpha$ ) reaction. Eleven  $\lambda_n = 5$  levels appeared in the (d, p) reaction, so some fragmenting of the shell model strength occurred. The  $8^-$  member is identified as the 138 keV isomer. The 344 keV level is a part of the  $7^-$  member, the level carrying the remainder of the  $7^-$  strength has not been identified. The 257 and 434 keV levels are tentatively identified as components of the  $6^-$  member of the configuration. The  $5^-$  member is identified as the 624 keV level. The  $9^-$ ,  $4^-$ ,  $3^-$  and  $2^-$  members have not been positively identified from the (d, p) data. Alexeev's  $5^-$  assignment to the 267 keV level is not firmly established and the  $5^-$  strength is already accounted for by the 624 keV level. If the observed strength of the 263 keV doublet is equally divided between the 257 and 267 keV levels, the 267 keV level only carries part of the strength expected for the  $4^-$  member. The 782 and 830 keV levels carry enough  $\lambda_n = 5$  strength to be the  $3^-$  and

$2^-$  members or to be the other part of the  $4^-$  member. The 742 keV level carries enough  $\lambda_n = 5$  strength to account for the  $4^-$  member or to account for the remaining 65% of the  $7^-$  member.

Alexeev et al. (1978) ran shell model calculations for the p-n multiplets in  $^{122}\text{Sb}$  and obtained good agreement between the calculated and experimental level energies. Then they compared the level spacings of the negative parity states in  $^{122}\text{Sb}$  with those in  $^{134}\text{Cs}$  and concluded that the same p-n multiplets are observed in both nuclei. They performed a shell model calculation for the  $(\pi g_{7/2}, \nu h_{11/2})$  and  $(\pi d_{5/2}, \nu h_{11/2})$  multiplets in  $^{134}\text{Cs}$  with the same model that was used for  $^{122}\text{Sb}$ . The force parameters for the calculation were obtained from fits to the level energies of ten negative parity states in  $^{134}\text{Cs}$ . From a comparison of the calculated and experimental level energies they associated the 176.4, 193, 267, 257 and 138 keV levels with the  $3^-$ ,  $4^-$ ,  $5^-$ ,  $6^-$  and  $8^-$  members of the  $(\pi d_{5/2}, \nu h_{11/2})$  multiplet. They also identified the 840, 571, 450, 383, and 344 keV levels with the  $3^-$ ,  $4^-$ ,  $5^-$ ,  $6^-$  and  $7^-$  members of the  $(\pi g_{7/2}, \nu h_{11/2})$  multiplet. The (d,p) particle data in the present study show the 138, 257, 267 and 344 with  $\lambda_n = 5$  angular distributions. The (d,p) reaction populates states from  $(\pi g_{7/2}, \nu h_{11/2})$  but would not populate states from  $(\pi d_{5/2}, \nu h_{11/2})$ . The present study conflicts with

the p-n multiplet assignments of Alexeev et al. (1978). They were not justified in believing that a model which works for  $^{122}\text{Sb}$  could predict anything about  $^{134}\text{Cs}$  which has four more protons and eight more neutrons.

### 6.5 Summary

A description of an experimental study of the energy levels in the odd-odd  $^{134}\text{Cs}$  nucleus has been presented. The (d,p) and (t, $\alpha$ ) reactions gave the spectroscopic strengths and the  $Q$ -values for many of the low-lying levels. The particle data were analyzed within the framework of the nuclear shell model. The  $\gamma$ -ray studies revealed the decay properties for these levels and provided the basis for a comparison with the results of the (n, $\gamma$ ) study of Alexeev et al. (1975, 1978).

Many of the spins that Alexeev et al. (1975) assigned to the positive parity states were not well established because they assumed that the spin of the 60 keV level was  $3^+$ . Their data did not provide a firm spin assignment for the 60 keV level, since  $4^+$  and  $5^+$  could not be excluded as possible spins. The present study provides conclusive evidence that the 60 keV level is indeed  $3^+$ . Alexeev's spin assignments for some of the positive parity states are more firmly established as a result of the present study. The spins of the

positive parity states from the present study generally agreed well with those of Alexeev et al. (1975). The spins of some negative parity states from the present study also agreed well with those of Alexeev et al. Unfortunately, the present study did not provide information on many negative parity states whose spins are not firmly set by the  $(n,\gamma)$  work. The branching ratios from the present study also agree well in most instances with those of Alexeev et al. The p-n multiplet structure of some levels in  $^{134}\text{Cs}$  have been identified from the present study. These p-n multiplet assignments conflict with the multiplet assignments made by Alexeev et al. (1978). Since it was concluded that the negative parity states Alexeev et al. (1978) identified with the p-n multiplets were in error, their shell model calculation was considered to be invalid. Hence no attempts were made to compare the level energies of the p-n multiplet members with their shell model calculated energies.

The current study has produced more information on the structure of  $^{134}\text{Cs}$ , but further studies are needed. If an enriched isotope  $^{135}\text{Cs}$  target becomes available, the  $(d,t)$  reaction promises to provide a better chance to investigate the negative parity levels since the  $l_D = 5$  levels should be stronger in the pick-up reaction than they were in the stripping reaction.

If a very highly enriched  $^{134}\text{Xe}$  target became available, the  $^{134}\text{Xe}(p,n\gamma)$  reaction would be another good experiment for further investigating  $^{134}\text{Cs}$ . Repeating the  $(d,p\gamma)$  experiment does not appear to have many benefits. The lifetimes of many of the levels in  $^{134}\text{Cs}$  are already known (Alexeev et al., 1975), so lifetime information from the  $(d,p\gamma)$  reaction is not necessary. It would be advantageous to improve the energy resolution for another  $(d,p\gamma)$  experiment since there are many close lying lines which were unresolved or poorly resolved. There were also many lines from the  $^{133}\text{Cs}(d,2n\gamma)$  reaction in the  $\gamma$ -ray spectrum which obscured lines from  $^{134}\text{Cs}$ . The Q-value for the  $(d,2n)$  reaction is  $\approx 3.512$  MeV, so the reaction threshold is well below the 11.85 MeV Coulomb barrier for deuterons on  $^{133}\text{Cs}$ . The deuteron beam energy could not be lowered enough so that the  $(d,2n)$  reaction would not compete with the  $(d,p)$  reaction. The  $(d,p)$  reaction did not allow large amounts of angular momentum to be transferred so there would not be very much anisotropy in the  $\gamma$ -ray angular distributions. The  $(^{130}\text{Te} + ^7\text{Li})$  reaction was unsuccessful in providing information on  $^{134}\text{Cs}$  at bombarding energies of 32 and 34 MeV. Lowering the bombarding energy may provide useful information on  $^{134}\text{Cs}$  from the  $^{130}\text{Te}(^7\text{Li},3n\gamma)$  reaction. If useful information can be gained from this reaction,  $\gamma$ -ray angular distributions should provide spin informa-

tion since the heavy ion reactions transfer large amounts of angular momentum. The (t, $\alpha$ ) reaction populated a level at 455 keV which could be the 451 keV level, the 454 keV level or both. The energy resolution was not good enough to determine this. Since the  $\gamma$ -ray studies with the (d,p) reaction provided much information, a similar  $\gamma$ -ray study with the (t, $\alpha$ ) reaction might also prove useful.

## BIBLIOGRAPHY

- Alexeev, V.L., Emelianov, B.A., Kabina, L.P., Kaminker, D.M., Khazov, Yu.L., Kondurov, I.A., Leushkin, E.K., Loginov, Yu, E., Rumjantsev, V.L., Sakharov, S.L., Smirnov, A.I. and Suslkov, P.A., Nucl. Phys. A 248, 249 (1975).
- Alexeev, V.L., Emelianov, B.A., Egorov, A.I., Kabina, L.P., Kaminker, D.M., Khazov, Y.L., Kondurov, I.A., Leushkin, E.K., Loginov, Y.E., Martynov, V.V., Rumiantsev, V.L., Sakharov, S.L., Sushkov, P.A., Börner, H.G., Davidson, W.F., Pinston, J.A. and Schrenkenbach, K., Nucl. Phys. A 297, 373 (1978).
- Archer, N., Hughes, L.B., Kennett, T.J. and Prestwich, W.V., Nucl. Phys. 83, 241 (1966).
- Austern, N., Direct Nuclear Reactions, John Wiley and Sons, Inc., New York (1970).
- Bassel, R.H., Phys. Rev. 149, 791 (1966).
- Becchetti, F.D., Jr. and Greenlees, G.W., Phys. Rev. 182, 1190 (1969).
- Berestovoi, A.M., Kondurov, I.A. and Loginov, Yu.E., Bull. Acad. Sci. USSR, Phys. Ser. 32, 269 (1968).
- Bertsch, G.F., The Practitioner's Shell Model, North Holland Publ. Co., Amsterdam (1972).
- Bevington, P., Data Reduction and Error Analysis for the Physics Sciences, McGraw-Hill, New York (1969).
- Brennan, M.H. and Bernstein, A.M., Phys. Rev. 120, 927 (1960).
- Brussaard, P.J. and Glaudemans, P.W.M., Shell Model Applications in Nuclear Spectroscopy, North Holland Publ. Co., Amsterdam (1977).
- Bultsev, V.S., Vylov, T., Kalinnikov, V.G. and Tikhonov, N.A., Bull. Acad. Sci. USSR, Phys. Ser. 38, 54 (1974).
- Buttle, P.J.A. and Goldfarb, L.J.B., Proc. Phys. Soc. 83, 701 (1964).

- Cerny, J., ed., Nuclear Spectroscopy and Reactions, part C-D, Academic Press, New York (1974).
- Conjeaud, M., Harar, S., Caballero, M. and Cindro, N., Nucl. Phys. A 215, 383 (1973).
- De Shalit, A. and Talmi, I., Nuclear Shell Theory, Academic Press, New York (1963).
- Flynn, E.R., Hardekopf, R.A., Sherman, J.D., Sunier, J.W. and Coffin, J.P., Nucl. Phys. A279, 394 (1977).
- Fransson, K. and Bemis, C.E., Jr., Nucl. Phys. 78, 207 (1966).
- Fuller, G.H., J. Phys. Chem. Ref. Data 5, 835 (1976).
- Goncharov, K.S. et al., Izv. Acad. Nauk. SSSR. Ser. Fiz. 41, 1673 (1977).
- Gove, N.B. and Wapstra, A.H., Nuclear Data Tables 11, 129 (1972).
- Green, I.M. and Moszkowski, S.A., Phys. Rev. B139, 790 (1965).
- Gritsyna, V.T., Klyucharev, A.P. and Remaev, V.V., J. Nucl. Phys. 3, 993 (1966).
- Hamilton, W.D., The Electromagnetic Interaction in Nuclear Spectroscopy, North Holland Publ. Co., Oxford (1975).
- Haxel, O., Jensen, J.H.D. and Suess, H.E., Phys. Rev. 75, 1766 (1949).
- Helton, V.D., Hiebert, J.C. and Ball, J.B., Nucl. Phys. A201, 225 (1973).
- Islam, A., Ph.D. Thesis, McMaster University, 1975.
- Jackson, D.F., Direct Reactions, Methuen, London (1970).
- Khan, A., M.Sc. Thesis, McMaster University (1977).
- Koops, J.E. and Glaudemans, P.W.M., Z. Phys. A - Atoms and Nuclei, 280, 181 (1977).
- Kunz, P.D., DWUCK4, unpublished (1974).
- Kuo, T.T.S. and Brown, G.E., Nucl. Phys. 85, 40 (1966).

- Kuo, T.T.S. and Brown, G.E., Nucl. Phys. A 103, 71 (1967).
- Lederer, C.M. and Shirley, V.S., eds., Table of Isotopes, 7th ed., John Wiley and Sons, Inc., New York (1978).
- Levin, F.S. and Feschbach, H., Reaction Dynamics, Gordon and Breach Science Publishers, New York (1973).
- Lohr, J.M. and Haerberli, W., Nucl. Phys. A 232, 381 (1974).
- Macphail, R.M., Ph.D. Thesis, McMaster University, 1973.
- Madueme, G.Ch., Edvardson, L.O. and Westbury, L., Phys. Scr. 13, 23 (1976).
- Markham, R.G. and Robertson, R.G.H., Nucl. Inst. and Meth. 129, 131 (1975).
- Mayer, M.G., Phys. Rev. 75, 1969 (1949).
- Mayer, M.G. and Jensen, J.H.D., Elementary Theory of Nuclear Shell Structure, John Wiley and Sons, Inc., New York (1955).
- Meyer, R.A. and Griffien, R.D., Phys. Rev. 186, 1220 (1969).
- Morek, T., Beuscher, H., Bochev, B., Haenni, D.R., Sieder, R.M., Kutsarova, T., Muller-Veggian, M. and Neskakis, A., Z. Phys. A - Atoms and Nuclei 298, 267 (1980).
- Nordheim, L., Phys. Rev. 78, 294 (1950).
- Northcliffe, L.C. and Schilling, R.F., Nuclear Data Tables A7, 233 (1970).
- Nunnally, L.L. and Loveland, W.D., Phys. Rev. C 15, 444 (1977).
- O'Neil, R.A., SPECTR, unpublished (1979).
- Padalko, V.Y., Zarubin, P.P. and Sergienko, V.A., Bull Acad Sci USSR., Phys. Ser. 38, No. 12, 101 (1974).
- Perey, F. and Buck B., Nucl. Phys. 32, 353 (1962).
- Perey, C.M. and Perey, F.G., Atomic Data and Nuclear Data Tables, 17, 87 (1976).
- Preston, M.A., Physics of the Nucleus, Addison-Wesley Publ. Co. (1962).

- Rosel, F., Fries, H.M., Alder, K. and Pauli, H.C., Atomic Data and Nuclear Data Tables 21, 110 (1978).
- Roy, R.R. and Nigam, B.P., Nuclear Physics, John Wiley and Sons, New York (1967).
- Satchler, G.R., Introduction to Nuclear Reactions, The MacMillan Press, London (1980).
- Schneid, E. and Rosner, B., Phys. Rev. 148, 1241 (1966).
- Sergeenkov, Yu.V. and Sigalov, V.M., Nuclear Data Sheets 34, 475 (1981).
- Shikata, Y., Sakakura, M. and Sebe, T., Z. Phys. A - Atoms and Nuclei, 300, 217 (1981).
- Siegbahn, K., ed., Alpha-, Beta- and Gamma-Ray Spectroscopy, North Holland Publishing Co., Amsterdam (1965).
- Storm, E. and Israel, H.I., Nuclear Data Tables A7, 565 (1970).
- Summers-Gill, R.G. and Oluwole, F.A., priv. comm. (1978).
- Summers-Gill, R.G., Islam, A. and Lee, A.G., McMaster Accelerator Laboratory Annual Report, 65 (1980).
- Sunyar, A.W., Michelich, J.W. and Goldhaber, M., Phys. Rev. 95, 570 (1954).
- van Hienen, J.F.A., Chung, W. and Wildenthal, B.H., Nucl. Phys. A 260, 159 (1976).
- von Ehrenstein, D., Morrison, G.C., Nolen, J.A., Jr. and Williams, N., Phys. Rev. C 1, 2066 (1970).
- Wapstra, A.H. and Bos, K., Atomic Data and Nuclear Data Tables 19, 177 (1977).
- Westgaard, L., Hansen, P.G., Jonsen, B., Ravn, H.L. and Sundell, S., Proc. Int. Conf. Nucl. Phys., Munich, J. de Boer and H.I. Mang, eds., North Holland Publ. co., Amsterdam, Vol. 1, 696 (1973).
- Wildenthal, B.H., Phys. Rev. Letters, 22, 1118 (1969).
- Wildenthal, B.H., Newman, E. and Auble, R.L., Phys. Rev. C 3, 1199 (1971).
- Wilkin, G.B., M.Sc. thesis, McMaster University, 1976.

Wong, S.S.M., Ph.D. Thesis, University of Rochester, 1966.

Yousif, A.A., Hamilton, W.D. and Michelakis, E., J. Phys. G  
7, 445 (1981).

Appendix A

The experimental data for the  $^{133}\text{Cs}(d,p)^{134}\text{Cs}$  reaction are presented in Table A-1.

Table A-1  
 Differential Cross-Sections for the Energy Levels Identified with  $^{134}\text{Cs}$  in the  
 $^{133}\text{Cs}(d,p)$  reaction

Lab Angle	Energy (keV)						
	G.S.	11	60	140	174	191	207
7.5	144(16)	141(14)	145(16)	21(7)	102(12)	211(22)	14(4)
10.0	122(13)	146(15)	128(40)	15(3)	85(11)	144(17)	12(4)
12.5	148(56)	181(66)	131(18)	19(3)	88(17)	68(9)	16(4)
15.0	158(17)	249(38)	128(16)	17(3)	91(12)	55(19)	16(5)
17.5	164(23)	248(35)	139(15)	17(3)	104(13)	45(7)	21(5)
20.0	202(28)	237(33)	162(18)	20(3)	128(49)	66(9)	19(4)
22.5	156(17)	303(36)	173(18)	20(16)	98(11)	112(14)	42(9)
25.0	243(28)	272(27)	212(22)	19(6)	118(39)	203(63)	29(8)
27.5	251(35)	296(41)	246(26)	22(4)	138(16)	268(29)	29(6)
30.0	244(34)	253(36)	221(23)	21(3)	133(16)	252(28)	18(5)
32.5	155(18)	215(26)	170(17)	14(3)	92(12)	204(22)	24(6)
35.0	126(17)	308(32)	210(23)	26(3)	128(18)	239(28)	28(5)
37.5	174(18)	235(26)	187(20)	23(3)	121(15)	181(21)	13(3)
40.0	168(29)	230(32)	165(17)	17(3)	119(15)	140(17)	17(6)
45.0	126(15)	169(19)	128(13)	20(3)	96(10)	68(7)	12(2)
60.0	150(17)	151(17)	140(15)	22(4)	79(9)	89(11)	11(4)
65.0	82(8)	92(9)	77(8)	21(3)	61(7)	47(6)	5(1)
75.0	63(7)	70(8)	52(6)	16(3)	36(5)		

NOTE: Cross-sections are in  $\mu\text{b}/\text{sr}$

Table A-1 (continued)

Lab Angle	Energy (keV)						
	235	263	344	377	435	455	501
7.5	216(24)	14(3)	13(2)	470(60)	14(2)	36(6)	
10.0	122(14)	17(3)	6(2)	310(33)	7(2)	12(3)	
12.5	86(10)	13(3)	7(2)	178(25)	6(2)	8(2)	
15.0	46(11)	18(3)	8(3)	87(22)	8(2)	9(2)	
17.5	39(6)	23(9)	8(4)	89(11)	8(2)	5(2)	
20.0	75(21)	20(5)	8(2)	159(44)	9(2)	12(2)	7(1)
22.5	113(12)	21(5)		270(28)	8(1)	15(3)	10(4)
25.0	210(190)	24(5)	8(2)	482(70)	13(9)	19(6)	12(7)
27.5	270(28)	25(6)		680(145)	14(2)	22(5)	12(2)
30.0	287(30)	22(4)		646(66)	11(3)	40(6)	15(3)
32.5	231(25)	22(5)	4(1)	531(55)	6(2)	26(4)	13(2)
35.0	268(28)	32(4)	9(2)	639(90)			
37.5	208(22)	23(3)	6(2)	471(48)	14(2)	47(6)	11(2)
40.0	154(19)	22(8)	7(2)	340(38)	9(1)	25(4)	11(1)
45.0	56(6)	10(1)	5(1)	125(13)	6(1)	10(1)	
60.0	102(16)	18(3)	6(2)	213(25)	10(1)	9(1)	7(1)
65.0			10(1)	208(22)	12(2)	18(2)	16(3)
75.0	42(6)	9(2)	3(1)	98(14)	4(1)	5(1)	4(1)

Table A-1 (continued)

Lab Angle	Energy (keV)						
	520	580	623	691	720	742	782
7.5	16(3)		13(2)	31(4)	13(2)	15(3)	12(3)
10.0		9(2)	12(3)	20(4)	5(2)	9(3)	5(2)
12.5		11(2)	16(4)	23(4)	5(2)	10(2)	7(2)
15.0		8(2)	15(3)	22(4)	8(2)	11(2)	8(2)
17.5		8(2)	23(4)	21(9)	10(1)	12(2)	10(2)
20.0		13(4)	15(3)	30(10)	7(1)	12(2)	9(2)
22.5		10(1)	12(2)	21(4)	10(1)	12(3)	6(1)
25.0	11(3)		14(3)	21(5)	10(1)	12(3)	11(4)
27.5	9(2)		18(3)	38(7)	13(3)	17(3)	7(6)
30.0	8(2)	16(3)		23(4)	15(3)	17(3)	10(2)
32.5	5(1)	12(2)	28(6)		12(2)	23(6)	5(2)
35.0		14(3)	33(6)		8(2)	11(2)	11(7)
37.5	8(2)	8(1)	20(4)	44(7)	11(2)	12(2)	12(2)
40.0	6(1)	6(2)	19(4)	21(5)	11(2)	12(2)	11(2)
45.0		5(1)	10(1)	25(5)	7(1)	10(1)	14(2)
60.0	4(1)	7(1)	12(2)	12(3)	4(2)	10(1)	10(1)
65.0	7(1)	8(3)	10(1)	14(2)		16(3)	10(2)
75.0		10(3)				7(1)	6(1)

Table A-1 (continued)

Lab Angle	Energy (keV)		
	830	911	936
7.5	8(2)	49(6)	20(9)
10.0	9(2)	33(6)	10(2)
12.5	5(2)	25(5)	11(2)
15.0		13(2)	13(8)
17.5		15(3)	11(2)
20.0	7(2)	25(5)	19(14)
22.5		66(8)	10(2)
25.0	8(2)	58(8)	11(4)
27.5	7(3)	59(8)	24(6)
30.0	12(3)	104(14)	29(9)
32.5	6(3)	59(8)	14(5)
35.0	16(3)	74(8)	45(8)
37.5	13(3)	45(20)	12(5)
40.0	13(2)	52(7)	14(2)
45.0	9(2)	27(5)	13(2)
60.0	11(2)		10(2)
65.0	9(5)	22(3)	9(2)
75.0	3(1)	13(2)	5(1)

## Appendix B

The experimental data for the  $^{135}\text{Ba}(t, \alpha)^{134}\text{Cs}$  reaction and for the  $^{135}\text{Cs}$  and  $^{137}\text{Cs}$  impurity peaks are presented in Table B-1.

Table B-1

Differential Cross-Sections for Energy Levels Identified in the (t,  $\alpha$ ) Reaction on  
the Barium Target

Lab Angle	Energy (keV)						
	g.s. + 11, 60	173	189	207	234	a	
7.5	889(92)	130(40)	406(66)	105(62)	151(23)	7120(2180)	
10.0	860(92)	157(22)	400(46)	234(31)	155(20)	5300(710)	
12.5	858(92)	162(62)	325(68)	192(63)	133(18)	2190(400)	
15.0	881(88)	157(62)	263(66)	189(63)	107(16)	1680(330)	
17.5	640(64)	174(39)	209(90)	67(11)	84(13)	1320(270)	
22.5	416(46)	116(27)	131(48)	44(8)	55(9)	1060(210)	
25.0	317(38)						
27.5	363(46)	87(19)	220(26)	62(14)	35(16)		
30.0	338(34)	136(68)	150(47)	59(18)	64(9)	1060(250)	
32.5	321(33)	82(18)	144(77)	30(20)	55(10)	1130(400)	
37.5	238(74)	58(12)	82(17)	54(18)	35(5)	450(100)	
40.0	353(35)	96(15)	151(26)	76(23)	54(7)	1060(180)	

a ground state of  $^{135}\text{Cs}$

NOTE: cross-sections are in  $\mu\text{b}/\text{sr}$

Table B-1 (continued)

Lab Angle	Energy (keV)						b
	344	377	455	513	586	723	
7.5			106(15)		28(7)	18(6)	1120(230)
10.0	22(6)		272(134)		42(7)	23(6)	2060(290)
12.5	78(12)	36(7)	198(23)	20(6)	51(17)	16(6)	1880(280)
15.0	32(7)	54(9)	165(20)	26(7)	31(16)		1830(260)
17.5	26(5)	13(3)	104(13)	19(4)	14(4)		1960(550)
22.5	15(3)	14(3)	92(11)	19(4)	14(4)	14(2)	1180(160)
25.0	8(2)	6(3)	106(22)	18(3)	12(2)	6(1)	900(190)
30.0	7(3)	2(1)	97(13)	14(4)	10(2)		960(110)
32.5	14(4)	10(3)	74(8)	11(2)	7(2)	3(1)	590(80)
37.5	6(1)	3(1)	57(7)	21(3)	26(9)	10(2)	910(120)
40.0	10(2)	10(3)	110(21)				

b ground state of  $^{137}\text{Cs}$

Table B-1 (continued)

Lab Angle	Energy (keV)						
	802	849	908	936	c	1282	1319
7.5	28(7)	46(8)	21(5)	23(6)	1490(390)	20(4)	19(5)
10.0	62(9)		12(6)		1760(280)	20(4)	14(4)
12.5	39(11)	26(7)	13(3)	32(6)	1200(240)		19(4)
15.0	43(7)	21(5)	8(3)	27(5)			
17.5	31(9)		6(2)	11(2)	825(125)	6(3)	12(3)
22.5	23(4)	14(2)	6(1)	7(3)	645(130)	4(1)	8(4)
30.0					580(135)	12(3)	17(3)
32.5	10(3)	6(2)	3(1)	4(2)	455(80)	4(1)	9(2)
37.5	20(5)	15(4)	8(1)	15(2)	985(140)	11(2)	20(3)
40.0							

c first excited state of <sup>137</sup>Cs

829